iScience

CellPress
OPEN ACCESS

Article

Spermatogonial Gene Networks Selectively Couple to Glutathione and Pentose Phosphate Metabolism but Not Cysteine Biosynthesis

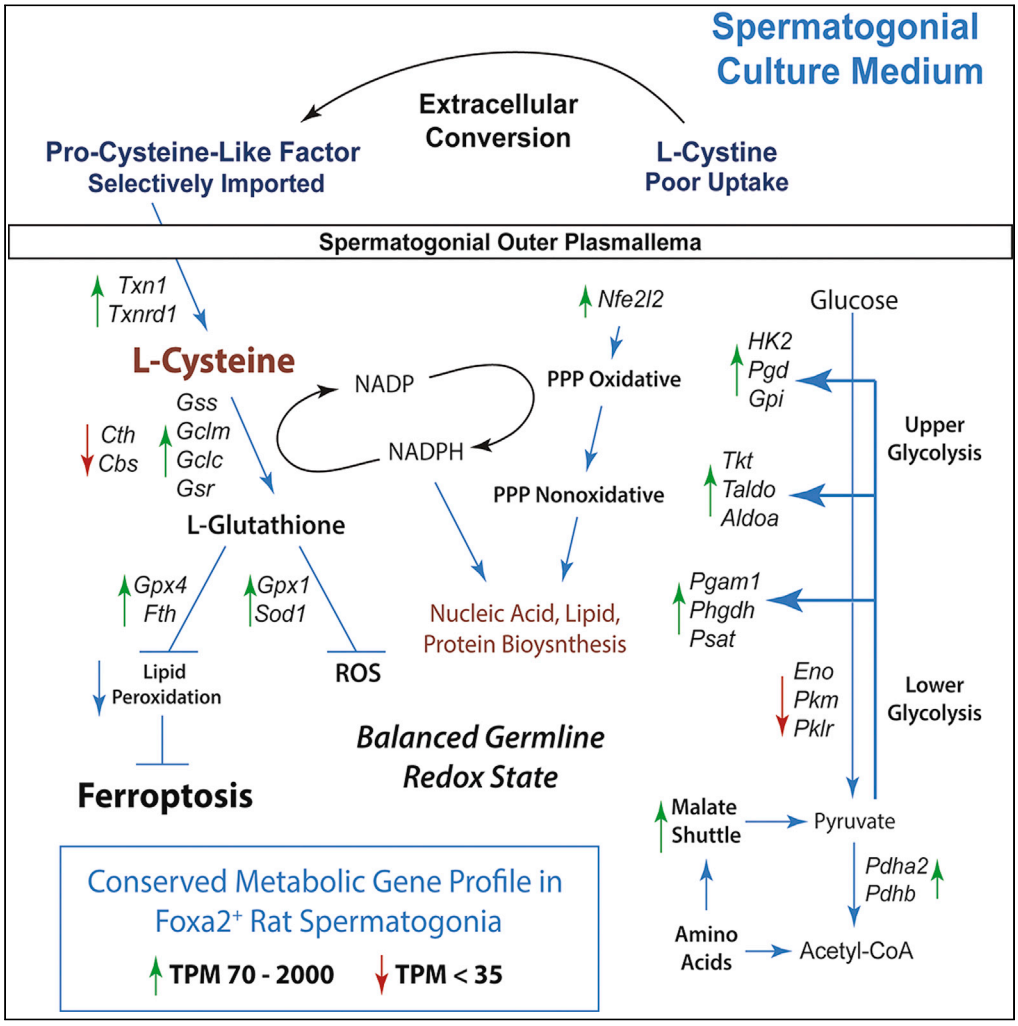

David Prokai, Ashutosh Pudasaini, Mohammed Kanchwala, ..., Xing Chao, Bruce R. Carr, F. Kent Hamra

kent.hamra@utsouthwestern.edu

HIGHLIGHTS

Foxa2-bound loci are enriched with spermatogonial stemness genes in the rat germline

Spermatogonial stemness genes couple to glutathione/pentose phosphate pathways

Mammalian spermatogonia are deficient in transsulfuration pathway gene products

Cysteine-like factors counteract spermatogonial ferroptosis in soma-depleted cultures

Prokai et al., iScience 24, 101880
January 22, 2021
https://doi.org/10.1016/j.isci.2020.101880

iScience

CellPress
OPEN ACCESS

Article

Spermatogonial Gene Networks Selectively Couple to Glutathione and Pentose Phosphate Metabolism but Not Cysteine Biosynthesis

David Prokai,[1,11] Ashutosh Pudasaini,[2,10,11] Mohammed Kanchwala,[4,11] Andrew T. Moehlman,[5,11] Alexandrea E. Waits,[5,11] Karen M. Chapman,[6,11] Jaideep Chaudhary,[7,11] Jesus Acevedo,[2,3] Patrick Keller,[2,3] Xing Chao,[4,8,9] Bruce R. Carr,[1,2] and F. Kent Hamra[2,3,12,*]

SUMMARY

In adult males, spermatogonia maintain lifelong spermatozoa production for oocyte fertilization. To understand spermatogonial metabolism we compared gene profiles in rat spermatogonia to publicly available mouse, monkey, and human spermatogonial gene profiles. Interestingly, rat spermatogonia expressed metabolic control factors *Foxa1*, *Foxa2*, and *Foxa3*. Germline Foxa2 was enriched in Gfra1^{Hi} and Gfra1^{Low} undifferentiated A-single spermatogonia. Foxa2-bound loci in spermatogonial chromatin were overrepresented by conserved stemness genes (*Dusp6, Gfra1, Etv5, Rest, Nanos2, Foxp1*) that intersect bioinformatically with conserved glutathione/pentose phosphate metabolism genes (*Tkt, Gss, Gclc, Gclm, Gpx1, Gpx4, Fth*), marking elevated spermatogonial GSH:GSSG. Cystine-uptake and intracellular conversion to cysteine typically couple glutathione biosynthesis to pentose phosphate metabolism. Rat spermatogonia, curiously, displayed poor germline stem cell viability in cystine-containing media, and, like primate spermatogonia, exhibited reduced transsulfuration pathway markers. Exogenous cysteine, cysteine-like mercaptans, somatic testis cells, and ferroptosis inhibitors counteracted the cysteine-starvation-induced spermatogonial death and stimulated spermatogonial growth factor activity *in vitro*.

INTRODUCTION

Spermatogonial stem cells maintain spermatozoa production throughout male reproductive life by the testis-specific process of spermatogenesis (Clermont, 1972). Spermatogonial stem cells maintain spermatogenesis by their abilities to self-renew or differentiate into progenitor spermatogonia that are primed for development into spermatozoa (de Rooij, 2017). Donor spermatogonial stem cells isolated from rodent testes effectively regenerate spermatogenesis and restore fertility to male-sterile recipients (Brinster and Avarbock, 1994; Brinster and Zimmermann, 1994). Remarkably, stem spermatogonia retain their ability to clonally regenerate spermatogenesis *in vivo* following long-term culture *in vitro* (Nagano et al., 1998). Spermatogonial culture systems, therefore, hold largely untapped potential for studying genetically encoded mechanisms that govern spermatogenesis and to provide sources of haploid gametes that would advance a broad spectrum of reproduction applications (Kubota and Brinster, 2006).

Knowledge gaps persist on metabolic states that support distinct premeiotic, meiotic, and post-meiotic steps in spermatozoan development (Rato et al., 2012). Sperm-specific metabolic enzymes essential for hypermotility have been systematically investigated using knockout mice and found to drive ATP production via lower glycolytic reactions (Danshina et al., 2010; Miki et al., 2004; Odet et al., 2008). Spermatozoan glycolytic flux further depended on Gapdhs and Pgk2 fueling a glucose-sensing $Ldhc_4$ complex (Odet et al., 2011, 2013). Spermatogonial and spermatocyte metabolism has yet to be investigated as rigorously as spermatozoan metabolism. Recent reports on spermatogonia demonstrated Myc- and JNK-mediated glycolysis increase the frequency of stem spermatogonia self-renewal divisions (Kanatsu-Shinohara et al., 2016, 2019). Beneficial effects of glycolysis on spermatogonial stem cell maintenance over time in sub-culture (Helsel et al., 2017a) may signify existence of premeiotic metabolic processes that promote

[1]Division of Reproductive Endocrinology and Infertility, University of Texas Southwestern Medical Center, Dallas, TX 75390, USA

[2]Department of Obstetrics and Gynecology, University of Texas Southwestern Medical Center, Dallas, TX 75390, USA

[3]Cecil H. & Ida Green Center for Reproductive Biology Sciences, University of Texas Southwestern Medical Center, Dallas, TX 75390, USA

[4]McDermott Center for Human Growth and Development, University of Texas Southwestern Medical Center, Dallas, TX 75390, USA

[5]Department of Neuroscience, University of Texas Southwestern Medical Center, Dallas, TX 75390, USA

[6]Department of Biophysics, University of Texas Southwestern Medical Center, Dallas, TX 75390, USA

[7]Advanced Imaging Research Center, University of Texas Southwestern Medical Center, Dallas, TX 75390, USA

[8]Department of Bioinformatics, University of Texas Southwestern Medical Center, Dallas, TX 75390, USA

[9]Department of Population and Data Sciences, University of Texas Southwestern Medical Center, Dallas, TX 75390, USA

[10]GenomeDesigns Laboratory, LLC, 314 Stonebridge Drive, Richardson, TX 75080, USA

[11]These authors contributed equally

[12]Lead Contact

*Correspondence: kent.hamra@utsouthwestern.edu

https://doi.org/10.1016/j.isci.2020.101880

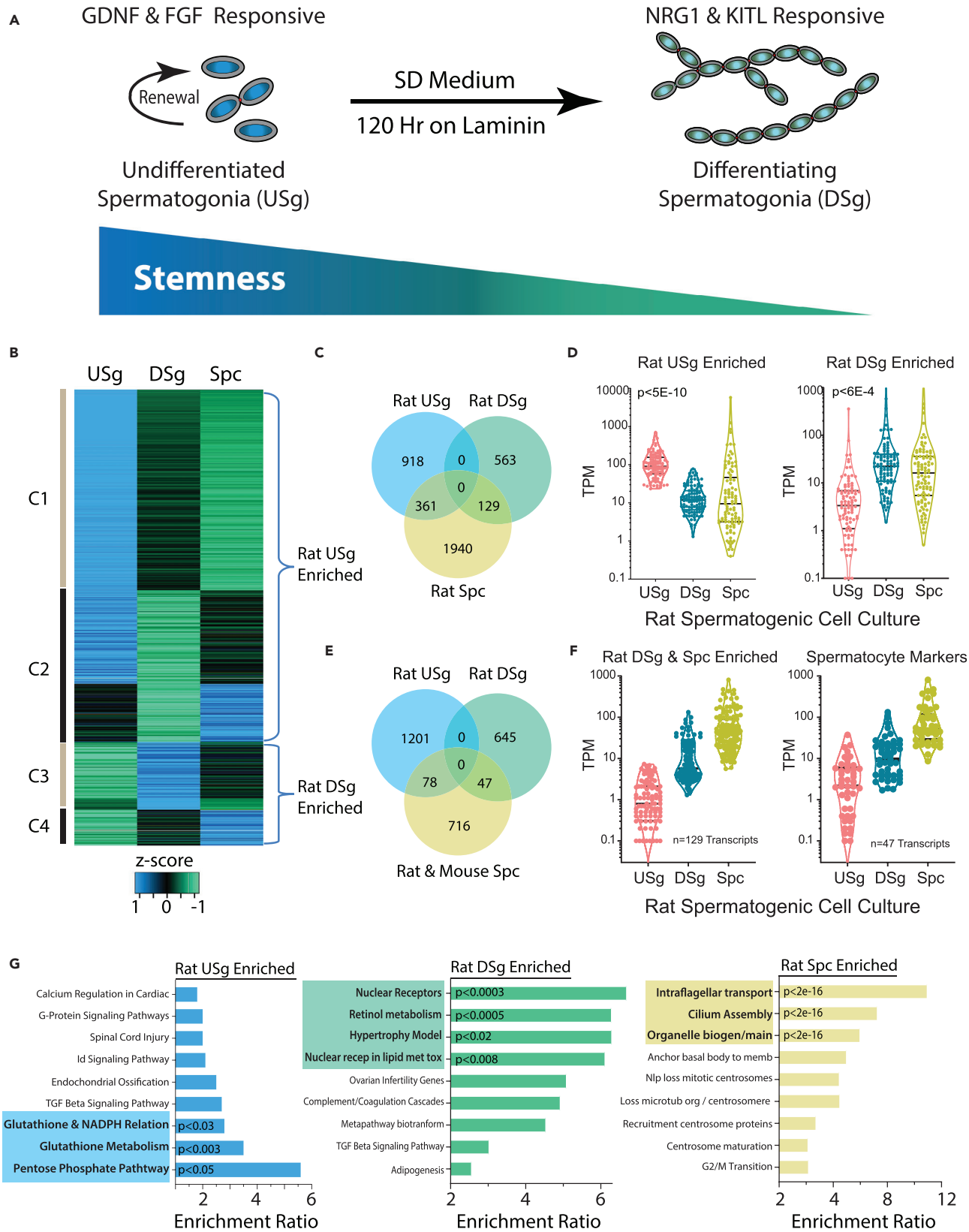
A
GDNF & FGF Responsive
Renewal
SD Medium
120 Hr on Laminin
NRG1 & KITL Responsive
Undifferentiated
Spermatogonia (USg)
Differentiating
Spermatogonia (DSg)
Stemness
B
USg DSg Spc
C1
C2
C3
C4
Rat USg
Enriched
Rat DSg
Enriched
z-score
1 0 -1
C
Rat USg Rat DSg
918 0 563
0
361 129
1940
Rat Spc
D
Rat USg Enriched
Rat DSg Enriched
p<5E-10
p<6E-4
TPM
USg DSg Spc
Rat Spermatogenic Cell Culture
E
Rat USg Rat DSg
1201 0 645
0
78 47
716
Rat & Mouse Spc
F
Rat DSg & Spc Enriched
Spermatocyte Markers
n=129 Transcripts
n=47 Transcripts
Rat Spermatogenic Cell Culture
G
Rat USg Enriched
Calcium Regulation in Cardiac
G-Protein Signaling Pathways
Spinal Cord Injury
Id Signaling Pathway
Endochondrial Ossification
TGF Beta Signaling Pathway
Glutathione & NADPH Relation p<0.03
Glutathione Metabolism p<0.003
Pentose Phosphate Pathtway p<0.05
Enrichment Ratio
Rat DSg Enriched
Nuclear Receptors p<0.0003
Retinol metabolism p<0.0005
Hypertrophy Model p<0.02
Nuclear recep in lipid met tox p<0.008
Ovarian Infertility Genes
Complement/Coagulation Cascades
Metapathway biotranform
TGF Beta Signaling Pathway
Adipogenesis
Enrichment Ratio
Rat Spc Enriched
Intraflagellar transport p<2e-16
Cilium Assembly p<2e-16
Organelle biogen/main p<2e-16
Anchor basal body to memb
Nlp loss mitotic centrosomes
Loss microtub org / centrosomere
Recruitment centrosome proteins
Centrosome maturation
G2/M Transition
Enrichment Ratio

Figure 1. RNA Profiling in Rat Stem and Differentiating Spermatogonia

(A) Soma-free *in vitro* culture system to study molecular and cellular mechanisms in rat undifferentiated spermatogonia (USg) derived and maintained in SG medium prior to inducing development into differentiating spermatogonia (DSg) by culture in SD Medium.

(B) Heatmap of 2-way hierarchal clustering using *Z* score for normalized values (Kendall's Tau distance measurement method). Differentially expressed gene clusters (C1, C2, C3, C4) in rat USg, DSg, and spermatocytes (Spc). Clusters C1 and C2 are enriched selectively in rat USg, whereas genes in Cluster C3 and C4 are selectively enriched in DSg.

(C) Intersection analyses on rat USg-enriched (n = 1279) versus rat DSg-enriched (n = 692) transcripts ($p < 0.02$, >2FC) with rat Spc-enriched (n = 2430) transcripts ($p < 0.02$, >2FC versus DSg).

(D) Rat spermatogenic cell gene profiles for transcripts selectively enriched in rat USg (left: $p < 5e\text{-}10$, n = 99) and gene profiles selectively enriched in rat DSg (right; $p < 0.0006$, n = 100). Transcripts per million kb (TPM).

(E) Intersection analyses on rat USg-enriched (n = 1279) and DSg-enriched (n = 692) transcripts ($p < 0.02$, >2FC) with conserved rat and mouse Spc-enriched transcripts (n = 841).

(F) Gene profiles for transcripts enriched in rat DSg and rat Spc (n = 129) (left) compared with transcripts enriched in rat DSg and the rat and mouse Spc marker transcripts (n = 47) (right).

(G) WebGenStalt.com Gene Ontology (GO) gene set enrichment ratios in rat USg- and DSg-enriched transcripts ($p < 0.02$, >2.8FC) and in rat Spc-enriched transcripts ($p < 0.02$, >4FC versus DSg). Shown: rat USg and DSg Wikipathway analyses, rat genome; rat Spc Reactome pathway analysis, human genome. Also see Figure S1 and Table S1.

the longer-term preservation and stability of replicating heritable DNA (Christodoulou et al., 2019; Milanese et al., 2019).

Rodent spermatogonial stem cell cultures provide *soma-free* platforms for dissecting biological processes in the germline that support spermatogenesis (Hamra, 2017). Undifferentiated spermatogonial lines endowed with germline stem cells are derived from rodent testes using culture media containing glial-cell-line-derived neurotrophic factor (Gdnf) and fibroblast growth factor 2 (Fgf2) (Kanatsu-Shinohara et al., 2003). Here, we exploited a rat culture system to annotate metabolic gene networks enriched in rat, mouse, monkey, and human spermatogonia. We found conserved (e.g. *Glutathione Biosynthetic Enzymes*) and species-dependent (e.g. *Forkhead Transcription Factors*) gene signatures enriched in rat undifferentiated spermatogonia.

Conserved spermatogonial gene profiles reported here are overrepresented by glutathione, NADPH, and pentose phosphate pathway gene sets that marked a 3.4-fold higher GSH:GSSG ratio in undifferentiated versus differentiating rat spermatogonia. We further report a dynamic metabolic shift during rat spermatogonial differentiation *in vitro* marked by reduced levels of the non-oxidative pentose phosphate pathway enzyme Transketolase (Tkt) and the accumulation of upper glycolytic/non-oxidative pentose phosphate pathway metabolites. Enrichment for glutathione and pentose phosphate pathway molecular markers across rat, mouse, monkey, and human premeiotic male germlines led us to identify an anti-ferroptotic pro-cysteine-like factor uptake pathway that stimulated clonal development of spermatogenic cells on laminin in synergy with the spermatogonial growth factor, Gdnf.

RESULTS

Gene Profiling in Rat Spermatogonia

To annotate rat spermatogonial gene expression profiles, we sequenced transcriptomes in rat spermatogonial lines before and after inducing their premeiotic differentiation in culture on laminin using spermatogonial differentiation medium (SD Medium) (Figure 1A, Table S1). Prior to inducing premeiotic differentiation with SD Medium, rat undifferentiated spermatogonial lines were derived and maintained on mouse embryonic fibroblasts (MEFs) using a culture medium containing GDNF and FGF2 (SG Medium) (Figures 1A and S1A). Rat undifferentiated spermatogonia (USg) cultured in SG Medium are enriched with spermatogonial stem cells (Wu et al., 2009). Unlike SG Medium, SD Medium contains all-trans retinoic acid and Neuregulin-1 and/or Kit ligand as essential growth factors for differentiating spermatogonia (DSg) *in vitro* (Chapman et al., 2015a; Hamra et al., 2007). Transcriptomes from rat spermatocyte cultures (Spc) (Hamra et al., 2002) were also sequenced to validate markers for spermatogonia entering meiosis *in vitro* (Table S1).

In silico analyses on the generated transcriptomes (USg versus DSg) revealed 4 major clusters (C1, C2, C3, C4) of differentially expressed genes (DEGs) (120 h) (Figure 1B). Genes modeling C1 were enriched in USg and progressively decreased in abundance from DSg to Spc (n = 918) (Figures 1C and 1D, and Table S1). Genes modeling C2 were transiently downregulated in DSg but upregulated with further differentiation (n = 361) (e.g. *Id1*, *Id2*, *Id3*, *Id4*, *Ctsh*, *Apoe*, *Cited2*, *Ier3*, *Phlda1*, *Rnc3*, *Penk*) (Figures 1C, 1D, and

S1B,and Table S1). In total, we identified 1,279 transcripts enriched in USg ($p < 0.02$, >2-fold) relative to DSg (Table S1). As notable examples, rat spermatogonial *Upk1b, Sgk1, Ctsh, Meox1, Foxa2, Hmha1, Gfra1, Fgfr3, Snap91, Ret, Dusp4,* and *Cited2* were 16.4 $\pm$ 1.9-fold ($\pm$SD) more abundant after culturing 120 h in SG Medium versus SD Medium (n = 12 transcripts, average TPM>200 in SD Medium, $p < 5e\text{-}10$, Table 1).

In contrast to USg gene profiles, we identified a total of 692 C3-like (n = 563) plus C4-like (n = 129) transcripts enriched in DSg compared with USg that increased in relative abundance during culture in SD Medium ($p < 0.02$, >2-fold) (Figures 1C and 1D, and Table S1). Spermatogonial *Cyp26a1, Mpped2, Kit, Erbb3, Lonrf3, Baz1a, Mob1b, Igfbp2, Ero1a, Tbx3, Hist1h1d,* and *Tgfbr1* were 6.5 $\pm$ 2.4-fold more abundant on average after culturing 120 h in SD Medium versus SG Medium (n = 12 transcripts, average TPM>45 in SD Medium, $p < 5 \times 10^{-5}$, Table 1). Changes in transcript abundance during culture in SD Medium were verified by qtPCR using *Zbtb16*, *Gfra1*, *Foxa2,* and *Snap91* as markers enriched in USg and *Stra8*, *Kit,* and *Erbb3* as markers enriched in DSg (Figure S1C).

Genes clustering such as C3 and C4 in DSg overlapped by 45% with genes downregulated in Stra8-deficient mouse preleptotene spermatocytes (Kojima et al., 2019) (n = 313 of 692; Figure S1D). More stringent filtering for transcripts marking the onset of meiosis in DSg cultures defined a gene set containing 841 conserved pachytene spermatocyte transcripts enriched in both rat and mouse Spc (Ball et al., 2016) (Table S1). The 841 conserved rat and mouse Spc transcripts uniquely overlapped with 6.1% (n = 78 of 1,279) and 6.7% (n = 47 of 692) of transcripts most enriched in USg and DSg, respectively (Figures 1E and 1F, and Table S1). The latter gene set (n = 47), marking meiotic entry by rat spermatogonia on laminin in SD Medium, included *Baz1a*, *Suco*, *Itgb3bp*, *Sephs2*, *Ngly1*, *Myo19*, *Gstt3*, *Nr2c1*, *Phf7*, and *Zfp949* (Figures 1E and 1F, and Table S1) and overlapped by 70% (n = 33 of 47) with Stra8-regulated genes in mouse preleptotene spermatocytes (Kojima et al., 2019) (Figures S1D and S1E), as reflected in the human testis transcriptome atlas (Guo et al., 2018).

Rat Undifferentiated Spermatogonia Are Enriched in Glutathione, NADPH and Pentose Phosphate Metabolism Transcripts

Gene ontology (GO) overrepresentation analyses were used to identify overlap between transcripts enriched in rat USg or DSg ($p < 0.02$, >2.8FC) (Table S1) and Wikipathway and Reactome pathway database gene sets (Table S2). Notably, transcripts enriched in rat USg were overrepresented by *Pentose Phosphate Pathway* (WP282, $p < 0.05$), *Glutathione Metabolism* (WP469, $p < 0.025$), and *Relationship between Glutathione and NADPH* (WP2562, $p < 0.003$) Wikipathway gene sets (Figure 1G and Table S2). In contrast to USg, transcripts enriched in rat DSg were overrepresented by *Nuclear Receptors* (WP217, $p < 0.0003$), *Retinol Metabolism* (WP1297, $p < 0.0005$), and *Nuclear Receptors in Lipid Metabolism and Toxicity* (WP139, $p < 0.001$) gene sets (Figure 1G and Table S2). USg undergoing spermatogenic differentiation in SD Medium containing RA (Figures 1F, S1D, and S1E) is consistent with RA-stimulated spermatogonial differentiation in rat testes (van Pelt and de Rooij, 1991).

The Rat Germline Is Endowed with Foxa-Family Proteins

Among genes that have yet to be rigorously studied in rat USg, *Foxa2* stood out as a gene effectively shut down by SD Medium (Table 1, Figure S1C) and displayed a gene signature that co-purified with spermatogonial stem cell activity in testis cell cultures (Hamra et al., 2004). Three Foxa-family genes encode for Forkhead Box DNA-binding domain transcription factors (Foxa1, Foxa2, Foxa3) (Lam et al., 2013) (Figure 2A) that regulate chromatin activity via their co-activation and linker histone domains and that are known for regulating somatic cell metabolic enzyme gene expression (Bochkis et al., 2008; Rausa et al., 2000; Wang et al., 2011; Wolfrum et al., 2004). *Foxa*-family genes are also critical for stem and progenitor cell fate determination in mesoderm, ectoderm, and endoderm (Monaghan et al., 1993; Weinstein et al., 1994).

To investigate *Foxa*-family genes in the rat germline in more detail, we conducted protein detection studies using antibodies as depicted in Figure 2A. Foxa2 labeling using monoclonal antibody (MAb) D56D6 was detected in nuclei of $Gfra1^+$ rat spermatogonial lines maintained in SG Medium on MEFs (Figures 2B and S2A) or laminin (Figures 2C and S2B). Although Foxa2 was abundant in type A spermatogonia maintained in SG Medium, in SD Medium, spermatogonial Foxa2 decreased in relative abundance over a 120-h culture period on either laminin or MEFs (Figures 2C and S2B). Immunoblot analysis revealed Foxa2 was downregulated by 72 h after culture in SD Medium, most like the type A spermatogonial marker Zbtb16 (Figure 2D). Like Foxa2, Foxa3 was detected by western blot in rat USg (Figure 2D). In contrast to Foxa2,

RNAs Enriched in Rat USg versus DSg					RNAs Enriched in Rat DSg versus USg				
Protein Coding Gene	Mean TPM			Species	Protein Coding Gene	Mean TPM			Species
	USg	DSg	Spc			USg	DSg	Spc	
Upk1b	202	4	3	R	*Cyp26a1*	1	131	2	R
Sgk1	184	9	65	R	*Kcnd2*	1	29	4	R
Ctsh	704	45	127	R M	*Nphs1*	1	23	2	R
Meox1	108	5	1	R	*Mpped2*	5	87	11	R
Foxa2	107	4	4	R M[a]	*Kit*	39	363	36	R M H[c]
Hmha1	169	9	7	R M	*Polq*	3	25	25	R
Hoxc4	83	6	3	R	*Ctgf*	3	25	46	R
Apoe	572	24	840	R M	*Kirrel2*	1	19	1	R
Irx2	59	3	4	R H	*Erbb3*	6	47	5	R H
Gfra2	83	7	2	R M	*Lonrf3*	38	257	43	R M
Lhx1	72	2	2	R M	*Elovl2*	2	15	37	R
Spry4	130	16	40	R M	*Foxn4*	3	26	2	R M
Fgfr3	225	29	5	R H	*Baz1a*	21	132	293	R M H
Tcl1a	183	18	<1	R H[b]	*Mob1b*	21	134	69	R
Adgrg1	91	9	66	R M	*Nrcam*	1	8	6	R M
Lbp	104	9	3	R	*Slc35c1*	3	25	25	R
Noto	148	5	2	R	*Cyp26b1*	5	36	8	R
Cited2	119	14	416	R M H	*Rarb*	2	33	2	R
Frzb	58	2	1	R M	*Ngfr*	1	11	10	R
Cldn4	117	10	5	R	*Igfbp2*	77	582	58	R M H[c]
Snap91	118	15	3	R M	*Trove2*	7	40	32	R H
Dusp4	156	12	18	R M H	*Fmo2*	<1	7	5	R
Ier3	138	19	939	R M	*Nr0b1*	<1	6	3	R
Tnfsf12	81	5	12	R M	*Ankrd34b*	6	35	3	R
Gfra1	102	15	2	R M H	*Dynlt3*	3	22	27	R
Phlda1	64	9	92	R M	*Dclre1c*	7	42	13	R
Mest	150	22	5	R H[b]	*Ero1a*	31	163	47	R
Enc1	227	38	36	R	*Tfcp2l1*	2	11	10	R
Rcn3	107	10	91	R M	*Kiaa0513*	4	22	14	R
Rnf125	63	7	12	R	*Tc2n*	6	42	36	R M H
Igsf21	127	11	1	R M	*Stra6*	1	10	4	R
Ret	212	39	7	R M	*Cpne7*	2	18	2	R, H[c]
Gpx2	108	8	7	R	*Mmd2*	1	7	24	R

Table 1. Rat Spermatogonial Gene Expression during Culture in SG versus SD MEDIUM

(Continued on next page)

RNAs Enriched in Rat USg versus DSg					RNAs Enriched in Rat DSg versus USg				
Protein Coding Gene	Mean TPM			Species	Protein Coding Gene	Mean TPM			Species
	USg	DSg	Spc			USg	DSg	Spc	
T	36	3	3	R M	*Tbx3*	15	86	22	R
Fblim1	77	10	14	R M	*Zfp763*	2	11	3	R M
Egr3	85	4	42	R M	*Hist1h1d*	357	1726	1227	R
Penk	441	14	1094	R M	*Tgfbr1*	12	65	50	R
Tfap2c	83	7	1	R	*Ncoa1*	14	62	51	R M

Table 1. Continued

Transcripts per Million Kb (Mean TPM values, Table S1) from rat undifferentiated spermatogonia (USg), differentiating spermatogonia (DSg), and spermatocyte (Spc) cultures (n = 2 rats/cell population). Left: R = Rat, enriched >7-fold in USg versus DSg, P < 5e-10; M = Mouse, enriched >2-fold in GFP-ID4 Bright versus GFP-ID4 Dim spermatogonia, p < 0.02.

[a]FPKM <1 in Mouse GFP-ID4 Bright spermatogonia (Helsel et al., 2017b); H=Human, enriched in spermatogonial transition gene clusters 1 > 2 up[b] or 1 > 2 down (Guo et al., 2018). Right: R = Rat, enriched >3-fold in DSg versus USg, $P < 5 \times 10^{-5}$; M = Mouse, enriched >2-fold in GFP-ID4 Dim versus GFP-ID4 Bright spermatogonia, p < 0.02; H=Human, enriched in spermatogonial transition gene clusters 2 > 3 up or 2 > 3 down[c].

spermatogonial Foxa3 did not decrease appreciably after culturing for 72 h in SD Medium (Figure 2D), and Foxa1 was not clearly detected over the 72-h culture period (Figure 2D). The germline marker, DAZL, was detected at similar levels at each time point and combined with Zbtb16, demonstrated the SD-Medium-stimulated downregulation of Foxa2 in type A spermatogonia (Figure 2D).

Foxa2 and Foxa1 selectively mark rat A_s and primed A_{al} spermatogonia subtypes

In adult rats, spermatogonial stem cells reside within a population of "A-isolated" (A_{is}) spermatogonia (Huckins, 1971b, 1971c, 1971d). More commonly, A_{is} spermatogonia are referred to as "A-single" (A_s) spermatogonia across species (Lok et al., 1983; Oakberg, 1971). A_s spermatogonia divide to renew germline stem cells but can also produce syncytia of spermatozoon progenitors termed A-paired (A_{pr}) and A-aligned (A_{al}) spermatogonia (Huckins, 1971c). To determine if Foxa-family proteins were expressed in A_s, A_{pr}, and/or A_{al} spermatogonial subpopulations, immunolocalization studies were conducted in rat seminiferous tubule whole mounts. An antibody raised the carboxy terminal domain of human Foxa1 (MAb 1519; Figure 2A) selectively labeled 8, 16, and 32-cell Gfra1$^+$, Rarg$^+$, Foxa2$^-$ spermatogonial syncytia in rats (Figures 2E and S3A–S3C). Foxa1 and Foxa2 were clearly detected in distinct populations of Gfra1$^+$ spermatogonia (Figure S3A). Only 0.2% of total A_s and A_{pr} and A_{al}-like spermatogonia scored were both Foxa1$^+$ and Foxa2$^+$, as represented by 2 double-positive A_{pr}-like spermatogonial clones identified in 1 of 174 tubular subsegments (0.5 mm/subsegment, ~9 cm total tubule length scored, 1,997 total immunopositive nuclei scored) or 1 of 38 tubular subsegments containing longer Foxa1$^+$, Foxa2$^-$ syncytia among distinct Foxa2$^+$, Foxa1$^-$ A_s, and A_{pr} spermatogonia (Figures S3A and S3B).

In contrast to Foxa1 MAb 1519's labeling profile in Gfra1$^+$ A_{al} USg (Figures 2E, S3A, and S3B), in adult rats the Foxa2 Mab D56D6 (Figure 2A) selectively labeled Gfra1$^+$ and Zbtb16$^+$ A_s and A_{pr} spermatogonia (Figures 2F, S3A, S3B, S4A, and S4B) and displayed progressively less intense labeling in cohorts of longer Zbtb16$^+$ and Gfra1$^+$ A_{al} spermatogonia (Figures 2F, S4A, and S4B). Distinct Foxa3$^+$ testicular cells were not observed in rat seminiferous tubule whole mounts or in rat USg cultures by immunofluorescence labeling, potentially due to the R32147 Foxa3 antibody being better suited for western blot assays (Figure 2A).

Interestingly, two additional MAbs generated to respective amino-terminal (2F83) and carboxy-terminal (JF10-02) domains of human FOXA1, respectively, displayed a labeling profile in seminiferous tubule whole mounts that overlapped with the combined labeling profiles obtained using Foxa1 MAb F1519 plus Foxa2 MAb F56D6 by clearly labeling all A_s, A_{pr}, and A_{al}-like Gfra1$^+$ spermatogonia (Figure S5A). In contrast, Foxa1 Mabs JF10-02 and 2F83 and Foxa2 MAb D56D6 did not label spermatogonia in adult mouse seminiferous tubules (Figure S5B). All three MAbs (JF10-02, 2F83, D56D6) selectively labeled rat hepatocytes; however, only Foxa1 Mab JF10-02 and Foxa2 MAb D56D6 labeled mouse hepatocytes (Figure S5C). Co-labeling with Foxa2 MAb 56D6 and Foxa1 MAb JF10-02 again revealed that the longer $A_{al\text{-}4}$ to $A_{al\text{-}32}$ Foxa1$^+$ spermatogonial syncytia in rat testes were Foxa2$^-$ (arrows; Figure S5A). Thus, Foxa1 MAbs 2F83

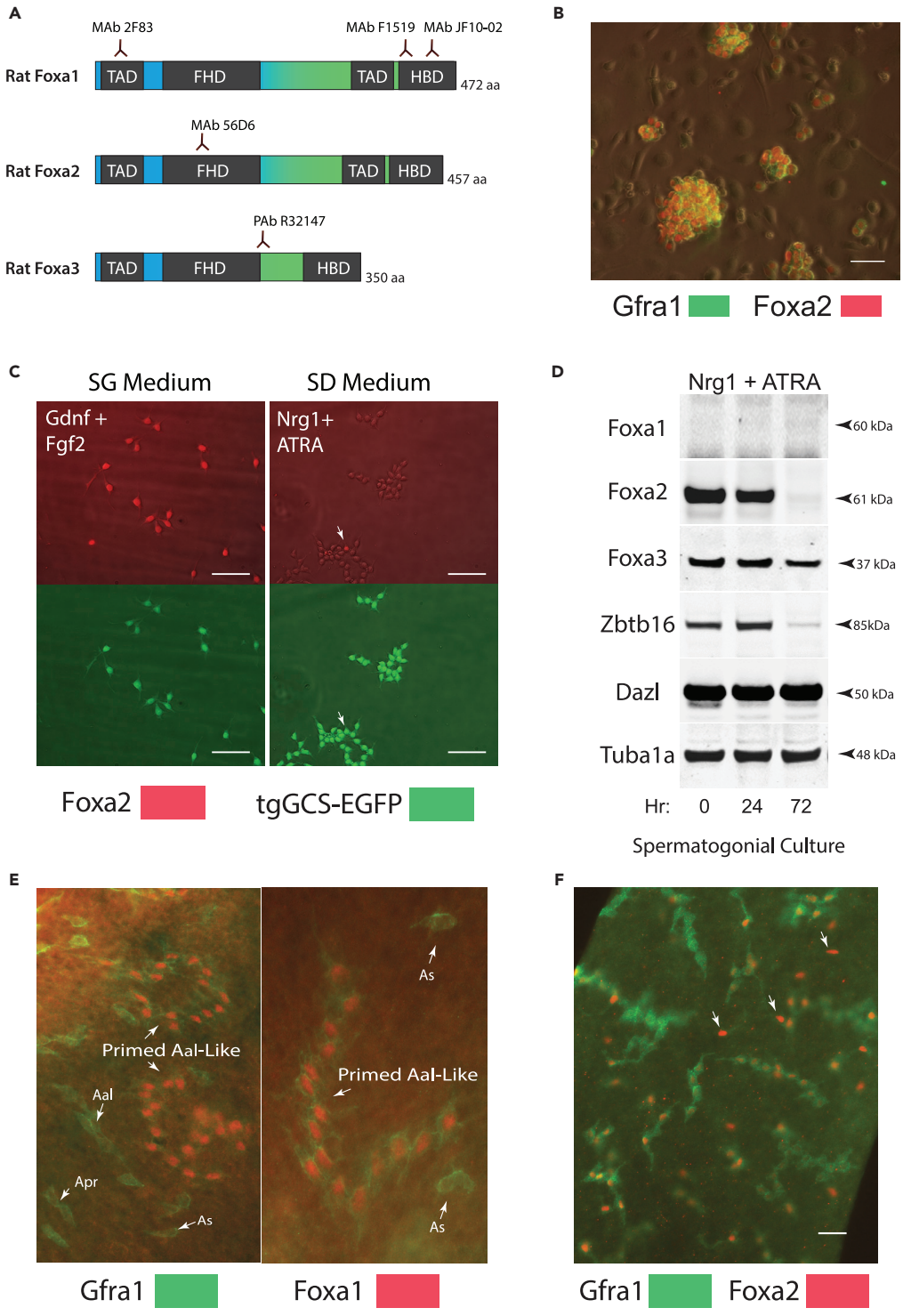

Figure 2. Rat Spermatogonial Stem Cell Lines Express Foxa2 and Foxa3

(A) Foxa family proteins encoded by rat *Foxa1*, *Foxa2*, and *Foxa3*. TAD, transcriptional co-activation domain. FAD, Forkhead box domain binds to DNA. Carboxy terminal winged helix histone binding domains (HBD) are related to linker histones. Monoclonal antibodies (MAb) raised to distinct Foxa1, Foxa2, and Foxa3 domains.

(B) Gfra1 and Foxa2 co-labeling in Brown Norway rat (BN) spermatogonial cultures on MEFs at passage 14. Scale: 40 μm.

(C) Foxa2 is abundant in tgGCS-EGFP^{+} Sprague-Dawley rat spermatogonial stem cells (passage 12) after culturing in SG Medium (Gdnf + Fgf2) and is effectively downregulated in rat spermatogonia after culturing in SD Medium (ATRA + Nrg1)

Figure 2. *Continued*
on laminin for 120 h. Top panels, Foxa2 MAb D56D6 (Red). Bottom panels, tgGCS-EGFP germline marker (Green). Arrow points to single germ cell that retained higher nuclear Foxa2 after culture in SD Medium. Scale: 60 μm
(D) Western blot on Foxa-family proteins in spermatogonial stem cell lines cultured on laminin at respective times after moving from SG (0 h) to SD Medium (24 h, 72 h). Dazl, germ cell marker loading control. Zbtb16 and Dazl combination marks rat type A spermatogonia. Tuba1a, loading control.
(E) Co-labeling for Foxa1 and Gfra1 in adult rat (d120) seminiferous tubule whole mount. Foxa1 was detected selectively in longer chains of Gfra1$^+$ A_{al}-like spermatogonia typically consisting of 8–32 labeled nuclei (Huckins, 1971c).
(F) Co-labeling for Foxa2 and Gfra1 in a rat seminiferous tubule whole mount (D120). Arrows point to Foxa2$^+$ A_s spermatogonia with relatively low Gfra1 labeling compared with longer Gfra1$^+$ A_{al} spermatogonia. Scale: 40 μm
Also see Figure S2.

and JF10-02 either recognized a distinct form(s) of rat Foxa1 in A_s and A_{pr} USg than in A_{al} USg or, quite possibly, the Foxa1 MAbs 2F83 and JF10-02 cross-reacted with Foxa2 and/or other Foxa2-like transcription factors in the rat germline (Table S1).

Next, we investigated Foxa2 localization in rat testes during early postnatal development. Rat spermatogonial stem cells develop from prospermatogonia that migrate from the center of seminiferous cords and colonize the basal compartment of the seminiferous epithelium on postnatal d4-7 (Hilscher et al., 1974). Foxa2$^+$ or GFRa1$^+$ prospermatogonia (Dazl$^+$) were not detected by postnatal d2 to d4 (Figure 3A). Between postnatal d4 and d16, however, Foxa2$^+$ germ cells progressively increased within the Gfra1$^+$ population (Figure 3A). Therefore, Foxa2 was induced in the rat germline concomitantly with a Gfra1$^+$ sub-population of undifferentiated spermatogonia (Figures 3A, S6A, and S6B) shortly after T2 prospermatogonia start their migration to colonize the basal lamina in developing seminiferous tubules (Hilscher et al., 1974).

In adult rats, Foxa2 was abundant in undifferentiated type A_s and A_{pr} spermatogonia as demonstrated by co-labeling with antibodies to Zbtb16, Gfra1, Cd9, and Snap91 (Figures 3B, S4A, and S4B). Populations of Cd9$^+$/Foxa2$^+$, Snap91$^+$/Foxa2$^+$, and Gfra1$^+$/Foxa2$^+$ undifferentiated A_s spermatogonia were identified by co-labeling with respective cytoplasmic and cell surface markers (Cd9, Snap91, Gfra1). Based on graded Gfra1 labeling within the undifferentiated A_s population (Figures 3B, 3C, and S6C), categories of Foxa2$^+$ spermatogonia were scored that exhibited relatively high, to low, to background levels of Gfra1 labeling (Figure 3D). Approximately 17% Foxa2$^+$ A_s spermatogonia demonstrated Gfra1 labeling at background levels (i.e. Gfra1$^-$) (Figures 3D and S6C). Longer Gfra1$^+$/Foxa2$^-$ syncytia containing 8 to 32 spermatogonia were commonly observed throughout rat seminiferous tubules and presumably developed from A_s spermatogonia one or more seminiferous epithelial cycles earlier (12.9 days/rat cycle) (Leblond and Clermont, 1952) (Figures 3E and S4B). Nuclear Foxa2 was also enriched in the stage VIII-IX-dependent Erbb3$^+$, Snap91$^+$, Zbtb16$^+$, Sall4$^+$, Gfra1$^+$ undifferentiated A_s spermatogonia population (Figures S6D and S6E) (Abid et al., 2014).

Analyses on seminiferous tubule cross-sections in adult rats similarly identified populations of Foxa2$^+$/Gfra1$^-$, Foxa2$^+$/Gfra1$^+$, and Foxa2$^-$/Gfra1$^+$ spermatogonia in each respective stage I-XIV comprising a rat spermatogenic wave (Figure 3E). Based on an "A_s spermatogonium-specific" labeling profile in seminiferous tubule whole mounts, Foxa2$^+$/Gfra1$^-$ A_s spermatogonia were detected during all stages of the seminiferous epithelial cycle and most commonly during epithelial stages XIV-II, V-IV, and XI-XII (Figure 3E). Foxa-family labeling profiles in rat seminiferous tubules build a model in which undifferentiated Gfra1$^-$ and Gfra1$^+$ A_s spermatogonial sub-types ultimately develop into syncytia of Foxa1$^+$, Foxa2$^-$, Rarg$^+$, Gfra1$^+$ type A_{al} spermatogonia that, based on studies in mice (Gely-Pernot et al., 2012; Ikami et al., 2015), are developmentally primed for transformation into Gfra1$^-$ type A1 differentiating spermatogonia (Figure 3F).

Spermatogonial *Foxa* Gene Family Profiles in Rat, Mouse, and Human

In preliminary analyses, Foxa1$^+$ and Foxa2$^+$ mouse spermatogonia were not identified by antibody labeling in seminiferous tubule whole mounts (Figure S5B). In additional experiments aimed at determining if *Foxa*-family expression profiles where conserved across species, we compared our rat spermatogonial line gene lists (Table S1) with published mouse and human spermatogonial gene lists (Table S3). Although *Foxa*-family transcripts were detected at relatively low levels in mouse spermatogonia (i.e. <1.0 FPKM) (Helsel et al., 2017b), *Foxa2* was in fact significantly ($p = 0.01$) more abundant (~3-fold) in USg (Id4-GFP^{Bright} = 0.78 FPKM) relative to DSg (Id4-GFP^{Dim} = 0.27 FPKM) (Helsel et al., 2017b).

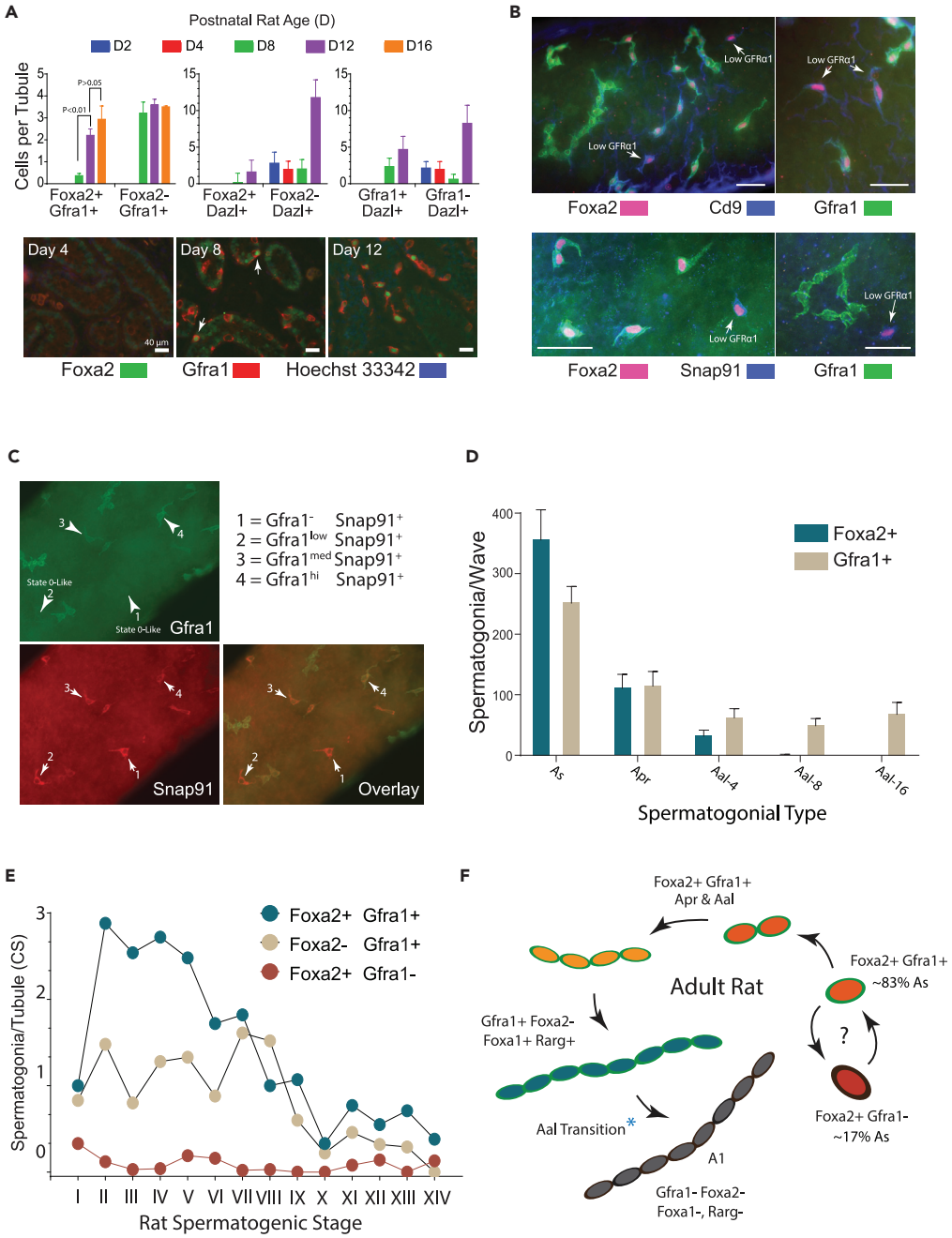

Figure 3. Foxa1 and Foxa2 Selectively Detect Spermatogonial Types in Rat Testes

(A) *Top*: relative abundance of Foxa2$^+$ and/or Gfra1$^+$ spermatogonia/seminiferous tubule cross-section in rats at postnatal days 2, 4, 8, 12, and 16 (mean, ±S.E.M, n = 3 rats, 50–60 tubules scored/rat; p values, one-way Anova). *Bottom*: immunolabeling in rat seminiferous cords/tubules scored in "top" panel. Foxa2$^+$, Gfra1$^+$ testis cells were first detected d8 (arrows). Scale: 30µm.

(B) Foxa2$^+$ A_s spermatogonial subtypes identified in rat. (*Top*) Co-labeling for Foxa2, Gfra1, and Cd9 revealed A_s spermatogonia with relatively high and low Gfra1 labeling intensities. Scale: 30µm. (*Bottom*) Co-labeling for Foxa2, Gfra1, and Snap91 revealed A_s spermatogonia with relatively high and low GFRa1 labeling intensities. Note: typical perinuclear cytoplasmic Snap91 localization. Scale: 30µm.

(C) Gradient of Gfra1 labeling in rat Snap91$^+$ A_s spermatogonia in tubule whole mount.

(D) Relative numbers of rat Gfra1$^+$ and Foxa2$^+$ A_s, A_{pr}, A_{al} spermatogonia/spermatogenic wave (mean counts ±SEM, 25–50, 0.5 to 2.0 mm tubule fragments/rat, n = 3 rats). Average spermatogenic wavelength in adult Sprague-Dawley rats = 2.6 cm (Perey et al., 1961).

Figure 3. *Continued*

(E) Relative numbers of Foxa2$^+$ and/or Gfra1$^+$ spermatogonia/seminiferous tubule cross-section (CS) per spermatogenic stage (mean counts, 110–120 tubule CS/rat, n = 3 rats).

(F) Summary of Foxa1 and Foxa2 antibody labeling profiles during steps in the development of Sprague-Dawley rat type A_s spermatogonia into syncytia of differentiating type A1 spermatogonia drawn from observations made in seminiferous tubule whole mounts and sections in the current study, and founded on the rat USg models proposed by Huckins (Huckins, 1971b, 1971c). Cytoplasmic Gfra1$^+$ (Green) marks A_s, A_{pr}, and A_{al} USg. Foxa2 nuclear labeling (red nucleus) is most intense in A_s and A_{pr} USg (Gfra1$^+$, Cd9$^+$, Snap91$^+$ or Gfra1$^-$, Cd9$^+$, Snap91$^+$) and then declines in intensity in Gfra1$^+$ A_{al} spermatogonia (orange nucleus). Foxa1 is selectively detected in 8-, 16-, and 32-cell Gfra1$^+$, Rarg$^+$, and Foxa2$^-$ spermatogonial syncytia (blue nucleus) prior to differentiating into Foxa1$^-$, Foxa2$^-$, and Gfra1$^-$ type A1 spermatogonia (gray nucleus). *In mice Rarg$^+$ A_{al} USg are primed for differentiation into type A1 spermatogonia. The developmental hierarchy of Gfra1$^+$ and Gfra1$^-$ undifferentiated type A_s spermatogonia remains to be defined (?).

Also see Figures S3-S6.

Similar to mouse, gene expression profiles generated by scRNA sequencing revealed that *Foxa*-family genes were also not selectively enriched in distinct monkey and human spermatogenic cell populations (Guo et al., 2018; Shami et al., 2020) when compared with rat spermatogonia (Tables S1 and S3). Clear immunolabeling profiles in human testis sections were not observed for FOXA1 and FOXA2; however, FOXA3 demonstrated moderate labeling in human spermatogonia, spermatocytes, and Leydig cells [Human Protein Atlas; (Pontén et al., 2008)]. Thus, authenticating species-dependent Foxa-family expression and potential genetic effects in the male germline will require more detailed analyses. However, when compared with mouse, human, and monkey spermatogonia (Guo et al., 2018; Helsel et al., 2017b; Shami et al., 2020), rat spermatogonia appeared to be selectively endowed with Foxa-family transcription factors and most conspicuously, Foxa1 and Foxa2 (Figures 2 and 3, and Tables S1 and S3).

Spermatogonial Gene Profiles Conserved in Rat, Mouse, and Human

Phenotypic novelty in the rat germline, marked by higher relative levels of Foxa-family gene products than observed in mouse, monkey, and human male germlines (Guo et al., 2018; Shami et al., 2020) (Tables 1 and S1), prompted questions regarding the make-up of conserved gene systems in spermatogonia functionally linked to *Foxa2*. To identify candidate conserved spermatogonial gene systems regulated by *Foxa2*, we conducted gene set enrichment analyses (WebGestalt.org) comparing our annotated rat spermatogonial line gene lists (Table S1) across differentially expressed human spermatogenic cell states reported by (Guo et al., 2018). Accordingly, rat USg shared the greatest percentage of enriched genes with human spermatogonial gene sets "1->2 down" and "2->3 down" (Figure 4A) that decreased in relative abundance during human spermatogonial differentiation (Guo et al., 2018) and that best modeled gene profiles enriched in rat undifferentiated spermatogonia prior to loss of germline stem cell activity during differentiation in culture (Hamra et al., 2004).

In contrast to rat USg, gene sets in DSg and Spc displayed the greatest overlap with human gene sets 1->2 up, 2->3 up, 3->4 up, and 4->5 up (Figure 4A). Spermatogenic cell gene sets 2->3 up, 3->4 up, and 4->5 up are predicted to be enriched with transcripts that increase in relative abundance during human spermatogenic cell differentiation (Guo et al., 2018). Transcripts identified as being enriched in both rat USg ($\geq$2-fold versus DSg, $p \leq 0.02$) (Table S1) and human spermatogonial gene sets 1->2 down and 2->3 down (Guo et al., 2018) provided a list of 122 conserved USg transcripts (Table S3) for comparative analyses with transcripts enriched in mouse USg ($\geq$2 fold-enriched Id4-GFP^{Bright} versus Id4-GFP^{Dim}, $p \leq 0.02$) (Helsel et al., 2017b).

Filtering for conserved gene profiles across rat, mouse, and human USg by intersection analyses detected 33 commonly enriched genes (Figures 4B and Table S3) that included established spermatogonial stemness markers (e.g. *Nanos2*, *Id4*, *Gfra1*, *Etv5*). Transcripts encoding *Dusp4*, *Cited2*, and *Gfra1* were among the most significantly enriched transcripts in rat USg ($p < 5 \times 10^{-11}$, Table 1) that were also enriched in mouse and human USg (Table S3). Notably, ~60% of the commonly enriched USg transcripts (n = 20 of 33) were more abundant in rat Spc versus rat DSg (Figure 4C), including *Cited2*, *Pqlc1*, *Serping1*, *Tkt*, *Optn*, *Axna5*, *Hspb1*, *Atp1b1*, *Dpysl2*, *Id4*, *Nfkbia*, *Gpx1*, *Scarb2*, and *Tjp* (Figure 4D). Conversely, ~40% of commonly enriched transcripts (13 of 33) were more abundant in rat DSg versus rat Spc (Figure 4C), including *Dusp4*, *Gfra1*, *Dusp6*, *Etv5*, *Nanos2*, *Ypel2*, *Bnc2*, *Fam43a*, *Rest*, *Pip4k2a*, *Farp1*, *Mgat4a*, and *Tmem55a* (Figure 4D). Thus, transcripts enriched across rat, mouse, and human USg formed two distinct gene clusters (Figure 4C) derived from rat gene clusters C1 and C2 (Table S1).

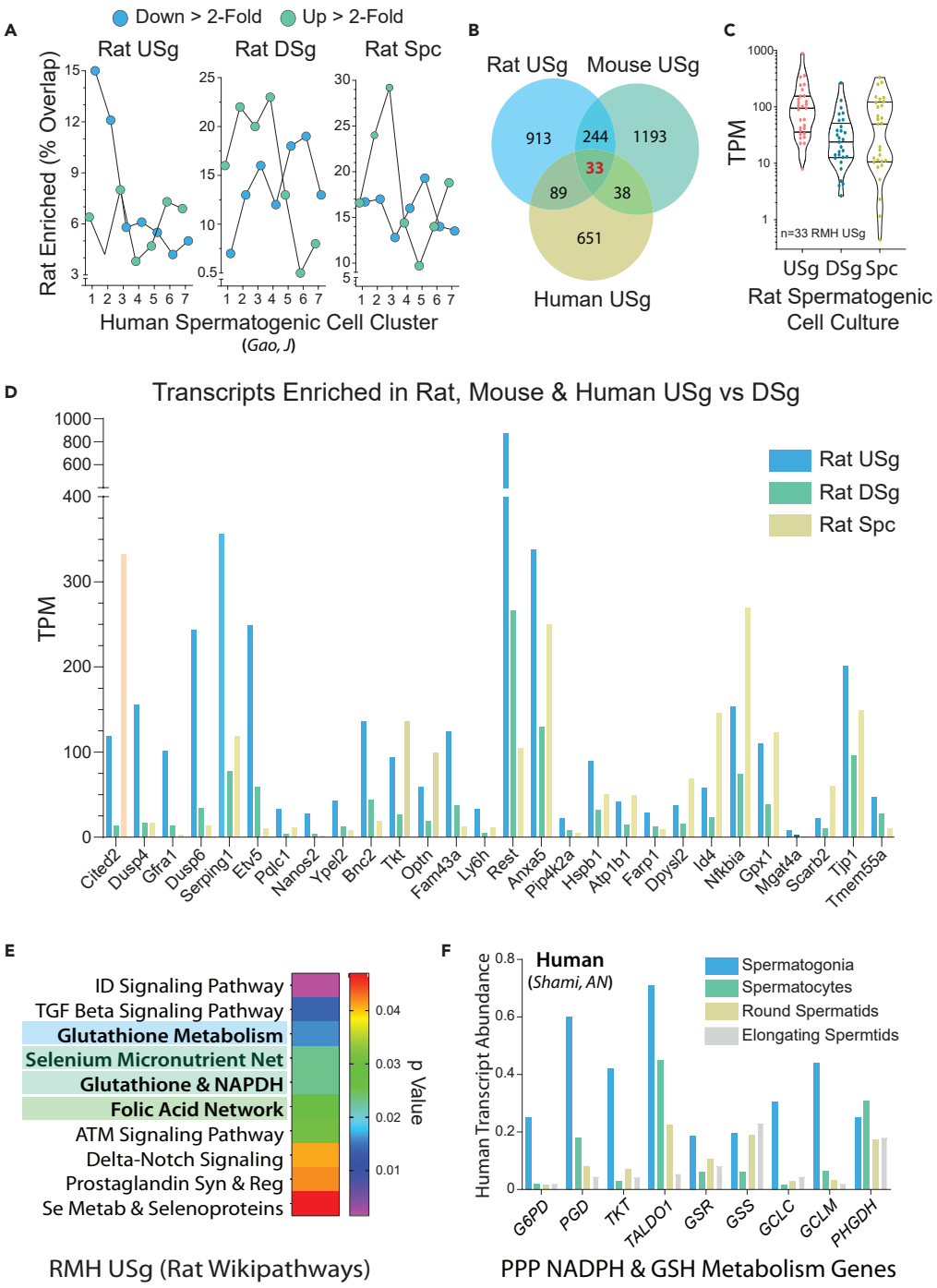

Figure 4. Rat, Mouse, and Human Spermatogonial Stemness Genes

(A) Overlap shared by rat USg-enriched, DSg-enriched, and Spc-enriched transcripts and human spermatogenic-cell-enriched gene clusters 1–7 reported in the *Testis Transcriptional Cell Atlas* (Guo et al., 2018).

(B) Intersectional analyses on gene sets enriched in rat, mouse, and human USg. Rat USg-enriched transcripts (n = 1279, $p < 0.02$, >2FC versus DSg); mouse USg-enriched transcripts (n = 1508, $p < 0.02$, >2FC GFP-ID4^{Bright} versus GFP-ID4^{Dim}); human USg-enriched transcripts (n = 811, gene sets: 1->2 Down and 2->3 Down) (Guo et al., 2018).

(C) Violin plot of conserved USg-enriched transcripts across rat USg, DSg, and Spc cultures reveals two distinct clusters.

(D) Expression profiles for transcripts composing the conserved USg-enriched gene set in rat USg, DSg, and Spc (n = 33 from panel "B").

Figure 4. *Continued*

(E) GO Wikipathway gene set enrichment analysis of USg-enriched transcripts conserved across rat, mouse, human (n = 33), plus USg-enriched transcripts conserved across rat and human (n = 89), plus USg-enriched transcripts conserved across mouse and human (n = 38) (see Venn diagram in panel "B").

(F) Relative abundance of human spermatogenic cell transcripts encoding pentose phosphate, NADPH, and glutathione metabolism enzymes. Ordinate represents relative transcript centroid values reported by (Shami et al., 2020).

Also see Figure S7, Table S2 and S3.

Ontology Gene Sets Conserved across Rat, Mouse, Monkey and Human Spermatogonia

To identify conserved gene systems in spermatogonia, we conducted Gene Ontology (GO) overrepresentation analyses (WebGestalt.org) by comparing transcripts enriched in rat, mouse, and human USg and DSg with gene sets in Wikipathway and Reactome pathway databases (Figure 4E and Table S2). Transcripts enriched in rat, mouse, and human USg (n = 33), together with transcripts enriched in rat and human USg (n = 89) and those enriched in mouse and human USg (n = 38) were pooled to generate a master conserved USg gene set (n = 160; Figure 4B) that was used for GO analyses.

Focusing on the protein-coding genes with annotated gene symbols across species (n = 135 of 160; Table S2), transcripts enriched across rat, mouse, and human USg were overrepresented by *Glutathione Metabolism* (WP469: *Gpx1, Gpx4*; $p = 1.6 \times 10^{-2}$), *Selenium Micronutrient Network* (WP1310:*Gpx1, Gpx4*; $p = 2.3 \times 10^{-2}$), and *Relationship between Glutathione and NADPH* (WP2562:*Tkt, Fth1, Gpx4*; $p = 2.3 \times 10^{-2}$) gene sets (Figure 4E and Table S2). Conserved USg transcripts were also overrepresented by *Id Signaling* (WP397:*Id4, Id1, Id2, Tcf3*; $p = 1.5 \times 10^{-3}$), *RAF-Independent MAPK1/3 Activation* (R-MMU-112409, $p = 8.3 \times 10^{-6}$), *Negative Regulation of MAPK Pathway* (R-MMU-112409, $p = 7.2 \times 10^{-5}$), and *MAPK Family Signaling Cascade* (R-MMU-5683057, $p = 1.6 \times 10^{-4}$) gene sets. The Mapk signaling gene sets were represented by *Gfra1, Fgfr3, Dusp4, Dusp5, Dusp6, Hspb1, Uba52, and Jak1* (Table S2).

By a similar approach, a set of 133 protein-coding transcripts enriched in rat, mouse, and human DSg (Table S2) were found to be overrepresented by *Nuclear Receptors* (WP217, $p = 2.7 \times 10^{-4}$), *Retinol Metabolism* (WP1297, $p = 4.2 \times 10^{-4}$), *Complement and Coagulation Cascades* (WP547, $p = 3.3 \times 10^{-3}$), *Adipogenesis* (WP155, $p = 4.2 \times 10^{-3}$), and *Nuclear Receptors in Lipid Metabolism and Toxicity* (WP139, $p = 7.1 \times 10^{-3}$) gene sets (Table S2), signifying SD Medium both stimulated and supported premeiotic spermatogenic differentiation (Figure 1F). Conserved Spc transcripts were enriched with gene sets that regulate spermatogenic cell metabolism and development, including *Hexose Metabolism in Proximal Tubules* (WP3916, $p < 2 \times 10^{-6}$), *Cilium Assembly* (R-MMU-5617833, $p < 5 \times 10^{-16}$), and *Intraflagellar Transport* (R-MMU-5620924, $p < 5 \times 10^{-16}$) (Table S2).

Enrichment for spermatogonial glutathione metabolism and pentose phosphate pathway gene sets across rat, mouse, and human USg (Figure 4E) are further supported by additional comparative analyses that we conducted using the recently reported primate single cell transcript centroid values in spermatogonia, spermatocytes, round spermatids, and elongating spermatids (Shami et al., 2020) (Figures 4F and S7). Like rat USg (Figure 1G and Table S2), human and monkey spermatogonia were selectively enriched with transcripts encoding non-oxidative (*TKT*, *TALD O 1*) and oxidative (*G6PD*, *PGD*) pentose phosphate pathway enzymes, glutathione biosynthesis pathway enzymes (*GSS*, *GCLC*, *GCLM*), and glutathione-dependent redox pathway enzymes (*GSR*, *GPX1*, *GPX4*, *SOD1*) when compared with spermatocytes (Figures 4F and S7).

Foxa2-bound loci are enriched with spermatogonial stemness genes in the rat germline

Due to the robust regenerative potential of rat spermatogonial stem cells (Hamra et al., 2002; Ogawa et al., 1999; Orwig et al., 2002; Wu et al., 2009), we hypothesized Foxa2 functioned as a genetic modifier in the rat germline by positively interacting with gene systems that promote a rat spermatogonial stem cell state. To identify candidate conserved gene systems in spermatogonia that interacted with Foxa2, we annotated Foxa2-bound genetic elements in rat USg chromatin (Chip-Seq; SG Medium) <1Mb from respective gene transcriptional start sites (peak score range 20-743) (Table S4). Distinct Foxa2-binding loci (n = 550; Table S4) were compared with transcripts enriched in rat USg (Table S1) and identified 106 genes in USg (n = 90) and DSg (n = 16) that are potentially regulated by binding Foxa2 (Figure 5A; Table S4). Approximately 45% of target genomic sequences harbored the canonical Foxa1/Foxa2 binding motif (TGTTTAC) (Figure S8A).

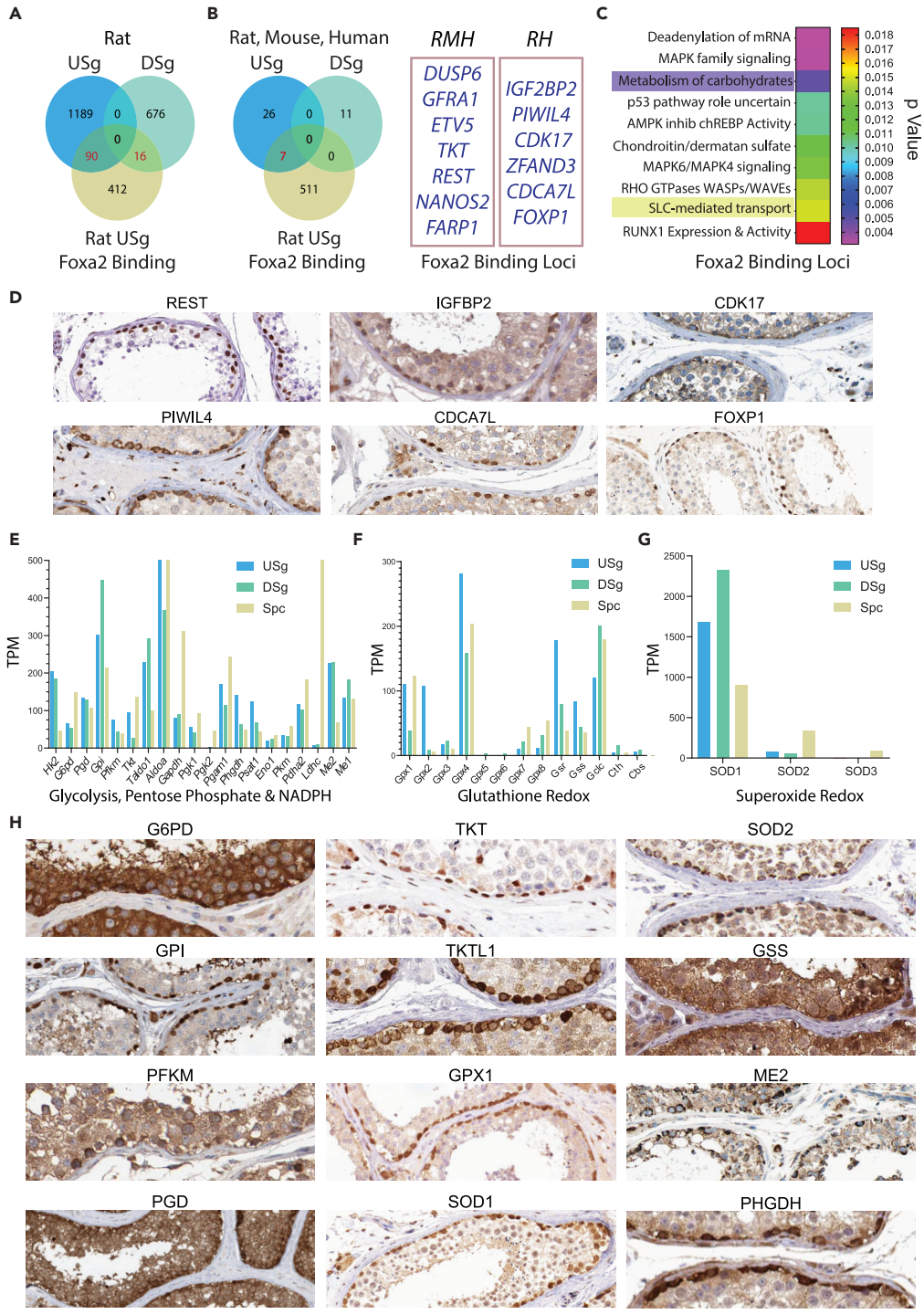

Figure 5. Foxa2-Binding Intersects with Spermatogonial Metabolism Gene Network

(A) Intersectional analyses on gene sets enriched in rat USg and DSg and Foxa2-binding loci identified by ChipSeq in rat USg.

(B) *Right*: intersectional analyses on conserved gene sets enriched in rat, mouse, and human USg and DSg and Foxa2-binding loci identified by ChipSeq in rat USg. *Left*: RMH = 7 genes enriched in rat, mouse, and human USg that interact with Foxa2 in rat. RH = 6 genes enriched in rat and human that interact with Foxa2 in rat.

(C) GO Reactome gene set enrichment analysis of Foxa2-binding loci in rat USg that intersect with USg-enriched transcripts conserved across rat, mouse, human (n = 33) + USg-enriched transcripts conserved across rat and human (n = 89).

Figure 5. *Continued*

(D) Antibody labeling profiles in human testis sections for spermatogonial proteins encoded by conserved USg-enriched, Foxa2-binding genes. Images modified from the Human Protein Atlas database (Pontén et al., 2008).

(E) Transcript profiles in rat USg, DSg, and Spc for genes linked to Glycolytic, Pentose Phosphate (PPP), and NADPH metabolic pathways that were selected by GO enrichment analyses.

(F) Transcript profiles in rat USg, DSg, and Spc for genes linked to glutathione redox pathways selected by GO enrichment analyses.

(G) Transcript profiles in rat USg, DSg, and Spc for genes linked to superoxide anion redox pathways selected by GO enrichment analyses.

(H) Labeling profiles in human testis sections for proteins marking conserved metabolic pathways enriched in rat, mouse, and human USg. Images modified from the Human Protein Atlas database (Pontén et al., 2008).

Also see Figure S8 and Table S4.

Rat USg-enriched transcripts inclusive to the Foxa2-binding gene set were compared with transcripts enriched across rat, mouse, and human USg and DSg (n = 33) (Figure 4B and Table S3) and identified a conserved spermatogonial Foxa2-binding gene signature (*Dusp6*, *Gfra1*, *Etv5*, *Rest*, *Tkt*, *Nanos2*, *Farp1*; n = 7 of 33) (*RMH*, Figure 5B and Table S4). In contrast, spermatogonial Foxa2-binding genes were not found to be inclusive to conserved DSg genes (n = 0 of 11) (Figure 5B). Comparisons using the conserved USg gene set (n = 33), plus transcripts enriched exclusively in rat and human USg (n = 89, Figure 4B), identified seven additional Foxa2-binding loci: *Igf2bp2, Piwil4, Cdk17, Zfand3, Cdca7l, and Foxp1* (*RH*, Figure 5B). Transcripts enriched exclusively in mouse and human USg (n = 38; Figure 4B) lacked genes that overlapped with Foxa2-binding loci identified in rat USg. Fifteen Foxa2-binding elements mapped to 13 distinct genes within or near genes encoding the 33 conserved USg stemness genes (Figure S8B).

Foxa2-binding loci in the USg stemness gene set were annotated as intergenic (*Gfra1, Piwil4, Cdk17, Zfand3, Cdca7l, Foxp1*), promoter (*Dusp6*) or intronic (*Etv5, Rest, Tkt, Igf2bp2*) regions (Figure S8B). Notably, *Dusp6* contained tandem Foxa2-binding loci within its promoter region (Promoter: −185 & −717 bp) (Figure S8B). *Etv5* also contained tandem Foxa2-binding loci with each binding motif localized to intron 21 of 24 (−78691 & −78,996 bp) (Figure S8B).

The Foxa2-binding locus linked to *Foxp1* stood out because *Foxp1* was abundant in USg (Figure S8C), and ~20% of Foxa2 ChipSeq-enriched target sequences contained consensus *Foxp1* binding motifs (Figure S8A). Rat Forkhead Box-family gene transcript profiles revealed *Foxa2, Foxa3, Foxo1, Foxp1, Foxm1,* and *Foxj3* were all relatively abundant in rat USg (Figure S8D). Like Foxo1 across mammals (Goertz et al., 2011) and Foxa2 in rats (Figures 3D–3F), Foxp1 was selectively expressed by Gfra1^{+} type A spermatogonia in adult rats (Figure S8E) and in type A-like spermatogonia in adult humans (Figure 5D). Based on mean TPM values > 30, rat USg hold the potential to abundantly express at least eight related Fox-family transcription factors (Figure S8D) that conceivably can compete for variations of the classical Foxa2 consensus DNA binding motif in the germline (Figure S8F).

Foxa2-Binding Spermatogonial Stemness Gene Ontology and Expression

To identify conserved pathways in spermatogonia that are functionally modified by Foxa2 enrichment, GO enrichment analyses were independently conducted on rat Foxa2-binding loci (n = 550; Table S4). Foxa2-binding loci were most significantly overrepresented by *Deadenylation of mRNA* (R-MMU-429947: $p = 3.15 \times 10^{-3}$), *Mapk Family Signaling Cascades* (R-MMU-5683057: $p = 3.17 \times 10^{-3}$), and *Metabolism of Carbohydrates* (R-MMU-71387: $p = 4.89 \times 10^{-3}$) gene sets (Figure 5C; Table S4).

The *Deadenylation of mRNA* gene set linked to *Nanos2*, due to inclusion of *Cnot6l, Cnot11,* and *Cnot8* (Table S2) and reported Nanos2 interactions with Cnot-family RNA decay factors that regulate germ cell RNA de-adenylation (Suzuki et al., 2010). *Mapk Family Signaling Cascades* included the USg-enriched growth factor receptor genes *Gfra1* (RMH) and *Fgfr1* (RH), as well as the RMH USg-enriched *Dusp6* (Table S2). Notably, the mouse *Metabolism of Carbohydrates* gene set contained the RMH USg-enriched *Tkt* (Reactome Pathway, $p < 0.005$) (Figure 5C), again linking Foxa2-binding to glutathione, NADPH, and pentose phosphate metabolic GO processes in USg (Figures 1G, and 4G).

In human testis (Human Protein Atlas), proteins encoded by the conserved USg gene set obtained by filtering on Foxa2-binding genes (Figure 5B) were selectively detected in spermatogonia (Figure 5D), consistent with transcript profiles in USg (Figures 1 and 4). Enrichment for proteins encoded by Foxa2-interacting gene sets in

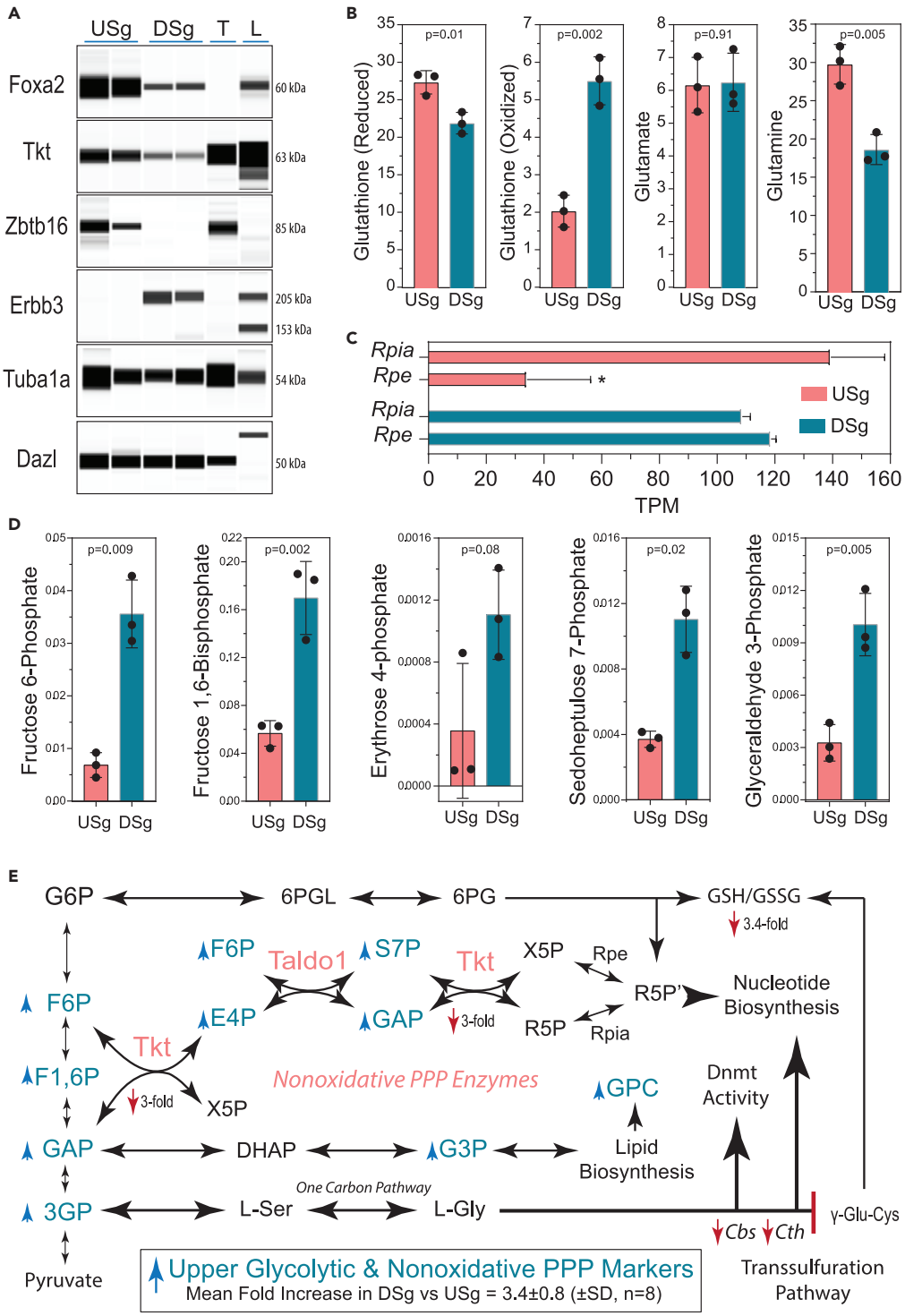

Figure 6. Accumulation of Upper Glycolytic and Pentose Phosphate Pathway Metabolites during Spermatogonial Differentiation in Culture

(A) Western blot analysis of transketolase in cultures of rat Foxa2^{+} USg before and after differentiation (DSg) on laminin in SD Medium for 120 h (n = 2 rat spermatogonial lines). T, adult rat testis; L, adult rat liver. Dazl, premeiotic and meiotic pan-germ cell marker; Zbtb16, type A spermatogonia marker; Erbb3, SD Medium-inducible spermatogonial marker; Tuba1a, soma and germ cell marker.

Figure 6. *Continued*

(B) Targeted LC-MS-based metabolite profiling measurements (Table S5) on relative levels of reduced (GSH) and oxidized (GSSG) L-glutathione in USg versus DSg in cultures prepared as described in panel (A) Relative levels of L-Glutamine and L-Glutamate in USg and DSg are shown for comparison (n = 3 replicate cultures/condition).

(C) Abundance of *Rpe* and *Rpia* transcripts in rat USg versus DSg (TPM; $p < 0.003$).

(D) Accumulation of upper glycolytic/pentose phosphate pathway metabolites in USg versus DSg cultures prepared as described in panel A.

(E) Summary of upper glycolytic/pentose phosphate pathway metabolite profiles in USg versus DSg (Table S5), prepared as described in panel A, but processed for targeted LC-MS-based metabolite profiling measurements (Also see Table S5).

human testes (Figure 5D) prompted additional analyses on spermatogonial metabolism to determine relative abundance of conserved glutathione, NADPH, and pentose phosphate metabolic GO gene-set-encoded (Figures 1G, 4G, and 5C) RNAs and proteins in human spermatogonia.

Glycolytic, Pentose Phosphate, Glutathione Mtabolism in Rat Spermatogonia

Spermatogonial glycolytic pathway gene sets that coupled to glutathione metabolism across rat, mouse, monkey, and human (Figures 4E, 4F, and S7) were evaluated in higher resolution developmentally using rat USg, DSg, and Spc. Like monkey and human spermatogonia (Figures 4F and S7), rat USg were enriched with glutathione, NADPH, and pentose phosphate metabolic enzyme gene sets (Figures 5E–5G) that connected to upper glycolytic (*Hk2, G6pd, Gpi, Pfkm*), oxidative (*Nfe2l3, G6pd, Pgd, Rpia, Rpe*), and non-oxidative (*Taldo, Tkt*) pentose phosphate pathway and serine/glycine biosynthetic enzyme (*Pgam1, Phgdh, Psat1, Shmt*) transcripts (Figure 5E and Table S1). Transcripts encoding lower glycolytic enzymes *Eno1, Pkm, Pkll, Ldha, Ldhb, Ldhc, and Ldhd* were less abundant in rat USg, whereas pyruvate and NADPH generating *Me1/Mdh1* and *Me2/Mdh2* genes, along with the pyruvate oxidizing *Pdha2* gene, were abundant in USg (Figure 5E and Table S1).

In agreement with GO analyses, rat USg were enriched with transcripts encoding glutathione reductase (*Gsr*) and glutathione peroxidases *Gpx1*, *Gpx2*, and *Gpx4* (Figure 5F). Rat USg also expressed relatively high levels of *Sod1*, encoding Superoxide dismutase (Mean TPM >1500) (Figure 5G). Cytotoxic superoxide anions generated by oxidative reactions are reduced to hydrogen peroxide by Sod1, and then Gpx-family enzymes rapidly neutralize H2O2 via redox reactions driven by reduced glutathione (Wang et al., 2011). In human testes, enzymes encoded by pentose phosphate, glutathione, and NADPH metabolism genes (Figures 4, 5, and S7) were selectively detected in spermatogonia (Figure 5H; Human Protein Atlas).

Consistent with USg being enriched with gene sets linked to glutathione metabolic processes (Figure 1G) and mirroring gene sets in primate spermatogonia (Figures 4F and S7), rat USg were endowed with transcripts encoding the essential glutathione biosynthetic enzymes, glutamate-cysteine ligase catalytic (Gclc)/modifier (Gclm) subunits, and glutathione synthetase (Gss) (Figure 5F). Glutamate-cysteine ligase catalyzes the first step in glutathione production by generating the dipeptide γ-glutamyl-cysteine (γ-Glu-Cys) from cysteine and glutamate (Koppula et al., 2018). Glutathione synthetase then catalyzes condensation of glycine and γ-glutamyl-cysteine to form the tripeptide, L-glutathione (Koppula et al., 2018). In human testes, GCLC (Atlas HPA036360), GCLM (Atlas CAB009568), and GSS (Atlas HPA054508) also appeared relatively abundant in spermatogonia (Figure 5H; Human Protein Atlas).

Western blot analyses demonstrated that Tkt was abundant in USg cultured in SG Medium but was rapidly downregulated during spermatogonial differentiation in SD Medium (Figure 6A). Transketolase's western blot profile during spermatogonial differentiation in SD Medium resembled the downregulation of Foxa2 and Zbtb16 and was distinct from upregulated Erbb3 (Figure 6A). A 3-fold decrease in Tkt levels in DSg versus USg was associated with a 3.4-fold decrease in GSH:GSSG (Figure 6B and Table S5), a significantly increased glutamate:glutamine (Figure 6B and Table S5), a 4-fold increase in *Rpe* transcripts (Figure 6C and Table S1), and a 3.4-fold increase in the accumulation of upper glycolytic and pentose phosphate pathway metabolite markers (Figure 6D and Table S5). Thus, USg gene sets (Figures 1 and 4) intersected bioinformatically with conserved glutathione/pentose phosphate metabolism gene sets (Figures 1G, 4E, 4F, 5E, and S7) that marked an elevated glutathione redox state in rat USg (Figure 6B).

Spermatogonia Depend on Extracellularly Supplied Cysteine to Drive Anabolism

Robust glutathione-linked metabolic enzyme gene profiles in rat spermatogonial lines contrasted with relatively low levels of transcripts encoding cystathionine beta-synthase (Cbs) and cystathionine gamma-lyase (Cth) that generate cysteine intracellularly from homocysteine *via* the transsulfuration pathway for protein biosynthesis,

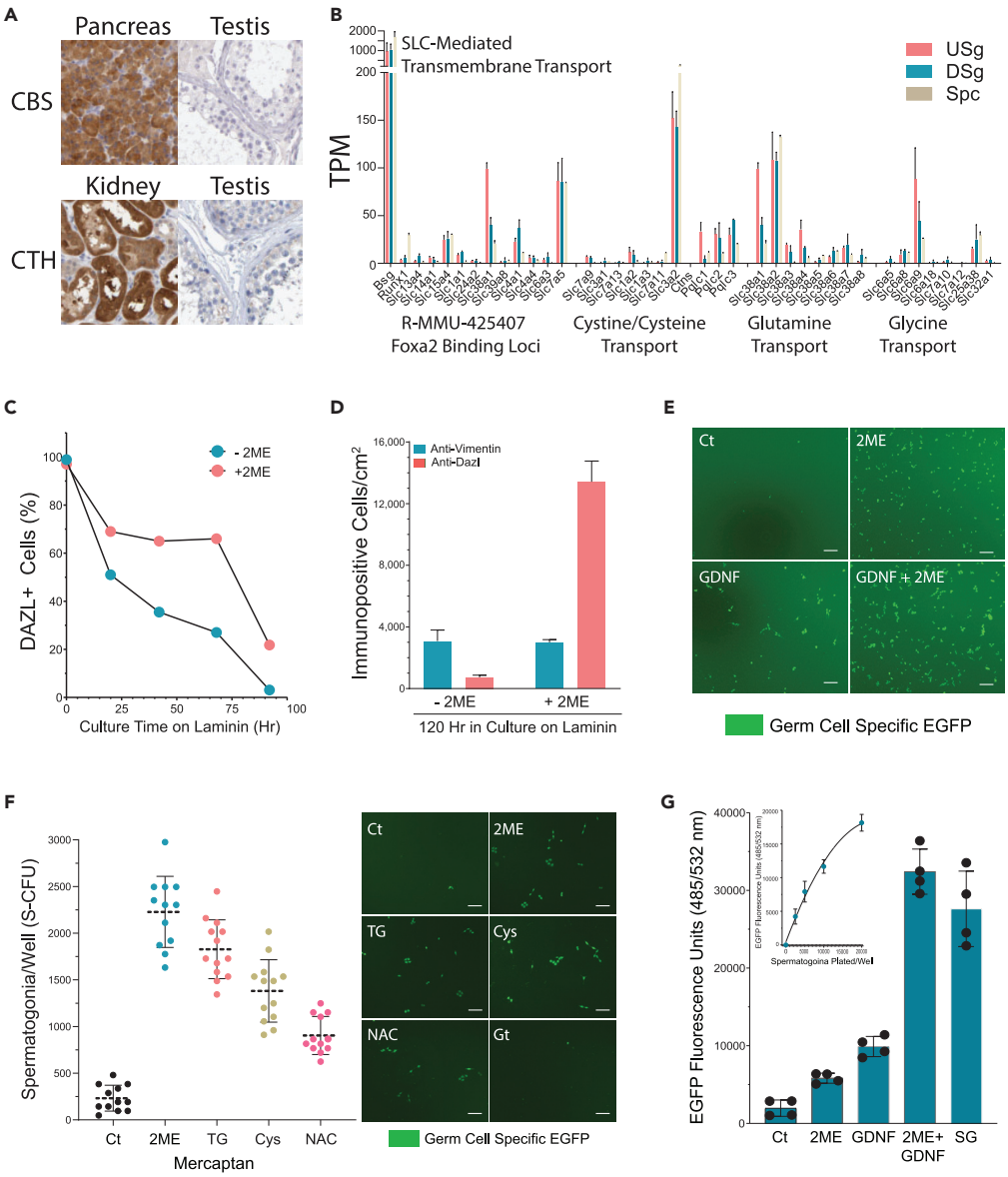

Figure 7. Cysteine-Like Factors Promote Spermatogonial Viability in Culture

(A) Antibody labeling profiles for CBS and CTH in human tissue sections modified from the Human Protein Atlas database (Pontén et al., 2008).

(B) Transcript profiles in rat USg, DSg, and Spc for genes linked to *SLC-mediated transmembrane transport* Reactome pathway gene set R-RNO-425407.

(C) Dazl^{+} cells/well scored over time on laminin with and without 2-mercaptoethanol (2ME) supplemented into the Control (Ct) DMEM:Hams F12 (1:1) culture medium containing 10% FBS. Representative of duplicate time course experiments (average values plotted, n = 2 wells/point).

(D) Relative numbers of Dazl^{+} (germ cell marker) and Vimentin^{+} (somatic cell marker) laminin-binding testis cells after 120 h in culture on laminin with and without 2ME supplemented into Ct medium. Mean, ±S.E.M. n = 3 wells/condition. Representative of duplicate experiments.

(E) Images of freshly isolated laminin-binding germ cells (tg*GCS-Egfp*$^{+}$) after 120 h in culture on laminin without (−2ME) and with (+2ME) 2ME supplemented into Ct medium with (+) and without (−) 10 nM rat GDNF. Representative Images from duplicate experiments. Scale, 100 μm

(F) (Left) Effects of L-cysteine and L-cysteine-like mercaptans on the viability of a rat spermatogonial stem cell line (tg*GCS-Egfp*$^{+}$ passage 16) based on spermatogonial colony forming unit (CFU) numbers scored/well after 120 h on laminin in: Ct, Control, or Ct plus 2ME, 50 μM 2-Mercaptoethanol; TG, 50 μM alpha-thioglycerol; Cys, 1 mM L-Cysteine; NAC, 1 mM N-

Figure 7. *Continued*
Acetyl-L-Cysteine; Gt, 1 mM L-Glutathione (S.E.M., n = 12 counts/well; representative of duplicate experiments) (Hamra et al., 2007). (Right) Respective images of cultures described for left panel. Scale, 100 μm.
(G) Relative levels of Egfp extracted from tg*GCS-Egfp*$^{+}$ spermatogonia (passage 14; 2000/0.96 cm^{2}) after 120 h in culture on laminin with (+2ME) and without (−2ME) 50 μM 2ME supplemented into Ct medium with (+) and without (–) 10 nM rat GDNF. SG Medium (SG). **Inset:** Fluorescence Units (485/532nm) extracted from cultures 20 h after plating different numbers of tg*GCS-Egfp*$^{+}$ germ cells in Ct medium on laminin (R = 0.907). Mean, ±S.E.M. n = 4 wells/condition. Representative of duplicate experiments.
Also see Figure S9.

protein unfolding, and glutathione biosynthesis for cellular redox balance and detoxification (Combs and DeNicola, 2019). Like relatively low *Cth* and *Cbs* levels that we observed as being conserved across rat, mouse, monkey, and human (Figures 5F and S7B), relatively low CBS and CTH levels were detected in human spermatogonia when compared with pancreatic and renal epithelia, respectively (Figure 7A; Human Protein Atlas).

Given low levels of spermatogonial *Cbs* and *Cth* in rodents and primates (Figures 5F and S7B), we formulated the hypothesis that spermatogonia require a mechanism(s) to uptake extracellular cysteine sources to promote germ cell growth and protect the germline from oxidative damage. Interestingly, we noticed Foxa2-binding loci were enriched in the *SLC-mediated transmembrane transport* gene set (R-MMU-425407) that included the cysteine uptake transporter gene *Slc1a1* (Aoyama et al., 2006) (Table S4). Still, analysis of R-MMU-425407 gene profiles in rat USg demonstrated relatively low levels of *Slc1a1* (Figure 7B) that did not support Slc1a1 representing a dominant source for cysteine uptake by spermatogonia in culture. Instead, the most abundantly expressed USg genes within R-MMU-425407 encoded Bsg (monocarboxylate transport chaperone), Slc15a4 (lysosomal His export), Slc38a1 (Gln uptake), Slc4a1 (HCO_3^-/Cl^- exchange), and Slc7a5 (Leu/Gln exchange) (Figure 7B).

Analysis of additional cysteine/cystine transport gene profiles across spermatogonia from rats, mice, monkeys, and humans expressed relatively high levels of the *Slc3a2* (Figure 7B; Table S2). Slc3a2 (alias CD98) functions in a complex with the Cystine/Glutamate exchanger, Slc7a11 (alias xCT) (Sato et al., 1999, 2005). Slc3a2/Slc7a11-mediated cystine uptake functions to fuel glutathione biosynthesis and buffer cell death by ferroptosis (Stockwell et al., 2017). Similarly, Slc3a2 functions in a complex with the related Leu/Gln exchanger, Slc7a5, that drives leucine uptake and mTor-dependent cell growth (Mastroberardino et al., 1998). Despite rat USg expressing relatively high levels for *Slc3a2* and *Slc7a5* for Leu uptake, as well as *Slc38a1/2* and *Slc6a9* for respective glutamine and glycine uptake (Figure 7B), rodent and primate spermatogonia displayed relatively low levels of cystine or cysteine uptake transporters, including low levels of the *Slc7a11* in the face of elevated *Nfe2l3* (mouse *Nrf2*) (Figures 7B and Tables S1 and S2) that feed into the *Gss-*, *Gclc-*, and *Gpx4*-dependent inactivation of lipid peroxides, as well as *Sod1*/*Gpx1*-dependent inactivation of ROS.

Spermatogonial culture medium is supplemented with glutathione, Sod1, catalase, and 2-mercaptoethanol (2ME) (Wu et al., 2009). Curiously, 2ME is also used to formulate culture media that promotes the growth of cancer and stem cell lines deficient in cystine uptake (Ishii et al., 1981; Ishii and Mann, 2014). Adding 2ME to culture medium generates "mixed disulfide" bonds with oxidized forms of cysteine (e.g. cystine) (Ishii et al., 1981). Cysteine- 2ME "mixed disulfides" are transported through an alternate L-system solute uptake pathway and then reduced intracellularly by Txn and Txnd as a mechanism to generate cysteine within cells (Willis and Schleich, 1995).

Supporting our hypothesis that spermatogonia require a mechanism(s) to uptake extracellular cysteine sources to promote germ cell growth, a standard FBS-containing culture medium effectively promoted survival and syncytial development of freshly isolated rat type A spermatogonia (Figures 7C–7E) and rat spermatogonial stem cell lines (Figures 7F, 7G, and S9A) only after supplementation with cysteine or cysteine-like mercaptans (i.e. 2ME, α-thioglycerol, N-acetyl-L-cysteine). With both freshly isolated and sub-cultured rat USg, we found that GDNF and 2ME synergistically stimulated germ cell viability on laminin and at levels comparable to SG Medium (Figures 7E and 7G). Standard FBS-containing culture medium, therefore, appeared to require importable pro-cysteine-like substrates that counteracted ferroptosis in the germline and effectively fueled GDNF-dependent spermatogonial growth.

Given poor cystine-dependent viability displayed by undifferentiated spermatogonia (Figures 7C–7E), plus the reported dependency of intracellular glutathione levels on cystine uptake to prevent ferroptosis in

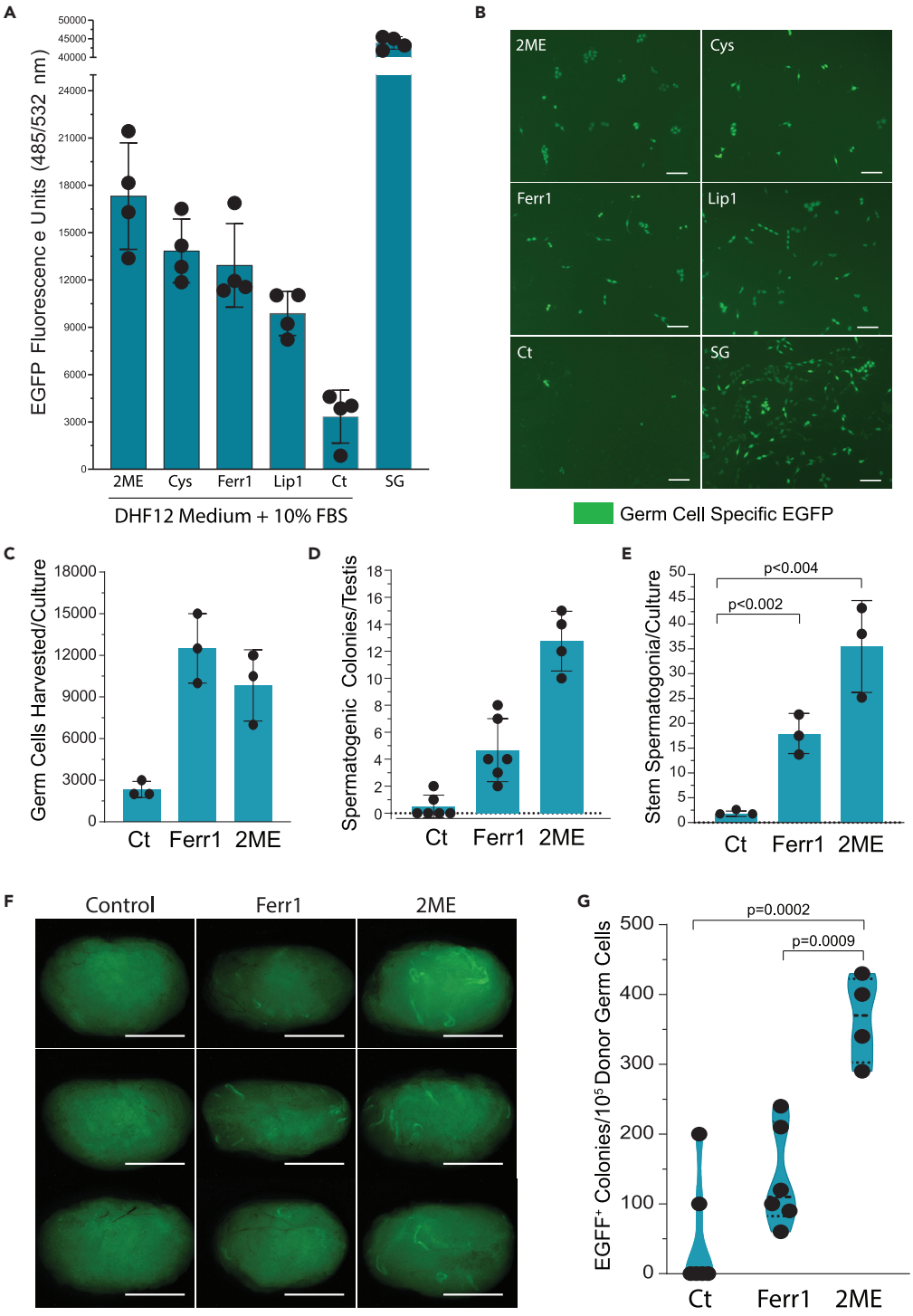

Figure 8. Cysteine-Like Factors Counteract Spermatogonial Stem Cell Ferroptosis

(A) Relative levels of Egfp extracted from tg*GCS-Egfp*$^{+}$ spermatogonia (passage 16; 4000/0.96 cm^{2}) after culture 120 h on laminin in the Control (Ct) 10% FBS-containing culture medium as described in panel 7G with and without 50 μM 2-Mercaptoethanol (2-ME), 1 mM L-Cysteine (Cys), 1 μM Ferristatin-1 (Ferr1), 0.1 μM Liproxstatin-1 (Lip1), or with 100% SG Medium (SG). Mean ±S.E.M. n = 4 wells/condition. Representative of duplicate experiments.

(B) Images of tg*GCS-Egfp*$^{+}$ spermatogonial cultures described in panel 8A with and without 50 μM 2ME, 1 mM Cys, 1 μM Ferr1, 0.1 μM Lip1, or with SG Medium. Scale: 100 μm

Figure 8. *Continued*
(C) tg*GCS-Egfp*$^{+}$ Germ Cells harvested per culture condition in Ct, Ferr1, or 2ME (average counts plotted/condition, n = 2–4 wells/condition), as described in panel 8B. One hundred twenty hours post-plating, 40,000 tg*GCS-Egfp*$^{+}$ spermatogonia/9.6 cm^{2}, n = 3 cultures.
(D) tg*GCS-Egfp*$^{+}$ donor-derived spermatogenic colonies that developed by d32 post-transplantation of tg*GCS-Egfp*$^{+}$ germ cells into recipient rat testes. Donor germ cells were harvested and transplanted 120 h after plating in each respective Ct, Ferr1, or 2ME medium at 0.5–4x10^{3} cells/testis/rat, as described in panel 8C. Ct, 3 colonies/3,000 cells transplanted (n = 6 rats); Ferr1 = 28 colonies/20,000 cells transplanted (n = 6 rats); 2ME = 51 colonies/14,000 cells transplanted (n = 4 rats).
(E) Numbers of stem spermatogonia harvested per culture calculated by germ cell numbers harvested/culture in panel C x average spermatogonial stem cell concentration/number donor germ cells transplanted/condition (Ct, Ferr1, 2ME) in panel D.
(F) Testes form recipient rats described in panels 8D and 8E illustrating more donor-derived spermatogenesis (EGFP + tubules) generated by cultures with Ferr1 or 2ME in the culture medium versus Ct. Scale, 0.5 cm.
(G) Relative spermatogonial stem cell activity in cultures described in panel 8C based on mean numbers of donor-derived spermatogenic colonies formed/10^{5} EGFP^{+} germ cells transplanted/testis obtained from study in panel 8D.
Also see Figure S9.

absence of cysteine-generating transsulfuration pathways (Zhu et al., 2019), we tested the hypothesis that ferroptosis inhibitors would restore a healthy intracellular redox environment(s) (Schafer and Buettner, 2001) to rat USg in the Ct medium. Supporting this hypothesis, we found ferroptosis inhibitors ferrostatin-1 and liproxstatin-1 (Figures 8A and 8B), and co-culture with rat somatic testis cells (Figure S9B), each effectively promoted spermatogonial survival in cultures lacking L-cysteine or L-cysteine-like mercaptans.

To quantify effects of L-cysteine-generating factors on USg, we measured relative numbers of rat spermatogonial stem cells/culture by *in vivo* spermatogenesis colony-forming assays (Hamra et al., 2004; Nagano, 2003). Spermatogenesis colony-forming assays were conducted by transplanting donor cultures into rat testes after 5 days on laminin in Ct medium with and without ferrostatin-1 or 2ME (Figures 8C–8G). Compared with Ct medium alone, Ct medium with ferrostatin-1, or Ct medium with 2ME, more effectively promoted spermatogonial stem cell maintenance in culture on laminin, as measured by greater relative numbers of tgGCS-EGFP^{+} germ cells harvested/culture (Figure 8C), greater tgGCS-EGFP^{+} donor-derived spermatogenic colonies produced/testis/culture (Figures 8D–8F), and greater relative spermatogonial stem cell activity based on numbers of EGFP^{+} spermatogenic colonies formed/testis/EGFP^{+} germ cell transplanted (Figure 8G).

Based on >20 times more total tgGCS-EGFP^{+} spermatogonial stem cells harvested/culture in medium with ferrostatin or 2ME versus control ($p < 0.003$; Figure 8E), and an ~7 times higher spermatogonial stem cell concentration/culture using medium with 2ME versus control ($p < 0.0002$; Figure 8G), rat USg are highly dependent on extracellularly provided sources of L-cysteine and/or pro-cysteine-like factors to balance their intracellular glutathione redox environment(s) (Stockwell et al., 2017).

DISCUSSION

Given the robust regenerative capacity of rat spermatogonial stem cell lines (Chapman et al., 2015b; Wu et al., 2009), we exploited a rat culture system (Hamra, 2017) to analyze the genomic landscape in undifferentiated spermatogonia and compare it with spermatogonia undergoing premeiotic differentiation *in vitro* on laminin (Figures 1E, 1F, S1D, and S1F). Rat spermatogonial transcriptomes served as a springboard to functionally annotate conserved metabolic processes critical for spermatogonial stem cell viability and growth *in vitro* (Figure S2). Here, we found that conserved molecular signatures in rodent and primate spermatogonia point to the diversion of glycolytic intermediates into oxidative and non-oxidative pentose phosphate pathways (PPP) (Christodoulou et al., 2019). Diverting metabolism through the PPP in spermatogonia, conceivably, may be more compatible with protecting germlines from metabolic stress-induced cellular damage (Milanese et al., 2019). For example, glycolytic flux through the PPP may promote genomic stability under conditions that are more favorable for preserving DNA integrity during the long term maintenance of male germline stem cells (Helsel et al., 2017a), and during their transition from a slower cell cycle in USg to a faster cell cycle in DSg (Huckins, 1971a, 1971c; Lok et al., 1983).

Here, we further define a spermatogonial stemness gene signature that is conserved across rat, mouse, and human USg (n = 33, Figure 4D) and that includes *Dusp6, Gfra1, Etv5, Tkt, Rest, Nanos2*, and *Farp1* as Foxa2-binding loci in the rat germline (Figures 5A–5D). Like in rat USg (Figure 1G and Table S2), conserved spermatogonial gene sets intersected with glutathione, NADPH, and pentose phosphate metabolism gene sets (Figures 4E and 4F, Table S2). Metabolically, *Foxa*-family transcription factors regulate responses to

changes in nutrient levels in somatic cells across species (Bolukbasi et al., 2017; Carrano et al., 2009; Lantz et al., 2004). In humans, *Foxa*-family genes upregulate metabolic processes during starvation (Wolfrum et al., 2004), function as genome modifiers repressed by insulin receptor/daf-2 signaling (Puigserver and Rodgers, 2006), and influence fasting glucose levels in humans (Xing et al., 2010).

In mice, spermatogonial stem cells are represented by undifferentiated ID4^{+}, Nanos2^{+}, Gfra1^{+}, Nanos3^{-}, and Neurog3^{-} A_s spermatogonia (Nakagawa et al., 2007, 2010; Oatley et al., 2011; Sada et al., 2009; Suzuki et al., 2009; Zheng et al., 2009). Here, in rats, we found Foxa2 to selectively mark populations of Gfra1^{+} and Gfra1^{-} undifferentiated A_s spermatogonia that were also Snap91^{+} and Cd9^{+} (Figures 3B and 3C). In rats, similar to *Foxa2*, *Snap91* transcripts co-purified with spermatogonial stem cells (Hamra et al., 2004, 2005). Accordingly, SNAP91 is localized to cytoplasm in human type A spermatogonia (von Kopylow et al., 2010). In rat seminiferous tubule whole mounts, Snap91 is a cytoplasmic marker enriched on endosome vesicle-like organelles in undifferentiated A_s and A_{pr} spermatogonia (Gfra1^{+}, Sall4^{+}, Cd9^{+}, Zbtb16^{+}) (Abid et al., 2014) (Figures 3B and 3C). Moreover, CD9 is a cell surface marker enriched on undifferentiated A_s, A_{pr}, and A_{al} type A spermatogonia in rats (Gfra1^{+}, Zbtb16^{+}; Figures 3B and 3C) (Abid et al., 2014; Kanatsu-Shinohara et al., 2004). In rats, only approximately 5% of total Snap91^{+} A_s spermatogonia were ErbbB3^{+} (Abid et al., 2014).

Here, the Foxa2^{+}, Gfra1^{+}, Snap91^{+}, Cd9^{+}, and Zbtb16^{+} A_s spermatogonia in rats further included the stage VIII-IX-specific Erbb3^{+} undifferentiated A_s spermatogonia (Figure S6DE). In contrast to robust Erbb3 labeling on a subset of undifferentiated stage-VIII-IX A_s spermatogonia, Erbb3 labeling was not detected in other USg or DSg types *in vivo* (Abid et al., 2014). *Erbb3* was previously demonstrated to be essential for development of rat DSg from USg *in vitro* on laminin in SD Medium supplemented with recombinant Neuregulin-1, however, the *Erbb3*-deficient germlines effectively regenerated spermatogenesis in recipient testes (Chapman et al., 2015b). Consistent with strict localization of Erbb3 immunolabeling to rat undifferentiated A_s spermatogonia during late stage VIII and stage IX of spermatogenesis (coincides with the peak in RA accumulation during stages VIII-IX of a mouse seminiferous epithelial cycle (Hogarth et al., 2015)), we demonstrate robust induction of Erbb3 in rat spermatogonia during culture in the RA-containing SD Medium (Table 1, Figures 6A and S1C). In mice, *Erbb3* transcripts are >5-fold enriched in GFP-ID4^{Bright} versus GFP-ID4^{Dim} spermatogonia (Helsel et al., 2017b), significantly change in abundance during spermatogonial differentiation (Tan et al., 2020), and total *Erbb3* transcript abundance peaks in mouse testes on postnatal ~ d8-11 (Schultz et al., 2003). In humans, *ERBB3* was found to be enriched in spermatogonia compared with spermatocyte/spermatid gene sets (Shami et al., 2020) and independently, was identified as being enriched in human early spermatocyte states and Sertoli cells (Young Adult Atlas) (Guo et al., 2018).

Based on their molecular profiles, the Gfra1^{+} and Gfra1^{-} sub-populations of Foxa2^{+} A_s spermatogonia reported here represent undifferentiated A_s spermatogonia (Figures 3B and 3C) that are specified in parallel with induction of Gfra1 in the rat germline (Dazl+) between postnatal d4 to d8 (Figure 3A). Distinct reports demonstrate that Gfra1^{+} and Gfra1^{-} testis cell fractions from mice each contain functional spermatogonial stem cells (Buageaw et al., 2005; Garbuzov et al., 2018). And, in mice, a key study reported that germline stem cells in a normal testis are GFRa1^{+} (Hara et al., 2014). Here, we make the unique observation, in seminiferous tubule whole mounts, that the Foxa2^{+}, Gfra1^{-}, Snap91^{+}, and Cd9^{+} spermatogonia are exclusively undifferentiated A_s spermatogonia and therefore, appear to represent a distinct developmental/cellular state compared with the Gfra1^{+} A_s, A_{pr}, and A_{al} spermatogonial populations (Figure 3F). Foxa2^{+} and Gfra1^{-} A_s spermatogonia are found during all stages of a seminiferous epithelial cycle (Figure 3E), and so would predominantly not represent the stage VIII-dependent differentiating A_s spermatogonia (Huckins, 1971c)(Figure S6C). It should be noted that evidence for a primitive Gfra1^{-} "State 0" USg population has been reported in human (Guo et al., 2018) and recently has been proposed to function as reserve germline stem cells (Caldeira-Brant et al., 2020).

Mouse type A_s spermatogonia develop into nascent syncytia of A_{al} progenitor spermatogonia characterized as Gfra1^{+} progenitor spermatogonia (Nakagawa et al., 2010). In mice, Rarg and Gfra1 localization is reported to be essentially mutually exclusive during an epithelial cycle, in that the "differentiation-primed" A_{al} spermatogonia in the mouse are Gfra1^{-}, Rarg^{+} (Ikami et al., 2015). Upon Rarg induction, Gfra1 is downregulated in A_{al} progenitor spermatogonia as they effectively transition toward Kit^{+}, Neruog3, and Rarg1^{-} type A1 differentiating spermatogonia (Gely-Pernot et al., 2012; Ikami et al., 2015). The transient populations of Gfra1^{-} and Rarg^{+} A_{al} progenitor spermatogonia are considered primed for differentiation into developmentally competent type A1 spermatogonia in the seminiferous epithelium of adult mice (Gely-Pernot et al., 2012; Ikami et al., 2015). *In vivo*, RA production peaks at stages VIII-IX and drives the development of Rarg^{+} progenitor

spermatogonia into type A1 spermatogonia (Gely-Pernot et al., 2012). Here, in rat, we found Foxa1 to selectively mark populations of Rarg^{+}, Gfra1^{+}, Foxa2^{-} type A_{al} spermatogonia (Figures 3E and S3A–S3C), which, based on mouse genetics (Gely-Pernot et al., 2012) and syncytia length in rat (Huckins, 1971c), seem to be primed for differentiation into type A1 spermatogonia (Gfra1^{-}, Foxa1^{-}, Foxa2^{-}, Rarg^{-}) (Figure 3F).

Curiously, transient sharp increases in Foxa1^{+} spermatogonia concentration along a spermatogenic wave predominantly occurred in peaks that either partially overlapped or that were fully separated by 0.5–2 mm valleys of tubule epithelium without Foxa1^{+} spermatogonia (1.0 $\pm$ 0.81mm/valley, n = 4 twin cohorts; Figure S3A). In a tubule fragment that contained two pairs of Foxa1^{+} spermatogonia cohorts, the subsegments containing each pair of Foxa1^{+} cohorts were ~3 cm apart (~1 rat spermatogenic wavelength) (Figure S3A) (Perey et al., 1961). The identification of heterogeneous populations of Foxa1^{+} and Foxa2^{+} USg (Gfra^{+}) in the same subsegments of a rat spermatogenic wave provides new molecular markers for mapping the topography of germline stem cell clone development in the rat seminiferous epithelium (Abid et al., 2014).

In human testes, *FOXA1, FOXA2,* and *FOXA3* were not significantly enriched in spermatogonial gene clusters. Still, state 0 and 1 clusters of human USg were significantly enriched in *FOXP1*, *FOXP4*, *FOXD1*, *FOXG1,* and *FOXC2* (Guo et al., 2018). Enrichment for *Foxp1* in USg (Figures 4B and 5D), together with enrichment for Foxa2-binding at consensus Foxp1- and Foxo1-binding elements in rat USg (Figure S8A), highlighted the potential for Foxa1 and Foxa2 to function as genetic modifiers at distinct developmental steps in the rat germline by competing for DNA binding in genes regulated by Forkhead Box family transcription factors (Figure S8F) (Goertz et al., 2011).

Based on conserved spermatogonial gene profiles linked to glutathione and pentose phosphate metabolism, and Foxa2's regulatory responses to metabolic stress signals in the soma of worms, flies, rodents, and primates (Panowski et al., 2007; Puigserver and Rodgers, 2006; Wolfrum et al., 2004; Wang et al., 2011), we hypothesize that rat USg coopted *Foxa2*-mediated genetic interactions to similarly help maintain germline stem cell integrity by counteracting metabolic stress (Wolfrum et al., 2004; Wang et al., 2011). By exploiting a rat culture system, we further report that the conserved germline gene networks enriched in spermatogonia predicted the functional expression of an anti-ferroptotic pro-cysteine-like factor uptake pathway in rat USg that selected against germline stem cell loss *in vitro* (Figure 8). Because cystine transporters are not abundantly expressed by rat USg in culture (Figures 7B and Tables S1 and S2), and standard eukaryotic cell culture medium contains cystine, but not cysteine, we propose a model analogous to that in L1210 mouse lymphoma cells (Ishii et al., 1981), wherein extracellular conversion of cystine into importable "cysteine-mercaptan disulfides" drives metabolic pathways that promote rat spermatogonial growth in culture.

Limitations of the Study

Comparisons between rodent and primate spermatogonial gene expression and molecular marker profiles in the current study are subject to evaluations being made between primary rat spermatogonial lines following subculture *in vitro* and more freshly isolated spermatogonia from mouse, monkey, and human testes. Thus, *in vitro* culture in rat spermatogonia, as well as time taken for testis cell isolation and histological processing protocols for mouse, monkey, and/or human specimens prepared under atmospheric conditions, may impact molecular profiles. The current study demonstrates Foxa2 is uniquely abundant in rat A_s spermatogonia and that Foxa2 binds to rat spermatogonial stemness genes, that included the gene encoding the non-oxidative pentose phosphate pathway enzyme Transketolase (*Tkt*) during rat spermatogonial culture *in vitro*. However, in the current study, a genetic interaction between Foxa2 and spermatogonial stemness genes or the ability of Foxa2 to function as a genetic modifier of germline metabolism by directly or indirectly regulating glutathione or pentose phosphate metabolism gene expression was not analyzed.

Resource Availability

Lead Contact

Further information and requests should be directed to and will be fulfilled by the Lead Contact, F. Kent Hamra (kent.hamra@utsouthwestern.edu).

Materials Availability

Rat spermatogonial stem cell lines are available for sharing from the Lead Contact with a completed Materials Transfer Agreement.

Data and Code Availability

The accession number for RNA and DNA sequencing data reported in this paper is NCBI GEO: GSE163302, and is summarized in supplemental data Excel files Tables S1–S5.

METHODS

All methods can be found in the accompanying Transparent Methods supplemental file.

SUPPLEMENTAL INFORMATION

Supplemental Information can be found online at https://doi.org/10.1016/j.isci.2020.101880.

ACKNOWLEDGMENTS

This work was supported by grants from The Eunice Kennedy Shriver National Institute of Child Health and Human Development, R01HD053889; The Office of the Director, R24OD011108; The National Institute on Drug Abuse, U44DA044885; The Department of Obstetrics and Gynecology's Reproductive Endocrinology and Infertility Fellowship Program (RF-21), UT Southwestern Medical Center, Dallas Texas; and GenomeDesigns Laboratroy, LLC., Richardson Texas. Chip Seq and RNA Seq were conducted by The McDermott Center Next Generation Sequencing (NGS) Core at UT Southwestern. Metabolite Profiling was conducted by the Children's Medical Research Institute Metabolomics Facility at UT Southwestern. We thank Audrey H. Nelson, Lauren G. Zacharias, and Hieu S. Vu for their help with experiments and Drs. R. Ann Word, Ralph J. DeBerardinis, and Bradley R. Cairns for their critical comments.

AUTHOR CONTRIBUTIONS

F.K.H. conceptualized the study. F.K.H., D.P., M.K., X.C., and B.R.C. designed the experiments. D.P., A.P., K.M.C., M.K., A.T.M., A.E.W., and J.C. performed most of the experiments. J.A. helped perform immunofluorescent labeling studies and transplantation assays. P.K. helped to perform protein assays and supporting western blots. F.K.H., D.P., M.K., A.P., A.T.M., A.E.W., J.C., B.R.C., M.K., and X.C. performed data analysis and/or helped prepare figures and tables. F.K.H. and B.R.C. obtained funding and coordinated the study. F.K.H. wrote the paper.

DECLARATION OF INTERESTS

A.P. is an employee of GenomeDesigns Laboratory, LLC., and F.K.H. is a founder and consultant of GenomeDesigns Laboratory, LLC and a member of its scientific advisory board. A provisional patent application has been filled on portions of this work (Inventor: F.K.H.). D.P., M.K., A.T.M., A.E.W., K.M.C., J.C., J.A., P.K., X.C., and B.R.C. declare no competing interests.

Received: November 26, 2019
Revised: November 2, 2020
Accepted: November 25, 2020
Published: January 22, 2021

REFERENCES

Abid, S.N., Richardson, T.E., Powell, H.M., Jaichander, P., Chaudhary, J., Chapman, K.M., and Hamra, F.K. (2014). A-single spermatogonia heterogeneity and cell cycles synchronize with rat seminiferous epithelium stages VIII-IX. Biol. Reprod. *90*, 32.

Aoyama, K., Suh, S.W., Hamby, A.M., Liu, J., Chan, W.Y., Chen, Y., and Swanson, R.A. (2006). Neuronal glutathione deficiency and age-dependent neurodegeneration in the EAAC1 deficient mouse. Nat. Neurosci. *9*, 119–126.

Ball, R.L., Fujiwara, Y., Sun, F., Hu, J., Hibbs, M.A., Handel, M.A., and Carter, G.W. (2016). Regulatory complexity revealed by integrated cytological and RNA-seq analyses of meiotic substages in mouse spermatocytes. BMC Genomics *17*, 628.

Bochkis, I.M., Rubins, N.E., White, P., Furth, E.E., Friedman, J.R., and Kaestner, K.H. (2008). Hepatocyte-specific ablation of Foxa2 alters bile acid homeostasis and results in endoplasmic reticulum stress. Nat. Med. *14*, 828–836.

Bolukbasi, E., Khericha, M., Regan, J.C., Ivanov, D.K., Adcott, J., Dyson, M.C., Nespital, T., Thornton, J.M., Alic, N., and Partridge, L. (2017). Intestinal fork head regulates nutrient absorption and promotes longevity. Cell Rep. *21*, 641–653.

Brinster, R.L., and Avarbock, M.R. (1994). Germline transmission of donor haplotype following spermatogonial transplantation. Proc. Natl. Acad. Sci. U S A *91*, 11303–11307.

Brinster, R.L., and Zimmermann, J.W. (1994). Spermatogenesis following male germ-cell transplantation. Proc. Natl. Acad. Sci. U S A *91*, 11298–11302.

Buageaw, A., Sukhwani, M., Ben-Yehudah, A., Ehmcke, J., Rawe, V.Y., Pholpramool, C., Orwig, K.E., and Schlatt, S. (2005). GDNF family receptor alpha1 phenotype of spermatogonial stem cells in immature mouse testes. Biol. Reprod. *73*, 1011–1016.

Caldeira-Brant, A.L., Martinelli, L.M., Marques, M.M., Reis, A.B., Martello, R., Almeida, F., and

Chiarini-Garcia, H. (2020). A subpopulation of human Adark spermatogonia behaves as the reserve stem cell. Reproduction *159*, 437–451.

Carrano, A.C., Liu, Z., Dillin, A., and Hunter, T. (2009). A conserved ubiquitination pathway determines longevity in response to diet restriction. Nature *460*, 396–399.

Chapman, K.M., Medrano, G.A., Chaudhary, J., and Hamra, F.K. (2015a). NRG1 and KITL signal downstream of retinoic acid in the germline to support soma-free syncytial growth of differentiating spermatogonia. Cell Death Discov. *1*, 15018.

Chapman, K.M., Medrano, G.A., Jaichander, P., Chaudhary, J., Waits, A.E., Nobrega, M.A., Hotaling, J.M., Ober, C., and Hamra, F.K. (2015b). Targeted germline modifications in rats using CRISPR/Cas9 and spermatogonial stem cells. Cell Rep. *10*, 1828–1835.

Christodoulou, D., Kuehne, A., Estermann, A., Fuhrer, T., Lang, P., and Sauer, U. (2019). Reserve flux capacity in the pentose phosphate pathway by NADPH binding is conserved across kingdoms. iScience *19*, 1133–1144.

Clermont, Y. (1972). Kinetics of spermatogenesis in mammals: seminiferous epithelium cycle and spermatogonial renewal. Physiol. Rev. *52*, 198–236.

Combs, J.A., and DeNicola, G.M. (2019). The non-essential amino acid cysteine becomes essential for tumor proliferation and survival. Cancers (Basel) *11*, 678.

Danshina, P.V., Geyer, C.B., Dai, Q., Goulding, E.H., Willis, W.D., Kitto, G.B., McCarrey, J.R., Eddy, E.M., and O'Brien, D.A. (2010). Phosphoglycerate kinase 2 (PGK2) is essential for sperm function and male fertility in mice. Biol. Reprod. *82*, 136–145.

de Rooij, D.G. (2017). The nature and dynamics of spermatogonial stem cells. Development *144*, 3022–3030.

Garbuzov, A., Pech, M.F., Hasegawa, K., Sukhwani, M., Zhang, R.J., Orwig, K.E., and Artandi, S.E. (2018). Purification of GFRalpha1+ and GFRalpha1- spermatogonial stem cells reveals a niche-dependent mechanism for fate determination. Stem Cell Rep. *10*, 553–567.

Gely-Pernot, A., Raverdeau, M., Celebi, C., Dennefeld, C., Feret, B., Klopfenstein, M., Yoshida, S., Ghyselinck, N.B., and Mark, M. (2012). Spermatogonia differentiation requires retinoic acid receptor gamma. Endocrinology *153*, 438–449.

Goertz, M.J., Wu, Z., Gallardo, T.D., Hamra, F.K., and Castrillon, D.H. (2011). Foxo1 is required in mouse spermatogonial stem cells for their maintenance and the initiation of spermatogenesis. J. Clin. Invest. *121*, 3456–3466.

Guo, J., Grow, E.J., Mlcochova, H., Maher, G.J., Lindskog, C., Nie, X., Guo, Y., Takei, Y., Yun, J., Cai, L., et al. (2018). The adult human testis transcriptional cell atlas. Cell Res. *28*, 1141–1157.

Hamra, F.K. (2017). Rattus norvegicus spermatogenesis colony-forming assays. Methods Mol. Biol. *1463*, 185–203.

Hamra, F.K., Chapman, K.M., Nguyen, D., and Garbers, D.L. (2007). Identification of neuregulin as a factor required for formation of aligned spermatogonia. J. Biol. Chem. *282*, 721–730.

Hamra, F.K., Chapman, K.M., Nguyen, D.M., Williams-Stephens, A.A., Hammer, R.E., and Garbers, D.L. (2005). Self renewal, expansion, and transfection of rat spermatogonial stem cells in culture. Proc. Natl. Acad. Sci. U S A *102*, 17430–17435.

Hamra, F.K., Gatlin, J., Chapman, K.M., Grellhesl, D.M., Garcia, J.V., Hammer, R.E., and Garbers, D.L. (2002). Production of transgenic rats by lentiviral transduction of male germ-line stem cells. Proc. Natl. Acad. Sci. U S A *99*, 14931–14936.

Hamra, F.K., Schultz, N., Chapman, K.M., Grellhesl, D.M., Cronkhite, J.T., Hammer, R.E., and Garbers, D.L. (2004). Defining the spermatogonial stem cell. Dev. Biol. *269*, 393–410.

Hara, K., Nakagawa, T., Enomoto, H., Suzuki, M., Yamamoto, M., Simons, B.D., and Yoshida, S. (2014). Mouse spermatogenic stem cells continually interconvert between equipotent singly isolated and syncytial states. Cell Stem Cell *14*, 658–672.

Helsel, A.R., Oatley, M.J., and Oatley, J.M. (2017a). Glycolysis-optimized conditions enhance maintenance of regenerative integrity in mouse spermatogonial stem cells during long-term culture. Stem Cell Rep. *8*, 1430–1441.

Helsel, A.R., Yang, Q.E., Oatley, M.J., Lord, T., Sablitzky, F., and Oatley, J.M. (2017b). ID4 levels dictate the stem cell state in mouse spermatogonia. Development *144*, 624–634.

Hilscher, B., Hilscher, W., Bulthoff-Ohnolz, B., Kramer, U., Birke, A., Pelzer, H., and Gauss, G. (1974). Kinetics of gametogenesis. I. Comparative histological and autoradiographic studies of oocytes and transitional prospermatogonia during oogenesis and prespermatogenesis. Cell Tissue Res. *154*, 443–470.

Hogarth, C.A., Arnold, S., Kent, T., Mitchell, D., Isoherranen, N., and Griswold, M.D. (2015). Processive pulses of retinoic acid propel asynchronous and continuous murine sperm production. Biol. Reprod. *92*, 37.

Huckins, C. (1971a). Cell cycle properties of differentiating spermatogonia in adult Sprague-Dawley rats. Cell Tissue Kinet. *4*, 139–154.

Huckins, C. (1971b). The spermatogonial stem cell population in adult rats. 3. Evidence for a long-cycling population. Cell Tissue Kinet. *4*, 335–349.

Huckins, C. (1971c). The spermatogonial stem cell population in adult rats. I. Their morphology, proliferation and maturation. Anat. Rec. *169*, 533–557.

Huckins, C. (1971d). The spermatogonial stem cell population in adult rats. II. A radioautographic analysis of their cell cycle properties. Cell Tissue Kinet. *4*, 313–334.

Ikami, K., Tokue, M., Sugimoto, R., Noda, C., Kobayashi, S., Hara, K., and Yoshida, S. (2015). Hierarchical differentiation competence in response to retinoic acid ensures stem cell maintenance during mouse spermatogenesis. Development *142*, 1582–1592.

Ishii, T., Bannai, S., and Sugita, Y. (1981). Mechanism of growth stimulation of L1210 cells by 2-mercaptoethanol in vitro. Role of the mixed disulfide of 2-mercaptoethanol and cysteine. J. Biol. Chem. *256*, 12387–12392.

Ishii, T., and Mann, G.E. (2014). Redox status in mammalian cells and stem cells during culture in vitro: critical roles of Nrf2 and cystine transporter activity in the maintenance of redox balance. Redox Biol. *2*, 786–794.

Kanatsu-Shinohara, M., Ogonuki, N., Inoue, K., Miki, H., Ogura, A., Toyokuni, S., and Shinohara, T. (2003). Long-term proliferation in culture and germline transmission of mouse male germline stem cells. Biol. Reprod. *69*, 612–616.

Kanatsu-Shinohara, M., Tanaka, T., Ogonuki, N., Ogura, A., Morimoto, H., Cheng, P.F., Eisenman, R.N., Trumpp, A., and Shinohara, T. (2016). Myc/Mycn-mediated glycolysis enhances mouse spermatogonial stem cell self-renewal. Genes Dev. *30*, 2637–2648.

Kanatsu-Shinohara, M., Toyokuni, S., and Shinohara, T. (2004). CD9 is a surface marker on mouse and rat male germline stem cells. Biol. Reprod. *70*, 70–75.

Kanatsu-Shinohara, M., Yamamoto, T., Toh, H., Kazuki, Y., Kazuki, K., Imoto, J., Ikeo, K., Oshima, M., Shirahige, K., Iwama, A., et al. (2019). Aging of spermatogonial stem cells by Jnk-mediated glycolysis activation. Proc. Natl. Acad. Sci. U S A *116*, 16404–16409.

Kojima, M.L., de Rooij, D.G., and Page, D.C. (2019). Amplification of a broad transcriptional program by a common factor triggers the meiotic cell cycle in mice. Elife *8*, e43738.

Koppula, P., Zhang, Y., Zhuang, L., and Gan, B. (2018). Amino acid transporter SLC7A11/xCT at the crossroads of regulating redox homeostasis and nutrient dependency of cancer. Cancer Commun. (Lond) *38*, 12.

Kubota, H., and Brinster, R.L. (2006). Technology insight: in vitro culture of spermatogonial stem cells and their potential therapeutic uses. Nat. Clin. Pract. Endocrinol. Metab. *2*, 99–108.

Lam, E.W., Brosens, J.J., Gomes, A.R., and Koo, C.Y. (2013). Forkhead box proteins: tuning forks for transcriptional harmony. Nat. Rev. Cancer *13*, 482–495.

Lantz, K.A., Vatamaniuk, M.Z., Brestelli, J.E., Friedman, J.R., Matschinsky, F.M., and Kaestner, K.H. (2004). Foxa2 regulates multiple pathways of insulin secretion. J. Clin. Invest. *114*, 512–520.

Leblond, C.P., and Clermont, Y. (1952). Definition of the stages of the cycle of the seminiferous epithelium in the rat. Ann. N. Y Acad. Sci. *55*, 548–573.

Lok, D., Jansen, M.T., and de Rooij, D.G. (1983). Spermatogonial multiplication in the Chinese hamster. II. Cell cycle properties of undifferentiated spermatogonia. Cell Tissue Kinet. *16*, 19–29.

Mastroberardino, L., Spindler, B., Pfeiffer, R., Skelly, P.J., Loffing, J., Shoemaker, C.B., and

Verrey, F. (1998). Amino-acid transport by heterodimers of 4F2hc/CD98 and members of a permease family. Nature *395*, 288–291.

Miki, K., Qu, W., Goulding, E.H., Willis, W.D., Bunch, D.O., Strader, L.F., Perreault, S.D., Eddy, E.M., and O'Brien, D.A. (2004). Glyceraldehyde 3-phosphate dehydrogenase-S, a sperm-specific glycolytic enzyme, is required for sperm motility and male fertility. Proc. Natl. Acad. Sci. U S A *101*, 16501–16506.

Milanese, C., Bombardieri, C.R., Sepe, S., Barnhoorn, S., Payan-Gomez, C., Caruso, D., Audano, M., Pedretti, S., Vermeij, W.P., Brandt, R.M.C., et al. (2019). DNA damage and transcription stress cause ATP-mediated redesign of metabolism and potentiation of anti-oxidant buffering. Nat. Commun. *10*, 4887.

Monaghan, A.P., Kaestner, K.H., Grau, E., and Schutz, G. (1993). Postimplantation expression patterns indicate a role for the mouse forkhead/HNF-3 alpha, beta and gamma genes in determination of the definitive endoderm, chordamesoderm and neuroectoderm. Development *119*, 567–578.

Nagano, M.C. (2003). Homing efficiency and proliferation kinetics of male germ line stem cells following transplantation in mice. Biol. Reprod. *69*, 701–707.

Nagano, M., Avarbock, M.R., Leonida, E.B., Brinster, C.J., and Brinster, R.L. (1998). Culture of mouse spermatogonial stem cells. Tissue Cell *30*, 389–397.

Nakagawa, T., Nabeshima, Y., and Yoshida, S. (2007). Functional identification of the actual and potential stem cell compartments in mouse spermatogenesis. Dev. Cell *12*, 195–206.

Nakagawa, T., Sharma, M., Nabeshima, Y., Braun, R.E., and Yoshida, S. (2010). Functional hierarchy and reversibility within the murine spermatogenic stem cell compartment. Science *328*, 62–67.

Oakberg, E.F. (1971). Spermatogonial stem-cell renewal in the mouse. Anat. Rec. *169*, 515–531.

Oatley, M.J., Kaucher, A.V., Racicot, K.E., and Oatley, J.M. (2011). Inhibitor of DNA binding 4 is expressed selectively by single spermatogonia in the male germline and regulates the self-renewal of spermatogonial stem cells in mice. Biol. Reprod. *85*, 347–356.

Odet, F., Duan, C., Willis, W.D., Goulding, E.H., Kung, A., Eddy, E.M., and Goldberg, E. (2008). Expression of the gene for mouse lactate dehydrogenase C (Ldhc) is required for male fertility. Biol. Reprod. *79*, 26–34.

Odet, F., Gabel, S., London, R.E., Goldberg, E., and Eddy, E.M. (2013). Glycolysis and mitochondrial respiration in mouse LDHC-null sperm. Biol. Reprod. *88*, 95.

Odet, F., Gabel, S.A., Williams, J., London, R.E., Goldberg, E., and Eddy, E.M. (2011). Lactate dehydrogenase C and energy metabolism in mouse sperm. Biol. Reprod. *85*, 556–564.

Ogawa, T., Dobrinski, I., and Brinster, R.L. (1999). Recipient preparation is critical for spermatogonial transplantation in the rat. Tissue Cell *31*, 461–472.

Orwig, K.E., Shinohara, T., Avarbock, M.R., and Brinster, R.L. (2002). Functional analysis of stem cells in the adult rat testis. Biol. Reprod. *66*, 944–949.

Panowski, S.H., Wolff, S., Aguilaniu, H., Durieux, J., and Dillin, A. (2007). PHA-4/Foxa mediates diet-restriction-induced longevity of C. elegans. Nature *447*, 550–555.

Perey, B., Clermont, Y., and Leblond, C.P. (1961). The wave of the seminiferous epithelium in the rat. Am. J. Anat. *108*, 47–78.

Pontén, F., Jirström, K., and Uhlen, M. (2008). The Human Protein Atlas–a tool for pathology. J. Pathol. *4*, 387–393.

Puigserver, P., and Rodgers, J.T. (2006). Foxa2, a novel transcriptional regulator of insulin sensitivity. Nat. Med. *12*, 38–39.

Rato, L., Alves, M.G., Socorro, S., Duarte, A.I., Cavaco, J.E., and Oliveira, P.F. (2012). Metabolic regulation is important for spermatogenesis. Nat. Rev. Urol. *9*, 330–338.

Rausa, F.M., Tan, Y., Zhou, H., Yoo, K.W., Stolz, D.B., Watkins, S.C., Franks, R.R., Unterman, T.G., and Costa, R.H. (2000). Elevated levels of hepatocyte nuclear factor 3beta in mouse hepatocytes influence expression of genes involved in bile acid and glucose homeostasis. Mol. Cell. Biol. *20*, 8264–8282.

Sada, A., Suzuki, A., Suzuki, H., and Saga, Y. (2009). The RNA-binding protein NANOS2 is required to maintain murine spermatogonial stem cells. Science *325*, 1394–1398.

Sato, H., Shiiya, A., Kimata, M., Maebara, K., Tamba, M., Sakakura, Y., Makino, N., Sugiyama, F., Yagami, K., Moriguchi, T., et al. (2005). Redox imbalance in cystine/glutamate transporter-deficient mice. J. Biol. Chem. *280*, 37423–37429.

Sato, H., Tamba, M., Ishii, T., and Bannai, S. (1999). Cloning and expression of a plasma membrane cystine/glutamate exchange transporter composed of two distinct proteins. J. Biol. Chem. *274*, 11455–11458.

Schafer, F.Q., and Buettner, G.R. (2001). Redox environment of the cell as viewed through the redox state of the glutathione disulfide/glutathione couple. Free Radic. Biol. Med. *30*, 1191–1212.

Schultz, N., Hamra, F.K., and Garbers, D.L. (2003). A multitude of genes expressed solely in meiotic or postmeiotic spermatogenic cells offers a myriad of contraceptive targets. Proc. Natl. Acad. Sci. U S A *100*, 12201–12206.

Shami, A.N., Zheng, X., Munyoki, S.K., Ma, Q., Manske, G.L., Green, C.D., Sukhwani, M., Orwig, K.E., Li, J.Z., and Hammoud, S.S. (2020). Single-Cell RNA sequencing of human, macaque, and mouse testes uncovers conserved and divergent features of mammalian spermatogenesis. Dev. Cell *54*, 529–547 e512.

Stockwell, B.R., Friedmann Angeli, J.P., Bayir, H., Bush, A.I., Conrad, M., Dixon, S.J., Fulda, S., Gascon, S., Hatzios, S.K., Kagan, V.E., et al. (2017). Ferroptosis: a regulated cell death nexus linking metabolism, redox biology, and disease. Cell *171*, 273–285.

Suzuki, A., Igarashi, K., Aisaki, K., Kanno, J., and Saga, Y. (2010). NANOS2 interacts with the CCR4-NOT deadenylation complex and leads to suppression of specific RNAs. Proc. Natl. Acad. Sci. U S A *107*, 3594–3599.

Suzuki, H., Sada, A., Yoshida, S., and Saga, Y. (2009). The heterogeneity of spermatogonia is revealed by their topology and expression of marker proteins including the germ cell-specific proteins Nanos2 and Nanos3. Dev. Biol. *336*, 222–231.

Tan, K., Song, H.W., Thompson, M., Munyoki, S., Sukhwani, M., Hsieh, T.C., Orwig, K.E., and Wilkinson, M.F. (2020). Transcriptome profiling reveals signaling conditions dictating human spermatogonia fate in vitro. Proc. Natl. Acad. Sci. U S A *117*, 17832–17841.

van Pelt, A.M., and de Rooij, D.G. (1991). Retinoic acid is able to reinitiate spermatogenesis in vitamin A-deficient rats and high replicate doses support the full development of spermatogenic cells. Endocrinology *128*, 697–704.

von Kopylow, K., Kirchhoff, C., Jezek, D., Schulze, W., Feig, C., Primig, M., Steinkraus, V., and Spiess, A.N. (2010). Screening for biomarkers of spermatogonia within the human testis: a whole genome approach. Hum Reprod *25*, 1104–1102.

Wang, X., Vatamaniuk, M.Z., Roneker, C.A., Pepper, M.P., Hu, L.G., Simmons, R.A., and Lei, X.G. (2011). Knockouts of SOD1 and GPX1 exert different impacts on murine islet function and pancreatic integrity. Antioxid. Redox Signal. *14*, 391–401.

Weinstein, D.C., Ruiz i Altaba, A., Chen, W.S., Hoodless, P., Prezioso, V.R., Jessell, T.M., and Darnell, J.E., Jr. (1994). The winged-helix transcription factor HNF-3 beta is required for notochord development in the mouse embryo. Cell *78*, 575–588.

Willis, J.A., and Schleich, T. (1995). 13C-NMR spectroscopic studies of 2-mercaptoethanol-stimulated glutathione synthesis in the intact ocular lens. Biochim. Biophys. Acta *1265*, 1–7.

Wolfrum, C., Asilmaz, E., Luca, E., Friedman, J.M., and Stoffel, M. (2004). Foxa2 regulates lipid metabolism and ketogenesis in the liver during fasting and in diabetes. Nature *432*, 1027–1032.

Wu, Z., Falciatori, I., Molyneux, L.A., Richardson, T.E., Chapman, K.M., and Hamra, F.K. (2009). Spermatogonial culture medium: an effective and efficient nutrient mixture for culturing rat spermatogonial stem cells. Biol. Reprod. *81*, 77–86.

Xing, C., Cohen, J.C., and Boerwinkle, E. (2010). A weighted false discovery rate control procedure reveals alleles at FOXA2 that influence fasting glucose levels. Am. J. Hum. Genet. *86*, 440–446.

Zheng, K., Wu, X., Kaestner, K.H., and Wang, P.J. (2009). The pluripotency factor LIN28 marks undifferentiated spermatogonia in mouse. BMC Dev. Biol. *9*, 38.

Zhu, J., Berisa, M., Schworer, S., Qin, W., Cross, J.R., and Thompson, C.B. (2019). Transsulfuration activity can support cell growth upon extracellular cysteine limitation. Cell Metab. *30*, 865–876.e5.

iScience, Volume *24*

Supplemental Information

Spermatogonial Gene Networks Selectively Couple to Glutathione and Pentose Phosphate Metabolism but Not Cysteine Biosynthesis

David Prokai, Ashutosh Pudasaini, Mohammed Kanchwala, Andrew T. Moehlman, Alexandrea E. Waits, Karen M. Chapman, Jaideep Chaudhary, Jesus Acevedo, Patrick Keller, Xing Chao, Bruce R. Carr, and F. Kent Hamra

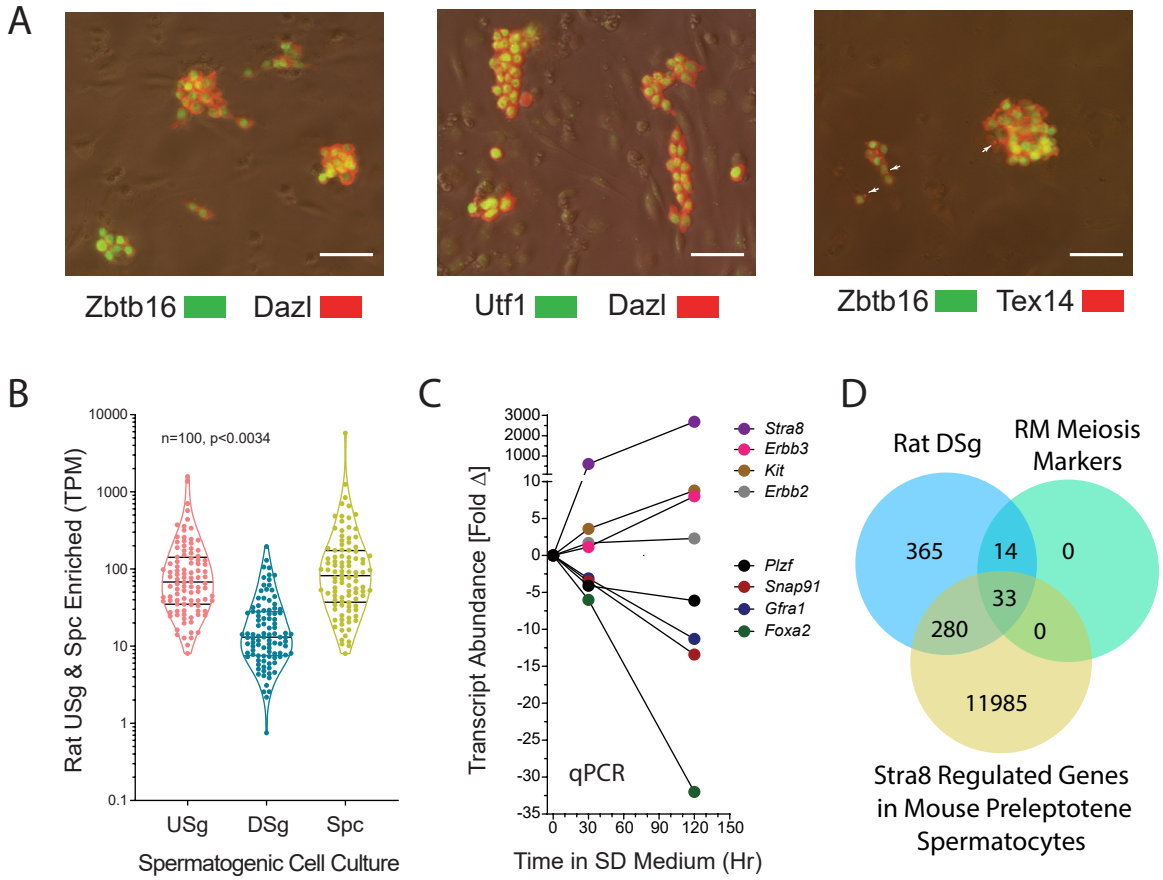

E

Meiotic Entry Markers

Rat Spermatogonia on Laminin in SD Medium

(d5, n=33 of 47 Conserved Rat & Mouse Pachytene Spermatocyte Markers)

Catsper2 Catsperg1 Ccdc173 Baz1a Agpat3 Phf7 Zfp949 Aurkc
Tmem30c Nr2c1 Cfb Efcab7 Slc2a8 Mcmdc2 Ngly1 Rdh11 Myo19 Lrrc6
Papss2 Gstt3 Cdc42ep3 Itgb3bp Clhc1 Dyx1c1 Mycbpap Polh
Sephs2 Rbm11 Lrguk Suco Chst1 Stambp Iqcg

Figure S1: Rat Spermatogonial Line Molecular Profiles, Related to Figure 1 and Table 1
(A) Brown Norway (BN) rat spermatogonial lines derived and sub-cultured on mouse embryonic fibroblasts (MEFs) in SG Medium (passage 8) co-express marker proteins for type A spermatogonia (Zbtb16, Utf1) and germ cells (Dazl, Tex14). Scale 40 µm
(B) Transcripts differentially enriched in rat undifferentiated spermatogonia (USg) and spermatocytes (Spc) versus differentiating spermatogonia (DSg). Transcripts/million RNA molecules (TPM).
(C) Relative abundance of marker transcripts in BN rat spermatogonial line (passage 14) measured by semi-quantitative PCR (qPCR) before (0 Hr) and after culture for 5 days in SD Medium (120Hr).
(D) Identification of Meiotic Entry Marker genes by overlap between transcripts enriched in rat DSg, conserved transcripts enriched across rat (R) Spc and mouse (M) pachytene spermatocytes (Ball et al., 2016) and genes regulated by Stra8 in mouse preleptotene spermatocytes (Kojima et al., 2019).
(E) Meiotic Entry Markers that are upregulated during rat spermatogonial differentiation on laminin (120h in SD Medium; n=33 common transcripts filtered for in panel "D").

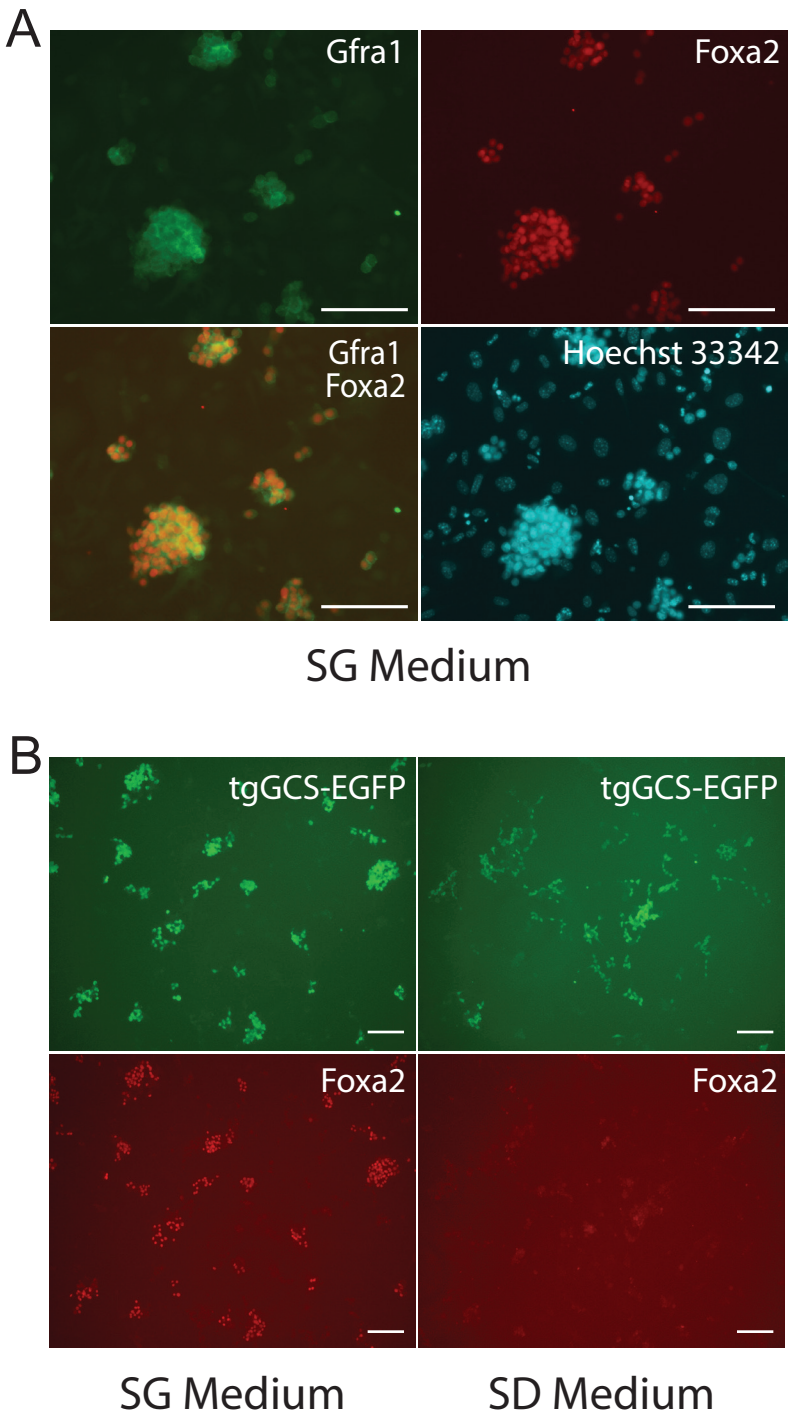

Figure S2: Spermatogonial Foxa2 is Abundant During Culture in SG Medium but is Down Regulated by Shifting Cultures into SD Medium, Related to Figure 2A-D

(A) Brown Norway rat spermatogonial lines derived and sub-cultured on MEFs in SG Medium (passage 14) co-express Gfra1 (green, cytoplasmic labeling) and Foxa2 (red, nuclear labeling). Hoechst 33342 (blue, nuclear labeling). Scale, 100 μm

(B) tgGCS-Egfp rat spermatogonial line (green, top panels) at passage12 after culture 120h in SG Medium (left panels) or SD Medium (Right panels). Note, reduction in Foxa2 labeling (red, bottom panels) intensity after culture in SD Medium. Scale, 100 μm

Figure S3

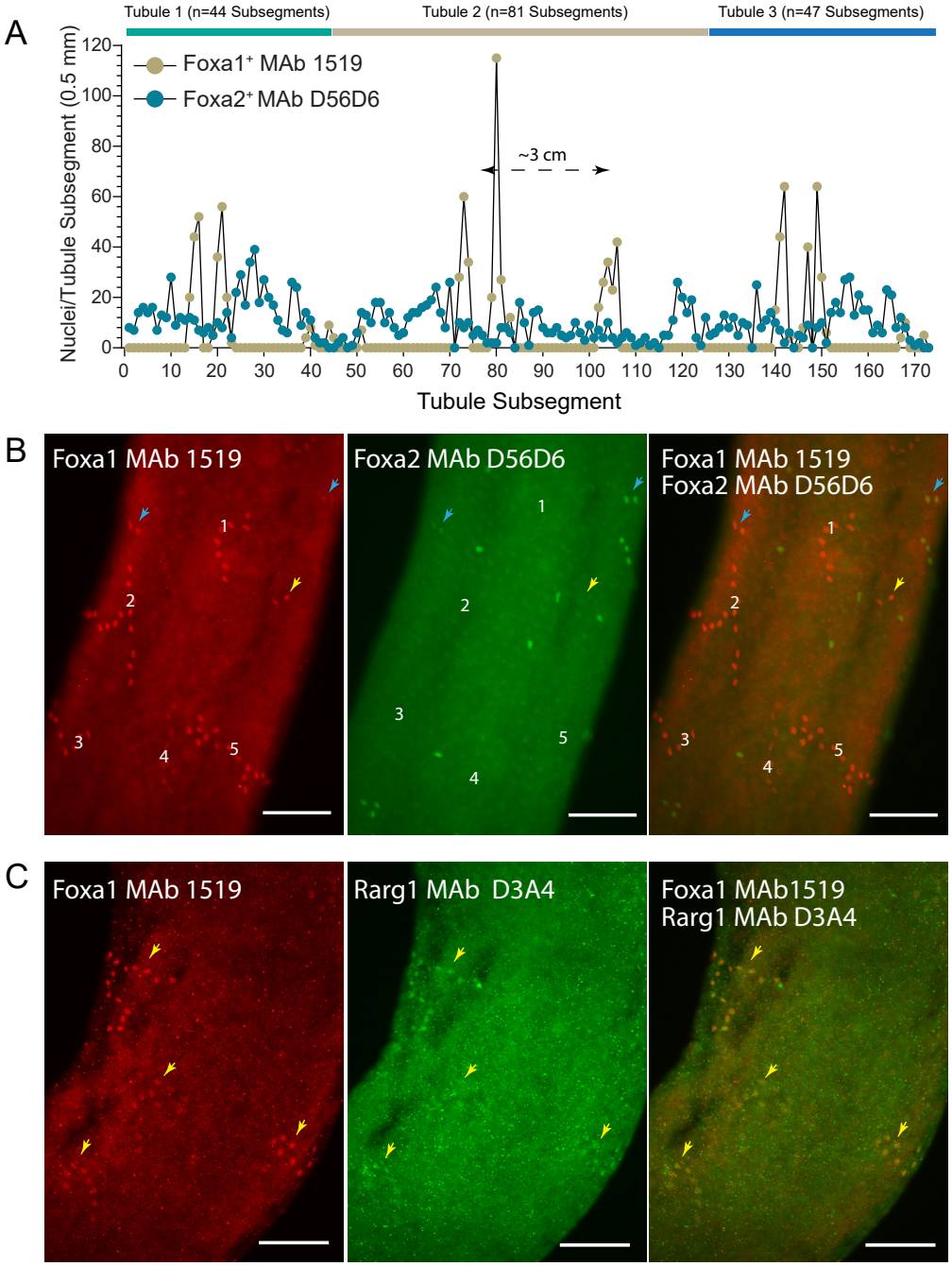

Figure S3: Nuclear Foxa1 and Foxa2 Mark Distinct Spermatogonial Types in Rats, Related to Figure 2E-F and Figure 3

(A) Foxa1+ (MAb 1519) and Foxa2+ (MAb D56D6) nuclei scored across contiguous subsegments (~0.5 mm long) of 3 seminiferous tubule whole mounts ranging from 2-4 cm long (Tubules 1-3) prepared from an adult rat (n=174 total subsegments, 1997 total nuclei scored, ~9 total cm). Note, the less prevalent "twin" cohorts of Foxa1+ spermatogonial nuclei enriched in distinct subsegments, whereas Foxa2+ nuclei were detected in most subsegments (~94%) analyzed across seminiferous tubules (n=163 of 174 total subsegments). The segmental order of spermatogenesis in, respective, Tubules 1-3 was not determined.

(B) Foxa1 MAb 1519 (red) and Foxa2 MAb D56D6 (green) co-labeling in a subsegment of a seminiferous tubule whole mount from an adult rat. Numbers 1-5 each overlay distinct Foxa1+, Foxa2- Aal-like spermatogonial syncytia. Note, co-labeling for rare double positive (Foxa1+, Foxa2+) Apr-like spermatogonial nuclei (Cyan Arrows), and a Foxa1+, Foxa2- Apr-like spermatogonial nuclei. Scale, 50 μm

(C) Foxa1 MAb 1519 (red) and Rarg1 MAb D3A4 (green) co-labeling (yellow arrows) in a subsegment of a seminiferous tubule whole mount from an adult rat. Scale, 50 μm

Figure S4

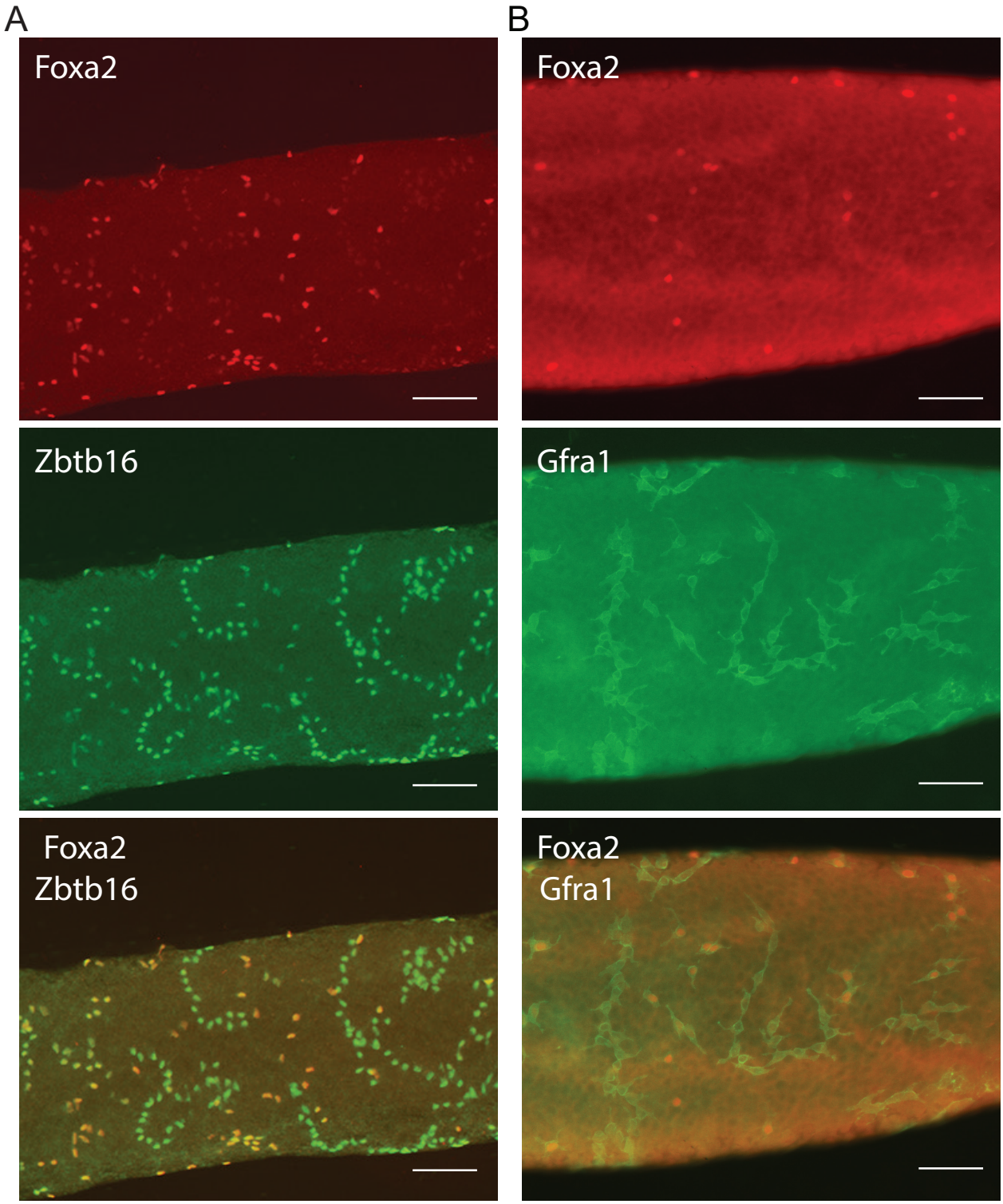

Figure S4: Foxa2 Selectively Marks Rat Undifferentiated As and Apr Spermatogonia, Related to Figure 2E-F and Figure 3

(A) Foxa2 MAb D56D6 (red) and ZBTB16 Mab 2A9 (green) co-labeling in a seminiferous tubule whole mount from an adult rat. Scale, 50 μm

(B) Foxa2 MAb D56D6 (red) and Gfra1 PAb AF560 (green) co-labeling in a seminiferous tubule whole mount from an adult rat. Scale, 50 μm

Figure S5

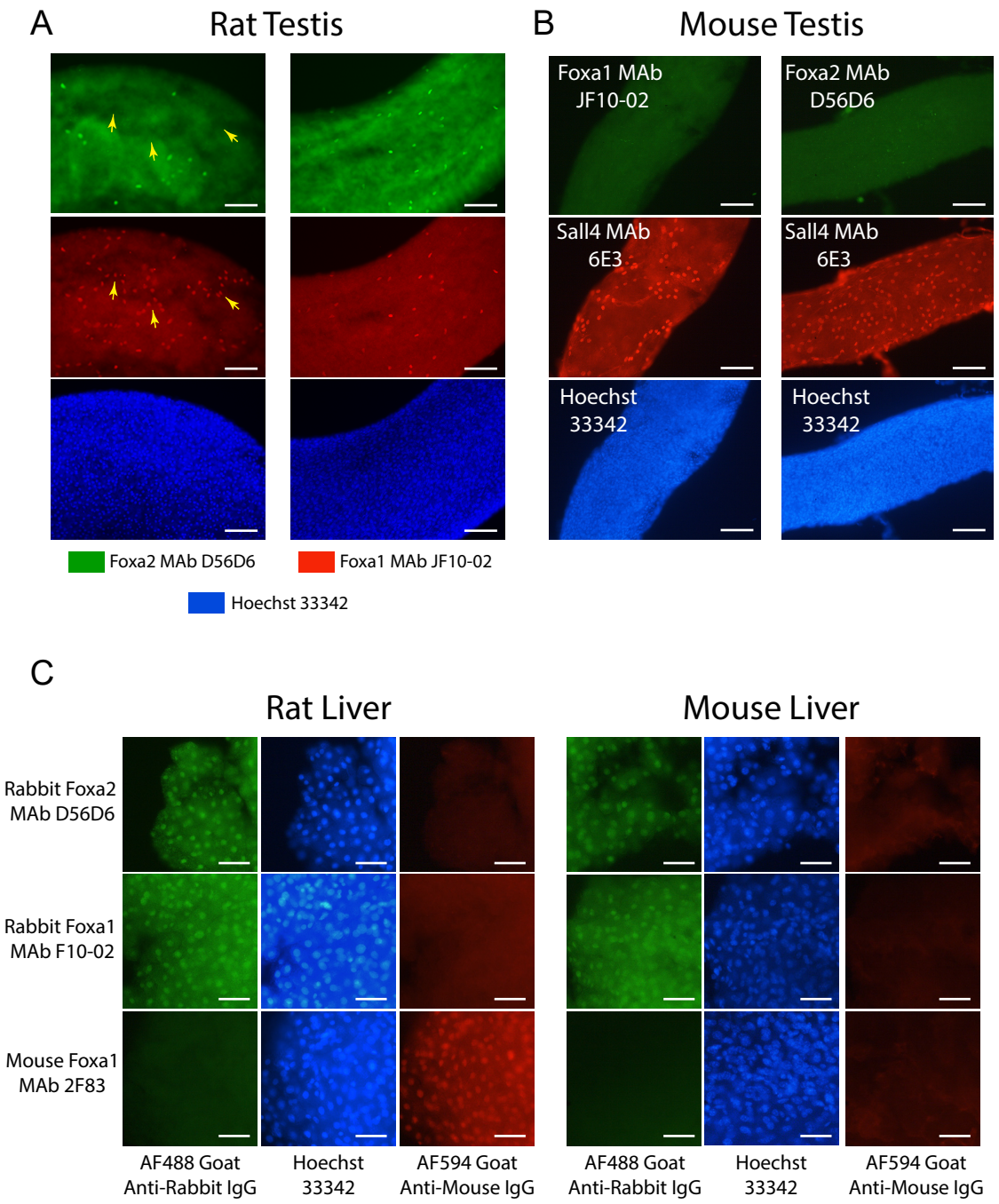

Figure S5: Foxa1 or Foxa2 MAb Labeling Profiles in Rat vs Mouse Liver and Testes, Related to Figure 2 and Figure 3

(A) Foxa1 MAb JF10-02 (red) and Foxa2 MAb D56D6 (green) co-labeling in 2 separate seminiferous tubule whole mounts from an adult rat shown in respective left and right panels. Note, Arrows in left panels point to Foxa1+, Foxa2- nuclei of Aal-like spermatogonia. Also note, Foxa1 MAb JF10-02 (red) labels the same As- and Apr-like nuclei as Foxa2 MAb D56D6 (green). Hoechst 33342 nuclear labeling (blue), Scale, 50 μm

(B) Co-labeling with Sall4 MAb 6E3 (red) and Foxa1 MAb JF10-02 (green) or Foxa2 MAb D56D6 (green) in seminiferous tubule whole mounts from an adult mouse. Scale, 50 μm

(C) Foxa1 MAb JF10-02, Foxa2 MAb D56D6 (green) and Foxa1 Mab 2F83 (red) labeling liver whole mounts from an adult rat (Rat Liver) and an adult mouse (Mouse Liver). Each sample was also individually co-labeled with respective rabbit or mouse isotype non-immune IgG (1 μg/ml) as background controls. Scale, 50 μm

Figure S6

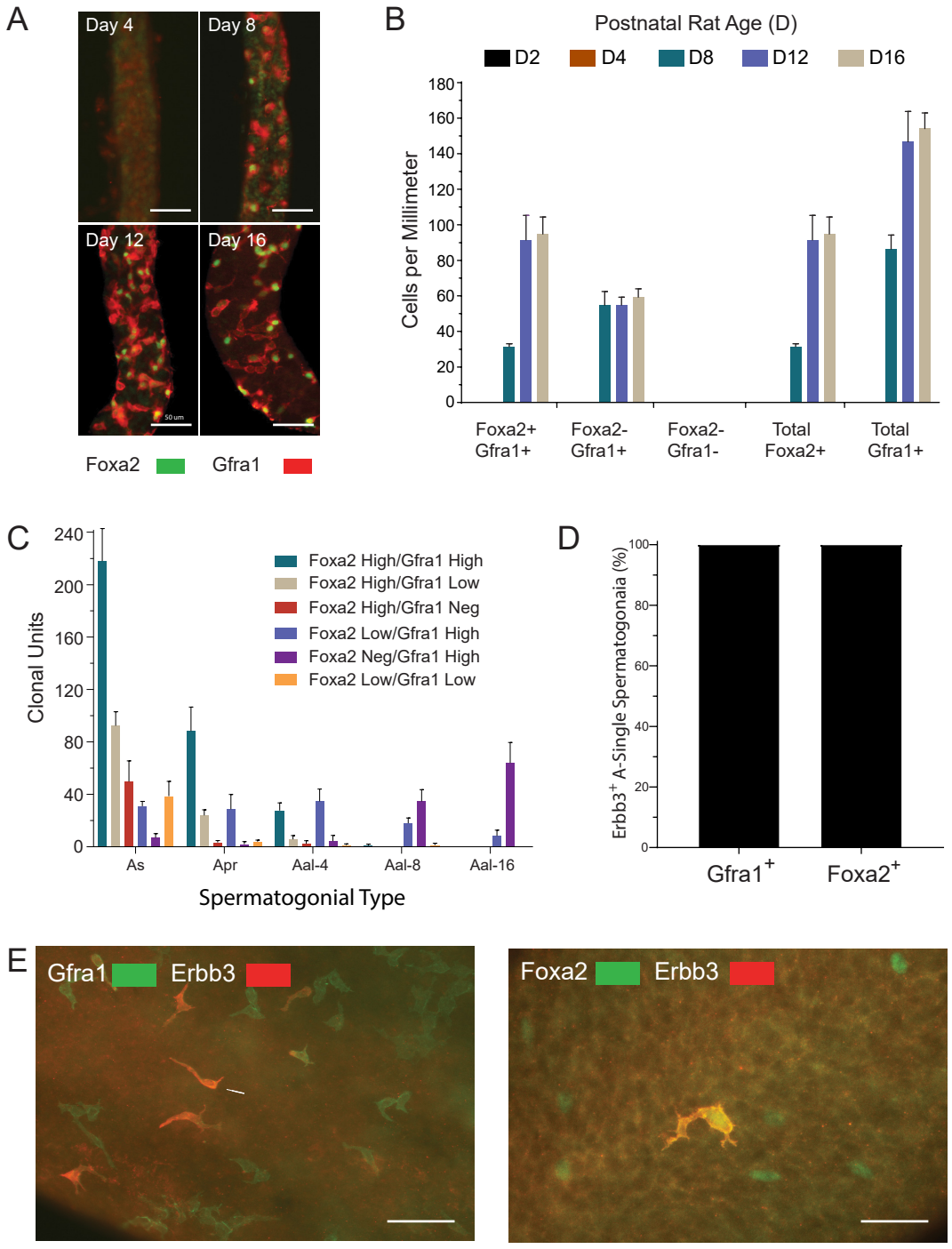

Figure S6: Postnatal Development of FOXA2+ Type A Spermatogonia, Related to Figure 2 and Figure 3

(A) Foxa2 and Gfra1 co-immunolabeling in D4, D8, D12 and D16 Sprague Dawley rat seminiferous tubules (whole mounts). Scale 50 μm

(B) Relative abundance of FOXA2+ and GFRA1+ spermatogonial types that develop postnatally in Sprague Dawley rat seminiferous tubules (D2 to D16).

(C) Gradient of GFRa1-immunolabeling in FOXA2+ As spermatogonia in adult Sprague Dawley rat seminiferous tubules (D110-120; mean counts ±SEM, 25-50, 0.5 to 2.0 mm tubule fragments/rat, n=3 rats).

(D) Erbb3+ As spermatogonia are Gfra1+ and Foxa2+ in Sprague Dawley rats (D110-120). Total n=34 Erbb3+/Foxa2+ and n=28 Erbb3+/Gfra1+ spermatogonia scored in tubule whole mounts (n=2 rats). Scale 40 μm

(E) Erbb3+, Gfra1+ and Erbb3- Gfra1+ As spermatogonia (arrows, Left) and Erbb3+, Foxa2+ and Erbb3-, Foxa2+ As spermatogonia (Right) in adult Sprague Dawley rat seminiferous tubules (D110-120). Scale 20 μm

Figure S7

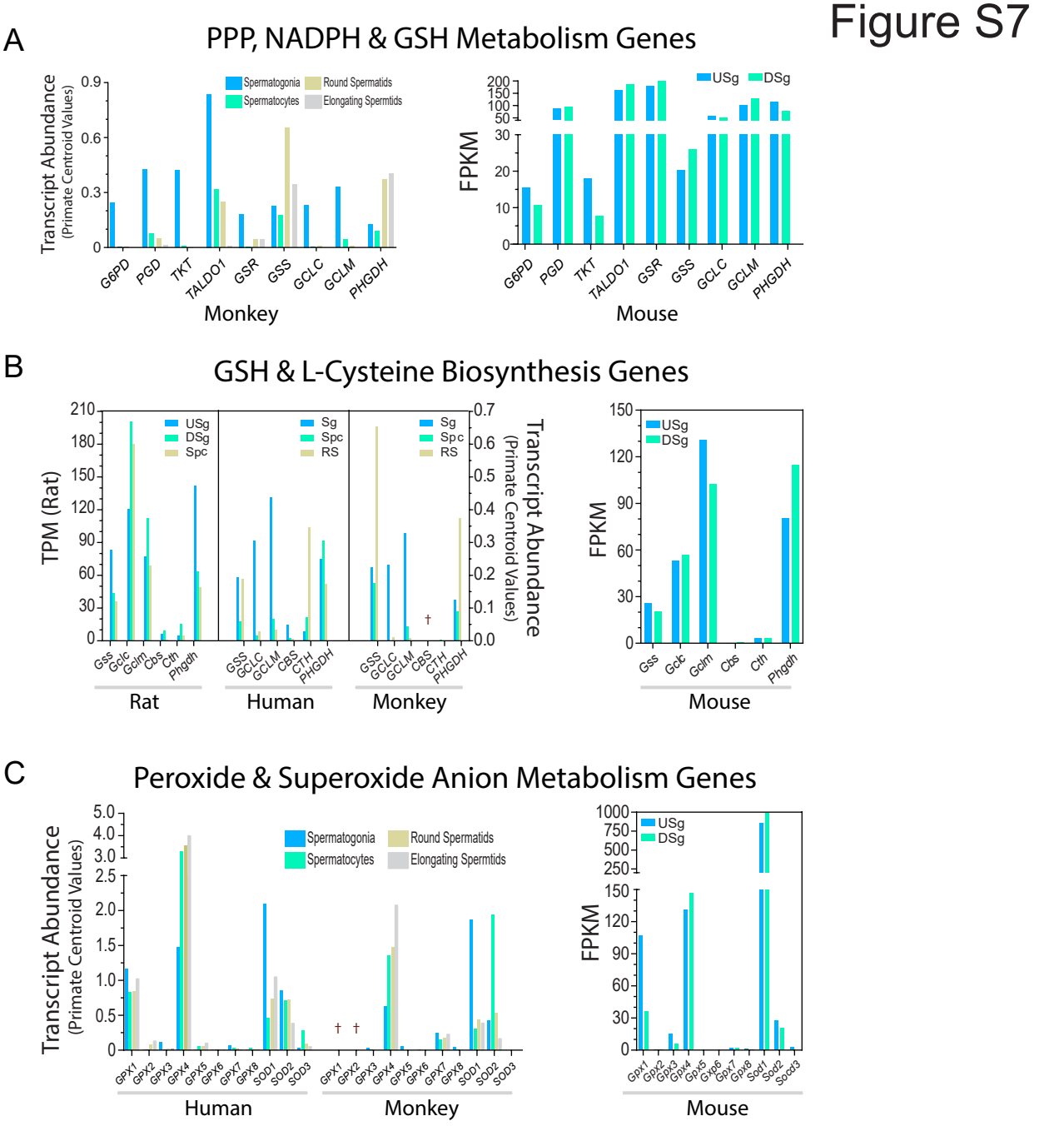

Figure S7: Conserved L-Glutathione Metabolism and Pentose Phosphate Pathway Gene Profiles in Rat, Mouse, Monkey and Human Spermatogenic Cells, Related to Figures 4-6

(A) Transcript profiles in Monkey and Mouse spermatogenic cells linked to the Pentose Phosphate (PPP), Nadph and L-Glutathione (GSH) metabolic pathways. Left Panel: Monkey transcript centroid values reported/spermatogenic cell type by (Shami et al., 2020). Right panel: Relative DNA fragments per kilobase of exon per million reads (FPKM) in flow sorted neonatal tgGFP-Id4 reporter mouse GFPbright (USg) vs GFPdim (DSg) spermatogonial populations isolated postnatal d8 by (Helsel et al., 2017).

(B) Relative abundance of Rat, Monkey, Human and Mouse spermatogenic cell transcripts encoding GSH biosynthesis pathway, L-Cysteine biosynthesis/transsulfuration pathway and 3-phosphoglycerate-oxidative L-Serine biosynthesis pathway enzymes. Left Panel: ordinate on left of graph represents relative TPM values for rat USg, DSg, Spc (Table S1, Figure 5E,F); ordinate on right of graph represents relative primate transcript centroid values reported/spermatogenic cell type (Shami et al., 2020). †no values recorded for monkey CBS. Right Panel: Relative FPKM values in flow sorted neonatal tgGFP-Id4 reporter mouse GFPbright (USg) vs GFPdim (DSg) spermatogonial populations by (Helsel et al., 2017).

(C) Relative abundance of Monkey, Human and Mouse spermatogenic cell transcripts encoding glutathione peroxidase and superoxide dismutase pathway enzymes. Left Panel: Relative primate transcript centroid values reported/spermatogenic cell type by (Shami et al., 2020). †no values recorded for monkey GPX1 or GPX2. Right Panel: FPKM values obtained from flow sorted neonatal tgGFP-Id4 reporter mouse GFPbright (USg) vs GFPdim (DSg) spermatogonial populations isolated postnatal d8 by (Helsel et al., 2017).

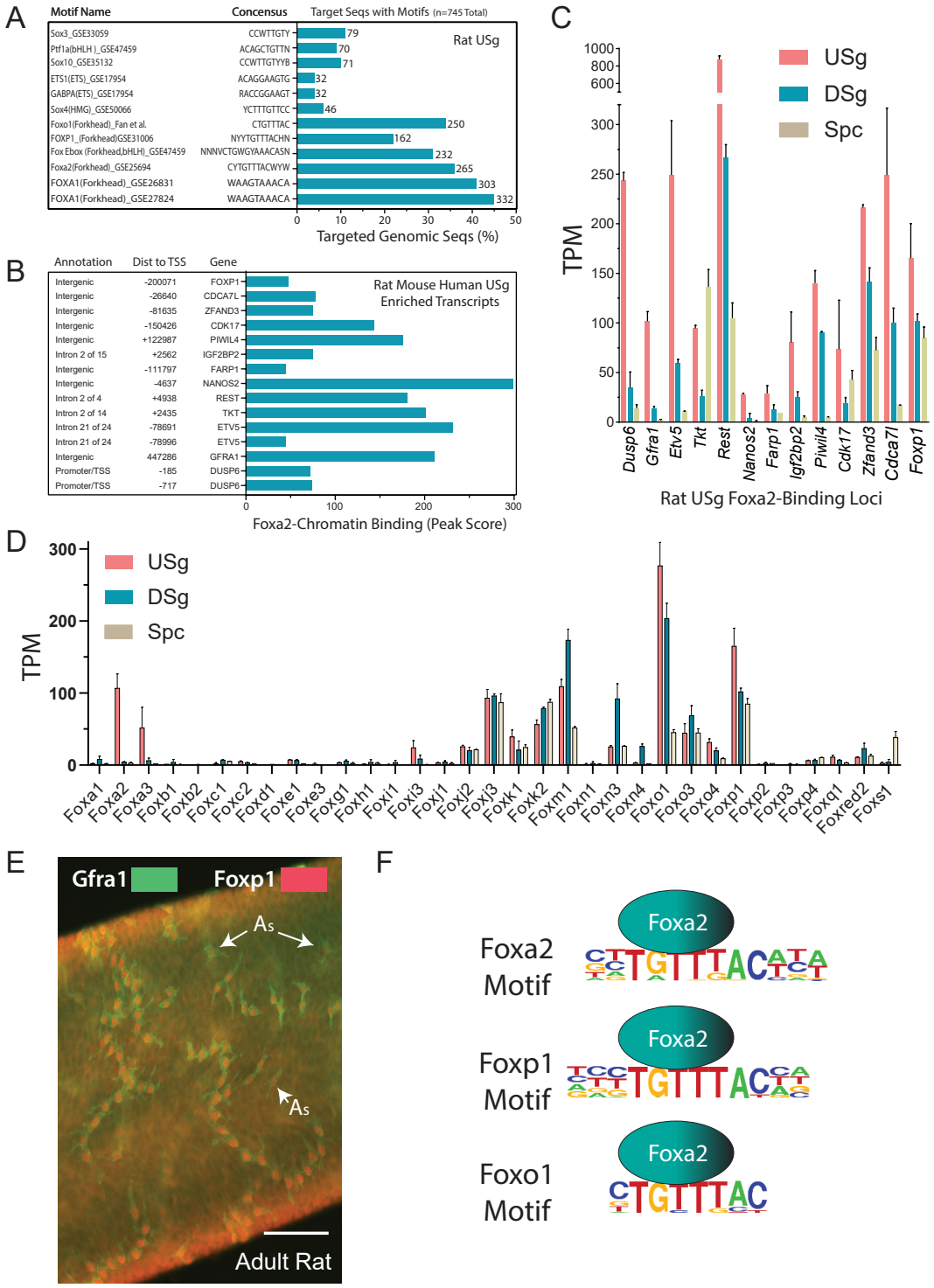

Figure S8: Foxa2-Binding Loci in Rat Undifferentiated Spermatogonia, Related to Figure 5A-C

(A) Target Foxa2-binding sequences identified by Chip-Seq. $p<0.0001$

(B) ChipSeq annotations for conserved USg-enriched genes (rat, mouse, human) that bind Foxa2 in rat USg (left) and respective peak scores (right)

(C) Transcript profiles in rat spermatogenic cell cultures for conserved USg-enriched genes (rat, mouse, human) that bind Foxa2 in rat USg

(D) Transcript profiles for conserved Fox-family genes in rat USg, DSg and Spc

(E) Co-immunolabeling for Foxp1 and Gfra1 in adult rat seminiferous tubule (D116), Scale, 50 µm. Arrows point to Foxp1+, Gfra1+ As spermatogonia

(F) Consensus Foxa2, Foxp1 and Foxo1 binding DNA motifs

Figure S9

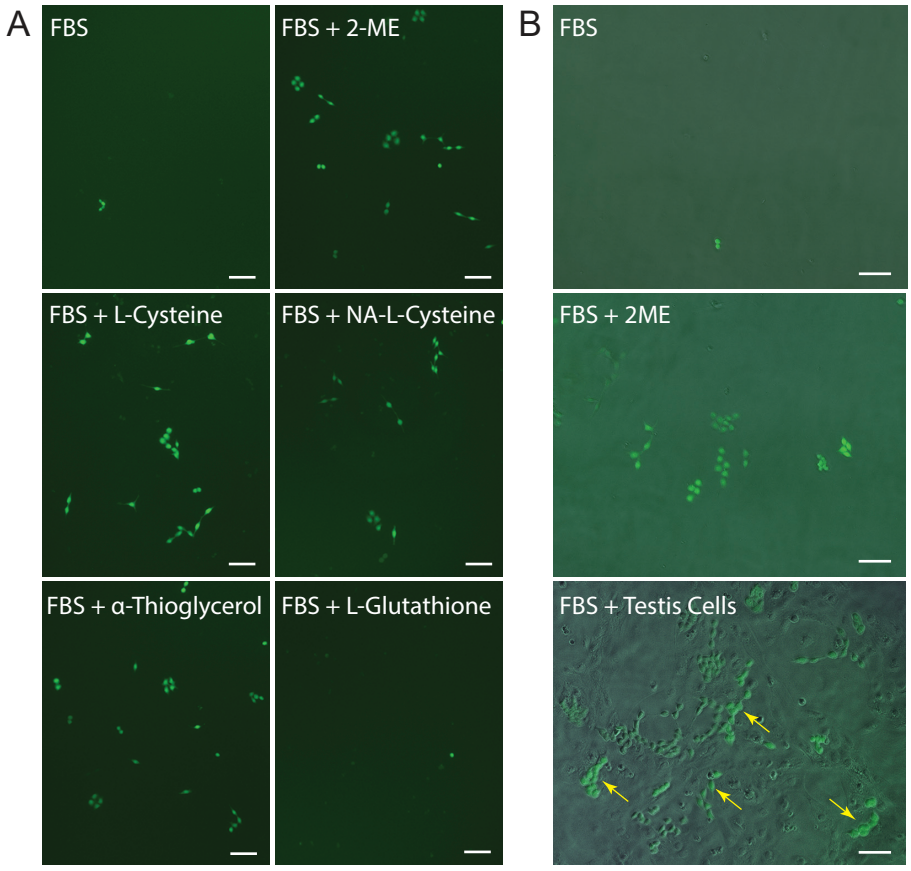

Figure S9: L-Cysteine-Like Mercaptans and Somatic Testis Cells Promote Spermatogonial Viability in Standard FBS-Containing Culture Medium, Related to Figure 7 and Figure 8

(A) Effects of L-cysteine and L-cysteine-like mercaptans observed on the viability of a spermatogonial stem cell line (tgGCS-Egfp+; passage 16) after 6d on laminin in control medium (FBS) with or without 2ME, 50 µM 2-Mercaptoethanol; TG, 50 µM alpha-thioglycerol; Cys, 1 mM L-Cysteine; NAC, 1 mM N-Acetyl-L-Cysteine. Images from 1 of 3 experiments. Scale, 60 µm

(B) Images of tgGCS-Egfp+ spermatogonia (passage 17) after culture in Ct medium (FBS) and Ct medium supplemented with 2ME (FBS + 2ME) or mitomycin C-treated wildtype rat somatic testis cells (FBS + Testis Cells) prepared as described (Hamra et al., 2002). Representative images from >3 experiments. Scale, 60 µm

(C) Left: Donor-derived spermatogenic colonies (green syncytia) in a recipient rat's seminiferous tubules d32 after transplanting tgGCS-EGFP+ rat spermatogonia cultured in Ct medium containing 2ME, as described Figure 8D. Right: Expanded view of region in yellow dashed box shown in Left panel. Yellow arrows point to the development of rat tgGCS-EGFP+ spermatogenic cell syncytia. Scale, 100 µm.

Transparent Methods

Animal Care and Use: Protocols for the use of rats in this study were approved by the Institutional Animal Care and Use Committee at UT-Southwestern Medical Center in Dallas, as certified by the Association for Assessment and Accreditation of Laboratory Animal Care International. Rats used for this study were housed in individually ventilated, Lab Products 2100 cages in a dedicated room with atmosphere controls set to 72ºF, 45-50% humidity during a 12h light/dark cycle (i.e. Light cycle = 6:00am-6:00pm, Central Standard Time adjusted for daylight savings time). Rats were fed Harlan Teklad Irradiated 7912, LM-485 Mouse/Rat Diet, 5% fat Diet and a continuous supply of reverse osmosis water. Wildtype Sprague Dawley rats were from Harlan/Envigo, Inc. and Brown Norway rats were form Charles Rivers, Inc.

Spermatogonial Culture: Rat spermatogonia were chosen for comparative analyses due to their traits that promote robust donor derived spermatogenesis in rat testes after being sub-cultured in SG Medium (Chapman et al., 2015b; Wu et al., 2009). Additionally, rat spermatogonial lines that are sub-cultured in SG Medium undergo spermatogonial differentiation *in vitro* on mouse embryonic fibroblasts (MEFs) or a laminin matrix after shifting into SD Medium (Chapman et al., 2015a; Hamra, 2017). Rat undifferentiated spermatogonial lines (Figure S1A) were derived from freshly isolated laminin binding spermatogonia and were maintained on MEFs using Spermatogonial Culture Medium (SG Medium), as previously detailed (Chapman et al., 2011; Wu et al., 2009). The base SG Medium formulation used contained: Dulbecco's Modified Eagle's Medium:Ham's F12 Nutrient Mixture (1:1)(Sigma), 6 ng/ml GDNF (R&D Systems), 6 ng/ml FGF2 (R&D Systems), 100 µM 2-mercaptoethanol (Sigma), 6 mM L-glutamine and a 1x concentration of the B27-Minus Vitamin-A Supplement solution (ThermoFisher). Spermatogonial lines were sub-cultured on feeder layers of MEFs (Chapman et al., 2011; Wu et al., 2009). Prior to *in vitro* or *in vivo* assays, spermatogonia were harvested from MEFs and incubated for 3-4 hours on gelatin-coated plates in SG Medium to deplete feeder cells (Hamra, 2017).

Isolating Undifferentiated Type A Spermatogonia: Seminiferous tubules were isolated from testes of 23-24 day old homozygous *SD-Tg*(*ROSA-EGFP*)*2-4*^{Reh}, or WT Brown Norway (Charles Rivers, Inc.) rats. The most advanced germ cell types in 23-day old male rats are spermatogonia and spermatocytes (Clermont and Perey, 1957). Rats of the *SD-Tg*(*ROSA-EGFP*)*2-4Reh* line were produced by pronuclear injection and are referred to as tg*GCS-EGFP* rats because they exhibit germ cell specific expression of enhanced green fluorescent protein during all steps in gametogenesis (Cronkhite et al., 2005). Tubules were enzymatically and mechanically dissociated into a cellular suspension to generate cultures of testis cells in serum-containing medium (Hamra et al., 2008; Hamra et al., 2002). The testis cell cultures were then used to isolate enriched populations of laminin-binding spermatogonia and laminin-non-binding spermatocytes by established methods (Hamra et al., 2008; Hamra et al., 2002) that first remove >95% of somatic testis cells from the germ cell population by negative selection on plastic and collagen, before positive selection for the spermatogonial stem cells based on their ability to bind to laminin (Hamra et al., 2002). *Note*, fractions of laminin-binding type A spermatogonia isolated by this procedure contain ~4% somatic cells, and ~5% differentiating spermatogonia plus spermatocytes; and fractions of laminin-non-binding germ cells contain >95% differentiating spermatogonia plus spermatocytes (Hamra et al., 2002; Hamra et al., 2004). The laminin-binding fraction of type A spermatogonia was used to initiate *in vitro* spermatogenesis colony forming assays and to derive rat spermatogonial stem cell lines.

In vitro Spermatogenesis Colony Forming Assays: Spermatogenesis colony forming assays were initiated by plating ~1000 to 10000 wildtype or tgGCS-EGFP rat spermatogonia/well (0.96cm^2) in Spermatogonial Culture Medium (SG Medium) at 36.5ºC, 5% CO_2 for analyses on USg, and then shifted cultures to SD Medium for analyses on differentiating spermatogonia (Hamra, 2017). Wells were pre-coated with ~5 µg/cm^2 laminin as described (Chapman et al., 2011). SD Medium is a modified formulation of the serum-free, SG Medium (Wu et al., 2009). To make SD Medium, SG Medium was modified to contain 6 ng/ml FGF2 (PGF0023, Life Technologies, Inc.), 2 ng/ml GDNF (512-GF, R&D Systems, Inc.), 40 ng/ml NRG1β1 T176-K246 (396-HB, R&D Systems, Inc.) and 3 µM all-trans-retinoic acid (R2625, Sigma, Inc.)(Hamra, 2017). Ferristatin-1 and Liproxstatin-1 were from R&D Systems, Inc and used at 1 and 0.1 µM, respectively.

Under standard, soma-free bioassay conditions using laminin matrix, on "day 0" (d0), spermatogonia were seeded in SG^F Medium (without GDNF) and maintained for 48 hr (n=2-10 wells/condition) before changing

them into SD Medium on d2. Medium was changed again on d4 and d6 using fresh SD Medium as needed. For most experiments, on d7-9 (i.e. d5-7 in SD Medium), medium was removed, and cells were either harvested for counting and transplanting germ cells (Hamra et al., 2004), lysed for measuring EGFP fluorescence units/cuture (Hamra, 2017), or were fixed in 4% paraformaldehyde, sodium phosphate buffer (0.1 M, pH 7.2) for 20-30 min on ice for molecular labeling and for scoring cells and colonies (Chapman et al., 2015a; Chapman et al., 2015b). Spermatogenesis colony forming units (S-CFU) were scored/well by counting numbers of single, paired and aligned tgGCS-EGFP^{+} spermatogenic cells (Hamra, 2017; Hamra et al., 2007).

In vivo Spermatogenesis Colony Forming Assays: WT Sprague Dawley rats at 12 days of age were injected (i.p.) with 12 mg/kg busulfan (4 mg/ml in 50% DMSO) and then used as recipient males at 24 days of age. Busulfan is a spermatogonial toxin commonly used to kill spermatogonia in recipient rat testes prior to transplantation because it increases the colonization efficiency by the donor stem cells (Hamra et al., 2002; Ogawa et al., 1999; Ryu et al., 2003). Donor tgGCS-EGFP^{+} spermatogonia (passage 14 and 16) were loaded into injection needles fashioned from 100 µl glass capillary tubes at a concentration of 0.5-4x10^{3} cells/65 µl SG medium containing 0.032% (wt/v) trypan blue and then the entire volume was transplanted into the seminiferous tubules of anesthetized rats by retrograde injection through the rete testes (Dym, 1976; Ogawa et al., 1999). Recipient males were analyzed 32 days post-transplantation and colonies of spermatogenesis expressing the tgGCS-EGFP transgene were scored using an IX70, Olympus fluorescence microscope (Olympus Inc.) equipped with Simple-PCI software (C-Imaging Systems, Compix, Cranberry Township, PA) (Hamra et al., 2004). Images of transgene expression in whole testes were captured using a Nikon SMZ1500 fluorescence stereomicroscope equipped with ACT-1 imaging software (Nikon Instruments, Inc. NY) (Hamra et al., 2004).

Immunofluorescence Labeling on Fixed Spermatogonial Cultures: In experiments that required molecular co-labeling, 4% paraformaldehyde fixed spermatogonial cultures were post-fixed in methanol for 5 min on ice and then washed 2x with phosphate buffered saline prior to fluorescence labeling with Hoechst 33342 dye and/or antibodies to Foxa2 D56D6, Rarg1 D3A4 (Cell Signaling Technology), Foxa1 JF10-02 (ThermoFisher), Foxa1 2F82 (Millipore), SNAP91 AP180-1, Foxa1 1519 (GeneTex), Snap91 clone (Abnova), Zbtb14 2A9 (Active Motif), Sall4 6E3 (Abnova), ERBB3 sc-285 (Santa Cruz), Gfra1 AF560 (R&D Systems), CD9 RPM.7 (BD biosciences), DazI-3 IgG (Hamra et al., 2002) and/or Tex14-1 IgG (Hamra et al., 2004). Isotype control antibodies: rabbit DA1E, mouse G2A1 and mouse E5Y6Q (Cell Signaling Technology). Spermatogenic colony scoring and imaging was conducted using an IX70, Olympus fluorescence microscope (Olympus Inc.) equipped with Simple-PCI software (C-Imaging Systems, Compix, Cranberry Township, PA).

Immunofluorescence Labeling in Seminiferous Tubule Whole Mounts: Seminiferous tubules (0.5 to 4 cm long pieces) from adult Sprague Dawley rat testes were dissected into 10 cm dishes containing Dulbecco modified Eagle medium:Ham F12 medium (1:1; DHF12 medium, catalog no. D8437; Sigma) at approximately 22–24°C. Individual tubules were teased apart from testes by blunt dissection, rinsed in fresh DHF12 medium, and fixed for 1 h at 4°C in 20 ml of 0.1 M sodium phosphate buffer (pH 7.2) containing 4% paraformaldehyde. Optimal co-labeling with antibodies was obtained by suspending the paraformaldehyde-fixed tubules in ice-cold methanol and then immediately incubating them for additional 20 min at −20°C. Following fixation, tubules were washed three times in 20 ml 1x phosphate buffered saline (PBS, ThermoFisher) for approximately 10 min/wash at 22–24°C before use. Freshly prepared tubule pieces were used directly for labeling with the antibodies raised to Foxa1, Foxa2, Rarg, Sall4, Zbtb16, Cd9 and Gfra1 (listed above) after pre-incubating for 1hr at 22-24ºC in blocking buffer (1x Roche Blocking Reagent, 0.1% v/v Triton X-100 in PBS). For the antibodies raised to Snap91 or Erbb3 (listed above), tubule pieces were aliquoted into microfuge tubes containing 800 µl of 10 mM sodium citrate (pH 6.0) and incubated at 70°C (4-5 min anti-Snap91; 7-8 min anti-Erbb3), washed 1x with PBS at 22–24°C and transferred into blocking buffer. Tubules were incubated overnight at 22–24°C with respective antibodies in fresh blocking buffer, and then processed for labeling with highly cross absorbed Alexa Flour 488, 594 and 647 secondary antibodies and Hoechst 33342 dye as described below for testis sections. After treatment with secondary antibodies, seminiferous tubule peices were cover slipped for viewing and imaging using Fluorogel mounting medium (17985-10; Electron Microscopy Sciences).

Immunofluorescence Labeling in Testis Sections: Frozen testis sections were prepared for immunofluorescence labeling from adult Sprague Dawley rats, as described (Abid et al., 2014), and then treated for 18–24 h at 22–24°C with respective antibodies diluted in blocking buffer: anti-Foxa2 D56D6 (Cell Signaling Technology) and anti-Gfra1 AF560 (R&D Systems). After treatment with primary antibodies, sections were washed three times for 10 min/wash in 50 ml of PBS and then incubated for 40 min at 22–24°C with respective Alexa Fluor 488 or Alexa Fluor 594 (Invitrogen, Inc.) secondary antibodies diluted to 4 µg/ml in PBS containing 2.5 µg/ml Hoechst 33342 dye. After treatment with secondary antibodies, sections were washed three times for 10 min/wash in 50 ml of PBS. After the third wash in PBS, sections were cover-slipped for viewing using Fluorogel mounting medium (17985-10; Electron Microscopy Sciences).

Analysis of Spermatogonial Subtypes:
Seminiferous tubule pieces used for analysis of epithelial subsegments containing $Foxa2^+$ and $Gfra1^+$ spermatogonia were imaged in whole mounts (Abid et al., 2014). Immunofluorescence-based data on numbers of spermatogonia were collected in testis sections and seminiferous tubule whole mounts after labeling with antibodies to spermatogonial markers, as detailed above in *Immunofluorescence labeling in seminiferous tubule whole mounts*. Spermatogonial counts in whole mounts were normalized per average spermatogenic wavelength in adult Sprague-Dawley rats (2.6 cm/wave) (Perey B *et al*., 1961).

$Foxa1^+$ (MAb 1519) and $Foxa2^+$ (MAb D56D6) nuclei were scored from images captured (0.5 mm l x 0.4 mm h) across the basal compartment of contiguous subsegments from 3 seminiferous tubule whole mounts (Tubules 1-3) of unknown segmental order prepared from an adult rat (n=174 total subsegments, 1997 total nuclei scored, ~9 total cm). The term “subsegment” is used in the current study based on scoring cells along contiguous ~0.5 mm regions of seminiferous tubules/image (single focal plane), as the mean length of full seminiferous tubule epithelial segments representing the respective 14 stages of rat spermatogenesis ranged from 0.4 mm (Stage X) to 3.2 mm (Stage VII) long (Perey et al., 1961). It was therefore calculated that most images of tubules scored would capture predominantly partial segments as defined for respective seminiferous epithelial stages (Perey et al., 1961). Images from fluorescence labeling were acquired using an IX70 fluorescence microscope (Olympus, Inc.) equipped with Simple-PCI software (Compix, Inc., Imaging Systems). Images captured included the full diameter of each tubular subsegment scored.

Western Blotting: Whole cell lysates were prepared in lysis buffer (50 mM Tris, 150 mM NaCl, 1 mM EDTA, 1% IGEPAL CA-630) with protease inhibitors (Complete EDTA-free protease inhibitor tablets, Roche Applied Science, Inc, cat # 11836170001), and phosphatase inhibitors (PhosSTOP, Roche Applied Science, Inc, cat # 4906845001). Samples were clarified by centrifugation in a microfuge at 4 degrees for 10 minutes. Samples were run on SDS PAGE gels under reducing conditions and transferred to nitrocellulose. Blots were probed overnight with primary antibodies as described (Hamra et al., 2002) and then washed and the probed with secondary antibodies labeled with IRDye 800CW or 680LT were from Li-Cor Biosciences, Inc. Blots were imaged on Odyssey Classic Quantitative Fluorescence Imaging System, Model 9120, also from Li-Cor Biosciences. The western blot analysis in Figure 6A was performed by Raybiotech, Inc. (Peachtree Corners, GA), using an automated Capillary Electrophoresis Immunoassay machine (WES™, ProteinSimple Santa Clara, CA). In brief, 3.0 µl of 0.2 µg/µl concentration samples was mixed with a master mix (ProteinSimple) to a final concentration of 1x sample buffer, 1x fluorescent molecular weight marker, and 40mM dithiothreitol (DTT) and heated at 95°C for 5 min. The samples, blocking reagent, wash buffer, primary antibodies, secondary antibodies, and chemiluminescent substrate were dispensed into designated wells in the manufacturer provided microplate. After plate loading, the separation electrophoresis and immunodetection steps took place in the fully automated capillary system. Auto-Western analysis was carried out at room temperature, and instrument default settings were used.

Rat Spermatogonial Metabolite Profiling by LC-MS: Cultures of USg on laminin in SG Medium (0 hr) and DSg on laminin in SD Medium (120h) were prepared as described above in *In vitro Spermatogenesis Colony Forming Assays* and harvested using PBS, 0.5% BSA as described (Hamra et al., 2002). Spermatogonial pellets were washed with 0.9% NaCl prior to extracting pellets with methanol using LCMS grade reagents. Methanol extracts made from each group of USg and DSg cultures (n=3 replicate cultures/group) where analyzed by targeted LC-MS-based metabolite profiling measurements (Table S5) at the Children’s Medical Institute Metabolomics Facility, UT Southwestern Medical Center in Dallas.

Data acquisition was performed by reverse-phase chromatography on a 1290 UHPLC liquid chromatography (LC) system interfaced to a high-resolution mass spectrometry (HRMS) 6550 iFunnel Q-TOF mass spectrometer (MS) (Agilent Technologies, CA). The MS was operated in both positive and negative (ESI+ and ESI-) modes. Analytes were separated on an Acquity UPLC® HSS T3 column (1.8 µm, 2.1 x 150 mm, Waters, MA). The column was kept at room temperature. Mobile phase A composition was 0.1% formic acid in water and mobile phase B composition was 0.1% formic acid in 100% ACN. The LC gradient was 0 min: 1% B; 5 min: 5% B; 15 min: 99%; 23 min: 99%; 24 min: 1%; 25 min: 1%. The flow rate was 250 µL min-1. The sample injection volume was 5 µL. ESI source conditions were set as follows: dry gas temperature 225 °C and flow 18 L min-1, fragmentor voltage 175 V, sheath gas temperature 350 °C and flow 12 L min-1, nozzle voltage 500 V, and capillary voltage +3500 V in positive mode and −3500 V in negative. The instrument was set to acquire over the full m/z range of 40–1700 in both modes, with the MS acquisition rate of 1 spectrum s-1 in profile format.

Raw data files (.d) were processed using Profinder B.08.00 SP3 software (Agilent Technologies, CA) with an in-house database containing retention time and accurate mass information on 600 standards from Mass Spectrometry Metabolite Library (IROA Technologies, MA) which was created under the same analysis conditions. The in-house database matching parameters: mass tolerance 10 ppm; retention time tolerance 0.5 min. Peak integration result was manually curated in Profinder for improved consistency and exported as a spreadsheet (.csv).

RNA Seq and Chip Seq on Rat Spermatogenic Cells: Total RNA and DNA was isolated from Brown Norway rat spermatogenic cell samples to best match rat reference genome Rnor 6.0 (NCBI: Gene). Replicate total RNA and DNA samples were each prepared from two rat spermatogonial lines derived and maintained on MEFs in SG Medium. Rat spermatogonial lines were harvested from 3x10cm dishes/line/condition at passages 8 and 9, respectively, and selected on gelatin coated plates for 1hr in SG Medium as described (Chapman et al., 2011; Hamra, 2017), yielding 3-4 million cells total/line/condition after preselection on gelatin-coated plates to deplete MEFs. The MEF-depleted spermatogonia were then either lysed directly and processed for ChipSeq or were plated onto replicate 10cm laminin-coated plates/line in SG Medium ($5\text{-}6x10^4$ spermatogonia/cm^2). On d2, half the cultures used for RNA sequencing were shifted to SD Medium as described above in *In vitro spermatogenesis colony forming assays*. Total RNA samples were extracted on ~d7 post-plating on laminin (d5 in SD Medium), and ~4 million Brown Norway rat laminin-non-binding spermatogenic cells, using the RNAqueous Kit (Ambion, Inc.). RNA concentration in each isolated sample was measured using the RiboGreen Kit (Invitrogen, Inc.). Genomic DNA samples were isolated using the DNA Mini-Prep Kit from Genesee Scientific (11-397B) and quantified using the Quant-iT™ PicoGreen™ dsDNA Assay Kit (ThermoFisher). RNA and Chip Seq analyses on rat spermatogonial transcripts and DNA fragments were conducted by The McDermott Center Next Generation Sequencing (NGS) Core at UT Southwestern Medical Center as describe by (Kollipara and Kittler, 2015). For qtPCR 50 ng of RNA from each cell sample was primed in a 20 µl reaction mix containing Oligo(dT) primers and Superscript III (Invitrogen, Inc.), according to manufacturer's protocol. Gene expression was analyzed by PCR using PfuTurbo in UltraHF Buffer from Stratagene, Inc. qtPCR conditions were as described (Wu et al., 2009), and PCR primers were designed to rat reference sequences (Rnor6.0) using the Primer/Blast: NCBI database.

Chip Seq Methods: Rat USg DNA (50 µg) was pretreated with protein G agarose beads (ThermoFisher) and Foxa2-DNA binding motifs co-precipitated using 5 µg of goat anti-human FOXA2 antibody sc-6554 (Santa Cruz Biotechnology) that was used to define the FOXA2 cistrome in the endometrium of the human uterus (Kelleher et al., 2019). Precipitates were washed, eluted from the beads with SDS buffer, and subjected to RNase and proteinase K treatment. Cross-links were reversed by incubation overnight at 65°C, and ChIP DNA was purified by phenol-chloroform extraction and ethanol precipitation (Kelleher et al., 2019). Single end reads of 75 bp were generated. After mapping reads to rat genome Rnor6.0 by bowtie2 (v2.2.3) with parameter "--sensitive", we perform filtering by (1) removing alignments with mapping quality less than 10, (2) removing duplicate reads identified by Picard MarkDuplicates (v1.127) http://broadinstitute.github.io/picard. Then enriched regions (peaks) were identified using MACS2 (v2.0.10)(Zhang et al., 2008), with a q-value cut-off of 0.05 for broad peaks. Peak regions were annotated by HOMER (Ross-Innes et al., 2012).

mRNA library preparation and bioinformatics analysis: Samples are run on the Agilent Tapestation 4200 to determine level of degradation thus ensuring only high-quality RNA is used (RIN Score 8 or higher). The Qubit fluorometer is used to determine the concentration prior to staring library prep. One microgram of total DNAse treated RNA is then prepared with the TruSeq Stranded Total RNA LT Sample Prep Kit from Illumina. Total RNA is depleted of its rRNA and fragmented before strand specific cDNA synthesis. cDNAs are then A-tailed and indexed adapters are ligated. After adapter ligation, samples are PCR amplified and purified with AmpureXP beads, then validated again on the Agilent Tapestation 4200. Before being normalized and pooled, samples are quantified by Qubit then run on the Illumina NextSeq 500 using V2.5 reagents. Raw data from machine are then de-multiplexed and converted to fastq files using bcl2fastq (v2.17, Illumina). The fastq files are checked for quality using fastqc (v0.11.2); http://www.bioinformatics.babraham.ac.uk/projects/fastqc and fastq_screen (v0.4.4) http://www.bioinformatics.babraham.ac.uk/projects/fastq_screen. Fastq files are mapped to rn6 reference genome (from igenomes) using STAR (Dobin et al., 2013). Read counts are then generated using featureCounts (Liao et al., 2014). TMM normalization and differential expression analysis is performed using edgeR (Robinson et al., 2010). Hierarchical clustering of differentially expressed genes is performed using hclust6 and heatmaps were generated using heatmap https://www.R-project.org/.

Spermatogenic Cell Transcript Authentication and Characterization: In rat testes, *Foxa2* was among 28 of 38 spermatogonial transcripts in Table 1 highly enriched in 2wk vs 6wk old rat testes (NCBI: Gene Database). In contrast, Spc marker transcripts were significantly enriched in 21wk vs 6wk rat testes containing more spermatocytes (Clermont and Perey, 1957) (NCBI: Gene Database). Enrichment of *Foxa2* in 2wk vs 6wk old rat testes is consistent with a spermatogonial gene profile (Hamra et al., 2004; Schultz et al., 2003). Transcripts selectively enriched in rat and human USg overlapped by 9.5% (n=122 of 1279), whereas, mouse and human USg transcripts overlapped by 4.7% (n=71 of 1508). Fifty-one transcripts enriched in rat USg vs DSg modeled gene profiles enriched in human USg cluster 1->2 Down (Guo et al., 2018), including *Utf1, Id1, Id2, Id4, Cdk17, Ffgr3, Nanos2, Nanos3, Fth1, Phgdh, Gpx4, Piwil4, Zbtb16 and Foxp1* (Figure 4A). Rat and mouse USg gene profiles were most related across species, overlapping by ~19.5% (n=277 of 1279). Significantly enriched transcripts in rat USg were highly conserved (71%, n=27 of 38) across at least two species when compared to genes enriched in DSg (32%, n=12 of 38) (Table 1). Lower conservation across rat, mouse and human DSg gene profiles potentially reflected greater species-dependent differences in progenitor spermatogonia amplification and differentiation programs. For example, rat and human USg enriched gene sets potentially encode markers for type A progenitor spermatogonia that persist into larger syncytia, and thus, may have been filtered for in the current study due to the GFP-ID4 bright and dim gene sets potentially being closer developmentally, due to a steep gradient of ID4 levels in A_s vs A_{al} spermatogonia (Oatley et al., 2011). Conversely, more genes commonly enriched in rat, mouse and human USg point to a greater similarity in molecular mechanisms that regulate germline stem cell fate.

Supplemental References

Abid, S.N., Richardson, T.E., Powell, H.M., Jaichander, P., Chaudhary, J., Chapman, K.M., and Hamra, F.K. (2014). A-single spermatogonia heterogeneity and cell cycles synchronize with rat seminiferous epithelium stages VIII-IX. Biol Reprod *90*, 32.

Chapman, K.M., Medrano, G.A., Chaudhary, J., and Hamra, F.K. (2015a). NRG1 and KITL Signal Downstream of Retinoic Acid in the Germline to Support Soma-Free Syncytial Growth of Differentiating Spermatogonia. Cell Death Discov *1*.

Chapman, K.M., Medrano, G.A., Jaichander, P., Chaudhary, J., Waits, A.E., Nobrega, M.A., Hotaling, J.M., Ober, C., and Hamra, F.K. (2015b). Targeted Germline Modifications in Rats Using CRISPR/Cas9 and Spermatogonial Stem Cells. Cell Rep *10*, 1828-1835.

Chapman, K.M., Saidley-Alsaadi, D., Syvyk, A.E., Shirley, J.R., Thompson, L.M., and Hamra, F.K. (2011). Spermatogonial Stem Cell Mediated Gene Transfer. Transgenic Technology, Vol 1, Eds. S. Pease & T. Saunders (Springer Press).

Clermont, Y., and Perey, B. (1957). Quantitative study of the cell population of the seminiferous tubules in immature rats. Am J Anat *100*, 241-267.
Cronkhite, J.T., Norlander, C., Furth, J.K., Levan, G., Garbers, D.L., and Hammer, R.E. (2005). Male and female germline specific expression of an EGFP reporter gene in a unique strain of transgenic rats. Dev Biol *284*, 171-183.
Dobin, A., Davis, C.A., Schlesinger, F., Drenkow, J., Zaleski, C., Jha, S., Batut, P., Chaisson, M., and Gingeras, T.R. (2013). STAR: ultrafast universal RNA-seq aligner. Bioinformatics *29*, 15-21.
Guo, J., Grow, E.J., Mlcochova, H., Maher, G.J., Lindskog, C., Nie, X., Guo, Y., Takei, Y., Yun, J., Cai, L*., et al.* (2018). The adult human testis transcriptional cell atlas. Cell Res *28*, 1141-1157.
Hamra, F.K. (2017). Rattus norvegicus Spermatogenesis Colony-Forming Assays. Methods Mol Biol *1463*, 185-203.
Hamra, F.K., Chapman, K.M., Nguyen, D., and Garbers, D.L. (2007). Identification of neuregulin as a factor required for formation of aligned spermatogonia. J Biol Chem *282*, 721-730.
Hamra, F.K., Chapman, K.M., Wu, Z., and Garbers, D.L. (2008). Isolating highly pure rat spermatogonial stem cells in culture. Methods Mol Biol *450*, 163-179.
Hamra, F.K., Gatlin, J., Chapman, K.M., Grellhesl, D.M., Garcia, J.V., Hammer, R.E., and Garbers, D.L. (2002). Production of transgenic rats by lentiviral transduction of male germ-line stem cells. Proc Natl Acad Sci U S A *99*, 14931-14936.
Hamra, F.K., Schultz, N., Chapman, K.M., Grellhesl, D.M., Cronkhite, J.T., Hammer, R.E., and Garbers, D.L. (2004). Defining the spermatogonial stem cell. Dev Biol *269*, 393-410.
Kelleher, A.M., Behura, S.K., Burns, G.W., Young, S.L., DeMayo, F.J., and Spencer, T.E. (2019). Integrative analysis of the forkhead box A2 (FOXA2) cistrome for the human endometrium. FASEB J *33*, 8543-8554.
Kollipara, R.K., and Kittler, R. (2015). An integrated functional genomic analysis identifies the antitumorigenic mechanism of action for PPARgamma in lung cancer cells. Genom Data *3*, 80-86.
Liao, Y., Smyth, G.K., and Shi, W. (2014). featureCounts: an efficient general purpose program for assigning sequence reads to genomic features. Bioinformatics *30*, 923-930.
Oatley, M.J., Kaucher, A.V., Racicot, K.E., and Oatley, J.M. (2011). Inhibitor of DNA binding 4 is expressed selectively by single spermatogonia in the male germline and regulates the self-renewal of spermatogonial stem cells in mice. Biol Reprod *85*, 347-356.
Perey, B., Clermont, Y., and Leblond, C.P. (1961). The Wave of the Seminiferous Epithelium in the Rat. Am J Anat *108*, 47-78.
Robinson, M.D., McCarthy, D.J., and Smyth, G.K. (2010). edgeR: a Bioconductor package for differential expression analysis of digital gene expression data. Bioinformatics *26*, 139-140.
Ross-Innes, C.S., Stark, R., Teschendorff, A.E., Holmes, K.A., Ali, H.R., Dunning, M.J., Brown, G.D., Gojis, O., Ellis, I.O., Green, A.R*., et al.* (2012). Differential oestrogen receptor binding is associated with clinical outcome in breast cancer. Nature *481*, 389-393.
Schultz, N., Hamra, F.K., and Garbers, D.L. (2003). A multitude of genes expressed solely in meiotic or postmeiotic spermatogenic cells offers a myriad of contraceptive targets. Proc Natl Acad Sci U S A *100*, 12201-12206.
Wu, Z., Falciatori, I., Molyneux, L.A., Richardson, T.E., Chapman, K.M., and Hamra, F.K. (2009). Spermatogonial culture medium: an effective and efficient nutrient mixture for culturing rat spermatogonial stem cells. Biol Reprod *81*, 77-86.
Zhang, Y., Liu, T., Meyer, C.A., Eeckhoute, J., Johnson, D.S., Bernstein, B.E., Nusbaum, C., Myers, R.M., Brown, M., Li, W*., et al.* (2008). Model-based analysis of ChIP-Seq (MACS). Genome Biol *9*, R137.